DIGEORGE SYNDROME GENE *TBX1*, REGULATES HEART AND CARTILAGE MORPHOGENESIS IN ZEBRAFISH BY PATHWAYS CONVERGING ON *ALCAMA*

by

Priya Choudhry

A dissertation submitted to the faculty of
The University of Utah
in partial fulfillment of the requirements for the degree of

Doctor of Philosophy

Department of Oncological Sciences

The University of Utah

December 2011

The University of Utah Graduate School

STATEMENT OF DISSERTATION APPROVAL

The dissertation of **Priya Choudhry**

has been approved by the following supervisory committee members:

Nikolaus Trede	, Chair	**07/27/2011** Date Approved
Dean Li	, Member	**07/27/2011** Date Approved
Joseph Yost	, Member	**07/27/2011** Date Approved
Tatjana Piotrowski	, Member	**07/27/2011** Date Approved
Jody Roseblatt	, Member	**07/27/2011** Date Approved

and by **Donald Ayer** , Chair of the Department of **Oncological Sciences**

and by Charles A. Wight, Dean of The Graduate School.

ABSTRACT

DiGeorge syndrome, characterized by congenital heart disease, craniofacial and immune system abnormalities, is the most common microdeletion syndrome with an incidence of 1 in 4000 live births. Congenital cardiac defects including conotruncal and ventricular septal defects are the leading cause of mortality. Experiments in mouse have identified *Tbx1* as the gene responsible for DiGeorge syndrome, and these findings were subsequently corroborated in human patients. However, the underlying pathways of *Tbx1* regulating heart, craniofacial and thymus development remain to be fully characterized. My dissertation focuses on using the zebrafish *tbx1*$^{-/-}$ mutant with craniofacial and immune defects similar to DiGeorge syndrome patients, to study the role and pathways of *tbx1* regulating heart and cartilage development.

I found that *tbx1*$^{-/-}$ mutants have defects in heart morphology, looping, function and differentiation. I showed that *tbx1* likely affects heart looping and differentiation by regulating cardiomyocyte proliferation and shape. I further demonstrated that *tbx1* regulates heart looping and differentiation via *wnt11r* and its downstream gene *alcama*. In addition to heart defects *alcama* morphants present cartilage abnormalities similar to those obtained by knockdown of *edn1*, a gene previously identified to act downstream of *tbx1* in cartilage development. Further investigation revealed that *alcama* functions downstream of Edn1 signaling in regulating neural crest differentiation and cartilage formation. In addition, I showed that Alcama on endoderm interacts with Nadl1.1 on

neural crest to mediate Edn1 signaling and regulate cartilage morphogenesis. Hence, I have demonstrated that Tbx1 regulates Alcama via Wnt11r in the heart and via Edn1 in pharyngeal endoderm.

For My Parents

TABLE OF CONTENTS

ACKNOWLEDGEMENTS

I would like to express special gratitude to my advisor, Nikolaus Trede, for his guidance and support during my graduate career. His energy, enthusiasm and love for science have given me motivation and courage especially during hard times. He has been very patient and encouraging, helping me to become a better scientist by encouraging me to think on my own. I also thank the rest of my committee: Dean Li, Joseph Yost, Tatjana Piotrowski and Jody Rosenblatt for their guidance, critical insights and helpful suggestions.

My sincere thanks to the members of the Trede lab, who have helped and encouraged me during my development as a scientist. They have helped me tremendously by showing me how to do experiments, give talks and write scientific documents in addition to providing friendship and support. Particularly noteworthy are Sarah Hutchinson, Deepa Joshi and Diana Bradley. Thank you to people in the CZAR for taking care of my fish and the microscopy and other core facilities for helping me obtain and analyze my results. Thank you to the people who have shared their plasmids and antibodies, particularly Shiela Samson and Josh Wythe. Thank you to the people from the Molecular Biology Program, Department of Oncological Sciences and Zebrafish Interest Group who have lent me technical support, and have provided a friendly and supportive environment for research. Thank you to Barbara Saffel, Tami Brunson, Dee DalPonte,

Jessica Hampton, and the International Center staff for making sure I stay in good academic and visa status.

Most importantly, I want to thank my parents for encouraging and supporting me during hard times. I have felt your love across the distance and will be forever grateful for your understanding. My brother has been my best friend and biggest supporter. To my friends here in Salt Lake City, you have helped me make a home away from home and provided great support over the years.

CHAPTER 1

INTRODUCTION

DiGeorge syndrome (DGS), characterized by cardiac abnormalities, craniofacial defects and thymus hypoplasia, is the most common microdeletion syndrome occurring in 1/4000 live births (Oskarsdottir et al., 2004). The clinical characteristics and severity of DGS are highly variable. The disease is predominantly sporadic and approximately 6-10% of cases are familial; sometimes one of the parents is identified only after a more severely affected child is diagnosed. Approximately 75-80% of patients have congenital heart disease with conotruncal defects (tetralogy of Fallot, aortic arch defects, and truncus arteriosus) and ventricular septal defects. Aortic arch defects include double aortic arch, right-sided aortic arch, cervical aortic arch and aberrant origin of subclavian arteries. 80% of patients have thymic hypoplasia resulting in decreased T cell numbers, but most are not clinically immunodeficient. IgA deficiency has also been identified. About 0.5% of cases have complete absence of T cells. This form is called Complete DGS and these patients require thymic transplantion as early as possible. Other features include hypocalcemia (resulting from parathyroid gland hypoplasia), palate anomalies, craniofacial abnormalities (auricular anomalies, small mouth, micrognathia, a short forehead, and some midfacial flattening), renal anomalies (urinary tract or renal agenesis or multidysplastic kidneys) neurological defects, speech disabilities, and feeding

disorders (Goldmuntz, 2005). Most of these affected structures are derived from the pharyngeal apparatus of the developing embryo, suggesting that DGS is a developmental defect arising during embryogenesis. I will now focus on the genetic basis of DGS.

1.1 *TBX1* is responsible for DGS

Most DGS patients have a 3Mb or a nested 1.5 Mb deletion of chromosome 22q11, implicating haploinsufficiency of a gene in the 1.5 Mb region (Morrow et al., 1995). To identify the gene responsible for the DGS phenotype among the 25 genes that map to the critical interval, various mice with deletions in the homologous region on chromosome 16 were generated (Fig. 1.1). Df1/+ mice carrying a 1.2 Mb deletion had outflow tract defects, suggesting that the critical gene was located in this region (Lindsay et al., 1999). A 550 Kb deletion of the proximal half of this region generated mice with no conotruncal abnormalities eliminating 13 genes (Puech et al., 2000). Mice with a large deletion spanning 1.5Mb (Lgdel/+) containing 24 genes exhibited parathyroid gland aplasia and perinatal lethality in addition to conotruncal anomalies (Merscher et al., 2001). These defects were rescued by complementation with BAC 316, thus narrowing the candidate genes to four: *Pnutl*, *Gp1bβ*, *Tbx1* and *Wdvcf*.

Only *Tbx1* is expressed in the pharyngeal apparatus, from which the craniofacial skeleton, thyroid, parathyroid and thymus are derived. *Tbx1*$^{+/-}$ mice have mild cardiovascular defects and ectopic parathyroid glands and are viable (Lindsay et al., 2001). *Tbx1*$^{-/-}$ mice have a severe phenotype with single cardiac outflow tract, aortic arch defects, thymus and parathyroid gland aplasia, absent outer and inner ear, cleft palate and neonatal lethality (Jerome and Papaioannou, 2001). Several frame-shift and missense

mutations in *TBX1* have been found in patients with a 22q11.2-like phenotype but without the chromosomal deletion, strongly suggesting that DGS is caused by haploinsufficiency of *TBX1* (Gong et al., 2001; Yagi et al., 2003). We will now examine *TBX1* function in more detail.

1.2 *TBX1* functions in a dose-dependent manner

Tbx1 is a member of the T-box gene family, a family of transcription factors that are characterized by a highly conserved DNA-binding region, the T box. The T-box also serves as an interaction domain for other transcription factors, and chromatin and histone modifying enzymes (Ryan and Chin, 2003; Smith, 1999). T-box proteins often function in combination with other transcription regulators or in a hierarchy, and are dose-dependent in their action. The dose-dependency of Tbx1 was confirmed by generating mouse transgenics. Mice carrying a duplication of the syntenic 22q11.2 region that is deleted in DGS and mice containing 8-10 copies of human *TBX1* exhibit some similarity to DGS patients (Ensenauer et al., 2003; Merscher et al., 2001). Normalization of *TBX1* expression by a gain of 8-10 copies of human *TBX1,* on a *Tbx1-/-* background rescues the DGS malformations (Liao et al., 2004). Additionally, 2 missense mutations, F148Y & H194Q found to cause DGS may function by increasing dimer stability and/or DNA affinity (Zweier et al., 2007). These findings indicate that *TBX1* operates in a dose-dependent manner, thus explaining why *TBX1* haploinsufficiency causes DGS in humans. This leads me to study the expression and role of *Tbx1*.

1.3 *Tbx1* expression

Most of the tissues and organs affected in DGS are derived from the pharyngeal apparatus, a vertebrate-specific, transient embryonic structure that gives rise to feeding and respiratory structures as well as the thyroid, parathyroid and thymus. The pharyngeal apparatus consists of five pharyngeal arches arising as a series of bulges on the lateral surface of the embryo. Cranial neural crest cells migrate from the rhombomeres to surround the core mesoderm of the pharyngeal arches. Each pharyngeal arch is composed of a cylinder of neural crest cells surrounding a core of mesodermal cells. The arches are separated from each other by ectoderm-lined pharyngeal clefts and endoderm-lined pharyngeal pouches.

Tbx1 is expressed in surface ectoderm, pharyngeal endoderm and core mesoderm but not neural crest (Fig. 1.2)(Vitelli et al., 2002). However, *Tbx1* mutation disrupts the migration of neural crest cells into the arches (Vitelli et al., 2002). Both conditional pharyngeal endoderm-specific and mesoderm-specific *Tbx1* null mice have malformations similar to those in *Tbx1* homozygous null mutants including thymus hypoplasia and cardiovascular defects (Arnold et al., 2006; Zhang et al., 2006). These data indicate that *Tbx1* expression in pharyngeal endoderm and mesoderm is necessary for proper patterning of the pharyngeal apparatus and proper formation of thymus and cardiac system.

Zebrafish *tbx1* is highly similar to mouse *Tbx1* in sequence and exon-intron structure. *tbx1* is first detected by *in situ* hybridization (ISH) at 6hpf during gastrulation in the involuting hypoblast cells and by 6-10 somites it is expressed in the paraxial mesoderm (Fig. 1.2) (Piotrowski et al., 2003). By 27 somites it is restricted to the

mesodermal core and epithelia of arches and the linear heart tube. From 48hpf *tbx1* expression is seen in individual arch muscles, pharyngeal endoderm, ear and heart. Thus, the expression of *tbx1* is conserved between mice and zebrafish. I have used zebrafish as a model system to study DGS.

1.4 Zebrafish as a model to study DGS

Though Tbx1 is an important developmental gene, and several mouse mutants have been generated, little is known about its downstream targets and pathways. New animal models that have a simpler developmental program and are easy to manipulate and examine are needed. Both heart and cartilage development is well described in zebrafish embryos and a plethora of developmental and structural markers is available. Transparency of the embryos allows live assessment of cardiac function, cellular morphology and cartilage/jaw structure.

The zebrafish mutant *vgo*^{tm208}/*tbx1*$^{-/-}$ has a premature stop codon in the T-box domain of *tbx1* (Piotrowski et al., 2003). The phenotypic similarities to DGS are striking with the exception that unlike mice and humans, the mutation is recessive in zebrafish. Homozygous mutants lack a thymus and pharyngeal pouches 2-6, resulting in fusion and loss of posterior pharyngeal arch-derived cartilage. In addition mutant embryos have reduced aortic arches, small otic vesicles and pericardiac edema. This dissertation will focus on identifying new targets of *tbx1* by studying heart and cartilage development in the zebrafish *tbx1*$^{-/-}$ mutant. This will, I hope, promote a deeper understanding of the molecular players involved and lead to better therapies. Before characterization of heart defects in *tbx1*$^{-/-}$ mutants, I will give an overview of heart development.

1.5 Heart development

Myocardial progenitors of the primary heart field (PHF) arise bilaterally, within the anterior portions of the lateral plate mesoderm as early as 10 somites (Brand, 2003; Yelon, 2001). The cardiomyocytes move toward the midline and begin cardiac fusion ending with a shallow cone with a central lumen (Fig. 1.3). The cone tilts and extends, forming the linear heart tube (LHT) by 24 hpf. Circulation begins at this stage and the heart tube extends from the midline to under the left eye. The ventricle jogs towards the midline by 33 hpf, curving the tube. The tube continues to bend and twist forming the completely looped heart by 48 hpf (Fig. 1.3).

At this stage, the heart is regionally specified to form the inflow tract (IFT), atrium, atrioventricular canal (AVC), ventricle and outflow tract (OFT). The ventricle is to the right of the atrium and the chambers look like inflated balloons with constrictions at both of their ends and the heart is fully functional. The early stages in the process of heart development are conserved among various organisms. Similar to zebrafish, the PHF arises as bilateral fields but their migration forms a cardiac crescent in mice, rather than a cardiac cone (Brand, 2003). In addition, the looping process continues on further to yield a four-chambered heart as compared to a two-chambered heart in zebrafish.

The secondary heart field (SHF) originates from the splanchnic mesoderm, medial to the PHF (Waldo et al., 2001). Cells from the SHF migrate towards the midline similar to the cells of PHF, but position themselves at the arterial pole of the heart tube. As the heart loops, these cells are added to the OFT and ventricle (Kelly and Buckingham, 2002). The SHF has been recently discovered in zebrafish. Similar to chick and mouse, the SHF cells are found in the most medial portion of the mesodermal heart

fields, migrate to the arterial pole after heart tube formation and later contribute to the bulbous arteriosus (BA) and ventricle (Hami et al., 2011).

1.5.1 Signaling pathways involved in heart development

Heart development is a complex process involving several pathways in a spatiotemporally regulated pattern. Study of signaling pathways during heart development has relied mainly on gene expression analysis and various mutants in *Drosophila,* zebrafish and mice. Gene expression analysis reveals that the PHF is already specified and patterned by the onset of somitogenesis (Yelon, 2001). Specified cardiomyocytes are marked by the expression of transcription factors *gata4*, *hand2* and *nkx2.5*. Mutants for the genes, *gata5, fgf8, bmp2b*, and *one-eyed pinhead* (*oep*) have reduced expression of *nkx2.5*, showing that these genes play a role in myocardial specification.

A different set of genes, including several T-box transcription factors, has been implicated in directing cardiac looping. The heart fails to loop in the zebrafish *tbx5-/-* mutant and *tbx20* has been shown to affect heart looping by negatively regulating *tbx5* expression (Brown et al., 2005; Garrity et al., 2002). Additionally, morpholino knockdown of *tbx2a* and *tbx3b* in zebrafish results in lack of heart looping and AVC formation (Ribeiro et al., 2007). Loss of noncanonical *wnt11r* signaling has also been shown to affect cardiac looping in *Xenopus* (Gessert et al., 2008). The relationship between these genes with respect to regulation of cardiac looping has not been determined so far.

The process and mechanism of cardiac looping is poorly understood. The signals directing migration and the signals creating competence to respond to migration signals are not known. It has been hypothesized that cardiac looping is driven by changes in cell shape (Auman et al., 2007) and cell proliferation (Qu et al., 2008; Ribeiro et al., 2007). Concomitant with looping, expression of several genes such as *notch1b* becomes restricted to specific regions of the heart. However, lack of looping in zebrafish morphants is often accompanied by defective expression of these region-specific genes. For example, *notch1b* expression is expanded into the ventricular endocardium of *tbx3b* and *tbx2a* morphant embryos (Ribeiro et al., 2007). Whether this region-specific expression induces abnormal looping directly, or is a secondary defect thereof, has not been determined.

In summary, these pathways cooperate or antagonize each other to promote cardiac morphogenesis. The hierarchy, epistasis and relationship between these signaling pathways with respect to heart morphogenesis remains to be elucidated. In this thesis I have examined if any of these pathways and mechanisms are mis-regulated in the hearts of the *tbx1*$^{-/-}$ mutant. My results suggest that *tbx1* regulates heart looping and subspecification via *wnt11r* and *alcama*. I will now summarize the literature regarding *wnt11r* and heart morphogenesis.

1.5.2 Wnt11r

Several publications indicate that Wnt11 signaling plays an important role during cardiac development. In *Xenopus*, maternal Wnt11 protein is enriched in the presumptive dorsal mesoderm and as zygotic transcription commences it becomes localized to the

dorsal marginal zone (Brade et al., 2006; Eisenberg and Eisenberg, 2006). *Wnt11* expression shows a conserved expression in precardiac mesoderm in quail, chick, mouse and *Xenopus* (Brade et al., 2006). Blocking *Wnt11* signaling inhibits cardiac specification while ectopic expression of *Wnt11* induces cardiac gene expression (Eisenberg and Eisenberg, 1999; Pandur et al., 2002; Schneider and Mercola, 2001). Furthermore *Wnt11* can induce expression of cardiac genes in *Xenopus* explants and noncardiac cells from humans and mouse (Belema Bedada et al., 2005; Eisenberg and Eisenberg, 1999; Flaherty et al., 2008; Garriock et al., 2005; Pandur et al., 2002; Schneider and Mercola, 2001; Ueno et al., 2007).

Garriock et. al. characterized *wnt11r*, a second *wnt11* gene in *Xenopus* and zebrafish that is an ortholog of chick and mammalian Wnt11 (Garriock et al., 2005). Unlike *wnt11, wnt11r* is not required for cardiac specification and does not form secondary axes when mis-expressed in *Xenopus* embryos. *wnt11r* expression begins in primary cardiac fields at the onset of differentiation, just prior to fusion of the heart tube and persists as the heart develops. Consistent with its expression pattern, knockdown of *wnt11r* leads to defects in heart morphogenesis and cardia bifida in some cases (Garriock et al., 2005). Furthermore, mutations in mouse *Wnt11* cause cardiac OFT defects such as truncus arteriosus, similar to those observed in *Tbx1-/-* mutants (Zhou et al., 2007). While both *Tbx1* and *Wnt11* signaling have been shown to be important in heart morphogenesis, my results provide the first link between them.

1.5.3 Alcama

Activated Leukocyte Cell Adhesion Molecule (ALCAM or Alcama in zebrafish), also known as CD166/neurolin/BEN/DM-GRASP/SC1/HCA, is a cell surface immunologlobulin superfamily member. Human ALCAM is a transmembrane glycoprotein having five immunoglobulin domains, a transmembrane domain and a short cytoplasmic tail. While it was initially identified in chicken for its role in neurite extension (Burns et al., 1991), ALCAM has now been shown to be involved in axonal pathfinding and axonal fasciculation (Diekmann and Stuermer, 2009; Weiner et al., 2004). In zebrafish, Alcama has been studied primarily for its role in neurogenesis (Diekmann and Stuermer, 2009; Fashena and Westerfield, 1999), although it is active in several other processes. Notably, ALCAM is expressed on dendritic and endothelial cells and can activate T-cells by binding to the CD6 receptor (Bowen et al., 2000; Fashena and Westerfield, 1999; Ofori-Acquah and King, 2008; Zimmerman et al., 2006). Furthermore, ALCAM has been shown to play a role in metastasis (Degen et al., 1998; Ofori-Acquah and King, 2008) and cell migration (Heffron and Golden, 2000).

ALCAM has a characteristic VVCCC immunoglobulin motif that is capable of interacting with itself or with other immunoglobulin motifs. It mediates cell-cell clustering through homophilic (ALCAM-ALCAM) as well as heterophilic (ALCAM-NgCAM and ALCAM-CD6) interactions (Bowen et al., 2000; DeBernardo and Chang, 1996; Degen et al., 1998). While Alcama is commonly used as a marker for pharyngeal endoderm and myocardium in zebrafish (Beis et al., 2005; Crump et al., 2004; Piotrowski and Nusslein-Volhard, 2000), its role in these tissues has not been elucidated thus far. However, *alcama* has been implicated to work downstream of *wnt11r* in regulating heart

morphogenesis in *Xenopus* (Gessert et al., 2008). In this thesis I have established that *tbx1, wnt11r* and *alcama* function in a linear pathway regulating heart morphogenesis in zebrafish. Furthermore, I have shown that *alcama* functions downstream of *tbx1* in cartilage morphogenesis. Before I do so, let me review cartilage development.

1.6 Cartilage development

Cartilage is derived from the neural crest of the pharyngeal arches. Each of the different cell types in the arch gives rise to distinct structures. Each pharyngeal arch is composed of a cylinder of neural crest cells surrounding a core of mesodermal cells. The arches are separated from each other by ectoderm-lined pharyngeal clefts and endoderm-lined pharyngeal pouches (Fig. 1.4). The ectoderm gives rise to sensory neurons while the endoderm forms the epithelial lining of the pharynx and the endocrine glands: thyroid, parathyroid and thymus. The mesoderm forms the musculature and endothelial cells of the arch arteries, and the neural crest forms the connective and skeletal tissues of each arch (Graham, 2003; Wurdak et al., 2006).

While the structure of the arch is conserved, each arch has an individual identity. The first arch (mandibular) forms the jaw, the second forms the hyoid apparatus, while the posterior (branchial arches) become incorporated into the throat. Neural crest cells that populate the pharyngeal arches arise as three streams from different parts of the brain. The neural crest cells that fill the first arch, arise from rhombomeres 1 and 2. The second arch neural crest cells arise from rhombomere 4. This pattern is common to mouse and zebrafish. The caudal arches are filled by neural crest cells emerging from

rhombomeres 6 and 7 in mouse and rhombomeres 6-8 in zebrafish (Graham, 2003; Piotrowski et al., 2003) (Fig. 1.4).

Although neural crest cells carry patterning cues with them, interaction with other cell types, particularly the endoderm, is required for correct patterning and formation of pharyngeal arches (David et al., 2002; Piotrowski and Nusslein-Volhard, 2000). Initial segmentation and expansion of pharyngeal arches and pouches, is followed by differentiation to form the mature cartilage. This pattern of development and differentiation is largely conserved across species with minor differences; for example the endoderm-derived gill clefts persist in fish but not in higher vertebrates. After reviewing cartilage development, I will describe what is known about Tbx1's role in cartilage development.

1.6.1 *tbx1* and cartilage development

The *tbx1*-deficient zebrafish *van gogh* mutants are characterized by small otic vesicles, and reduced pharyngeal skeleton whose elements are often fused. Mutant embryos fail to form segmented endodermal pouches, hence abolishing pharyngeal arch segmentation. The neural crest cells migrate in distinct streams, but fuse abnormally when they reach the pharyngeal arches (Piotrowski and Nusslein-Volhard, 2000). Elements of the first and second arches are reduced, while the branchial arches are highly reduced or absent. Transplantation of wild-type (WT) endodermal cells partially rescued pharyngeal cartilages, implying that neural crest-derived cartilage defects in *tbx1*$^{-/-}$ mutants result from defective signaling from the endoderm (Piotrowski et al., 2003).

In situ hybridization and transplantation analysis was used to place the genes *endothelin-1* (*edn1*) and *hand2* in a regulatory pathway downstream of *tbx1*(Piotrowski et al., 2003). *edn1* is co-expressed with *tbx1* in the mesodermal core, pharyngeal epithelia and endodermal pouches. Edn1 is a small diffusible peptide which regulates Hand2, a bHLH transcription factor expressed in the neural crest cells (Miller et al., 2000). *edn1* expression is reduced in *tbx1*$^{-/-}$, and *edn1*$^{-/-}$ mutants have malformed cartilage similar to *tbx1*$^{-/-}$. In addition, transplantation of wild-type endodermal cells can partially rescue *edn1* expression in *tbx1*$^{-/-}$, suggesting that *edn1* functions downstream of *tbx1* (Piotrowski et al., 2003). *hand2* expression is down-regulated in *tbx1*$^{-/-}$ and *edn1*$^{-/-}$ mutants and *hand2*$^{-/-}$ mutants also have cartilage defects. These results suggest that *tbx1* induces the expression of *edn1,* which in turn diffuses and induces *hand2* in the neural crest cells (Fig. 1.5).

While *edn1* has been identified as a target of Tbx1, it is not clear if it is a direct or indirect target. *edn1* and other genes in the Edn1 pathway are primarily required for correct formation of the mandibular and hyoid arches. The ventral cartilages of mutants in these genes are reduced in size, changed in orientation and fused to the dorsal cartilages (Kimmel et al., 1998; Piotrowski et al., 1996). On the other hand, all the pharyngeal cartilages are affected in the *tbx1*$^{-/-}$ mutant. The difference in severity of cartilage defects present in *tbx1*$^{-/-}$, *edn1*$^{-/-}$ and *hand2*$^{-/-}$ mutants suggests that Tbx1 signals differently in the anterior versus posterior arches and that there might be more molecular players involved.

In this dissertation, I study heart and cartilage defects in the zebrafish *tbx1*$^{-/-}$ mutant to identify downstream genes and further elucidate the mechanism of Tbx1 function. In this thesis I have identified Alcama as a new downstream target of zebrafish Tbx1 regulating heart and cartilage development. Using expression analysis and rescue experiments, I have demonstrated that Tbx1 regulates Alcama via Wnt11r in the heart and via Edn1 in pharyngeal endoderm.

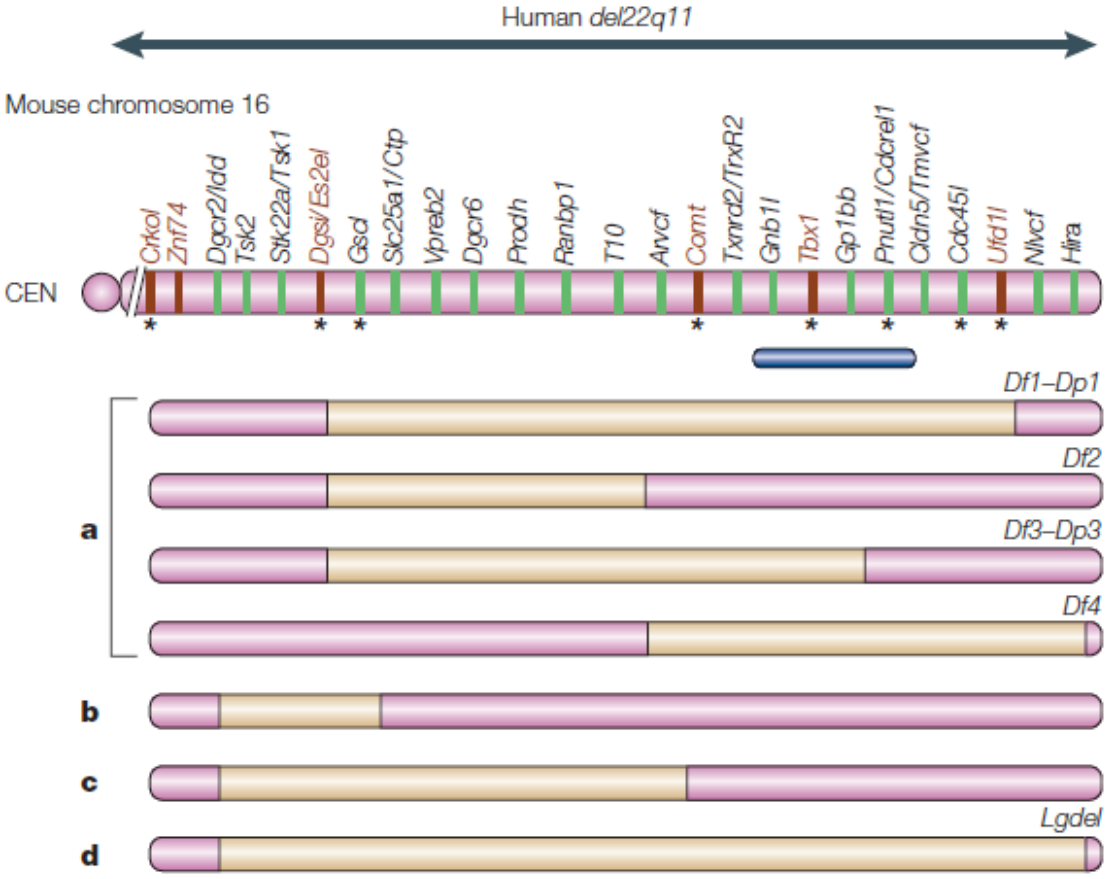

Figure 1.1 Map of region deleted in DGS patients (blue arrow) and its corresponding region on mouse chromosome 16 (pink)
The genes of the region deleted in DGS patients is highly conserved in the mouse genome. The deletions generated in different mouse models are shown in the lower part of the figure. The different BACs used for rescue are also depicted. The blue bar shows the BAC that rescues cardiovascular defects in Df1/+ and Lgdel/+ mutants. Adapted from Lindsay (2001).

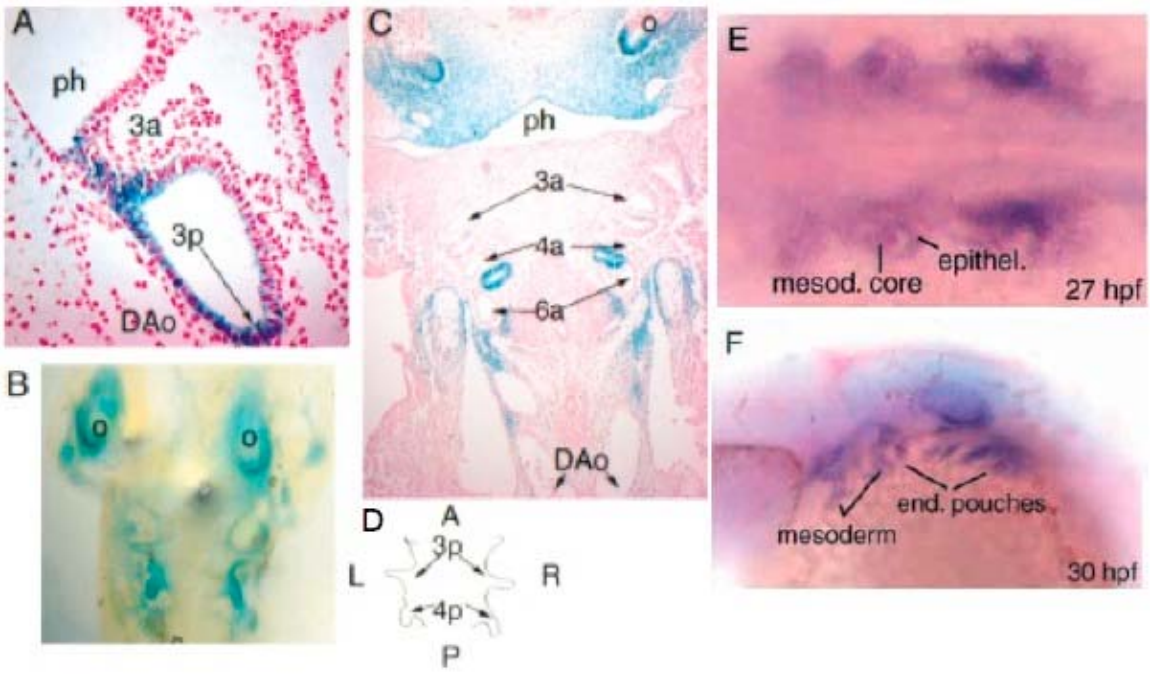

Figure 1.2 *Tbx1* expression in mouse and zebrafish
X-gal staining showing *Tbx1* expression in E9.5 (A), E10.5 (B) and E11.5 (C) mouse embryos. At each stage, the most caudal area of the pharyngeal endoderm shows the strongest Tbx1 expression. (D) is an outline of the pharynx: A, anterior; P, posterior; L, left; R, right. Adapted from (Vitelli et al., 2002). (E) Dorsal view of 27 hpf and (F) lateral view of 30 hpf zebrafish larva showing tbx1 expression withing the mesodermal cores, epithelia and endodermal pouches. Adapted from Piotrowski et al. (2003).

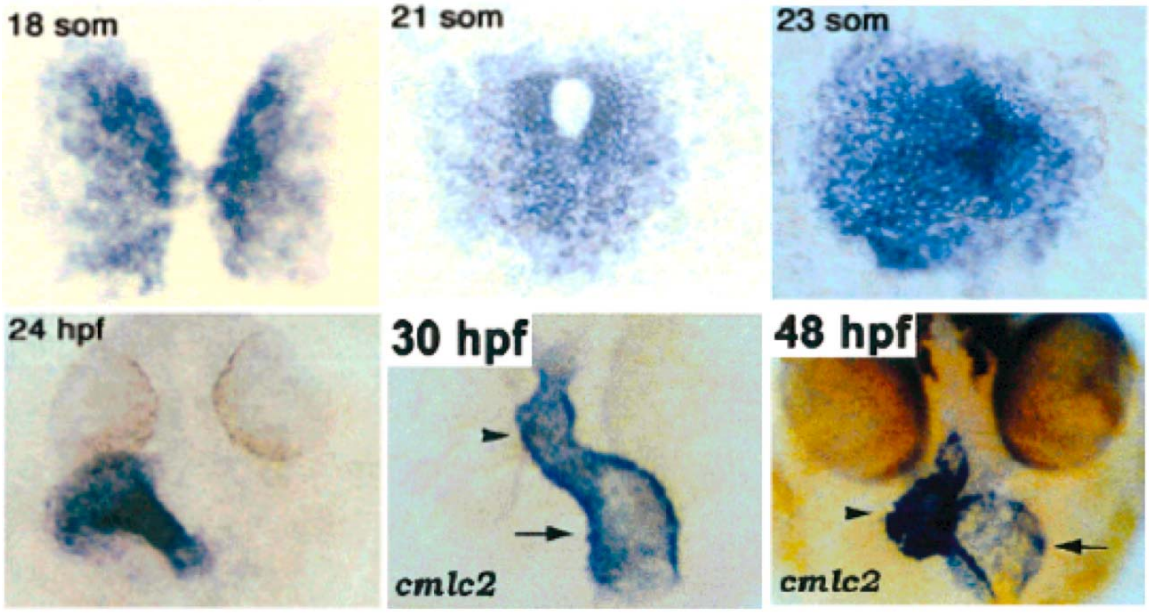

Figure 1.3 Zebrafish Heart formation
Cmlc2 ISH showing cardiomyocyte fusion (18 somites), cone formation (21 somites), cone tilting (23 somites) and linear heart tube (24 hpf). Images are dorsal views with anterior to the top. Cardiac jogging begins at 30 hpf and looping is complete at 48 hpf. Images are head-on views, with the embryo's left side to the right of the figure. The ventricle is indicated with arrowheads, and the atrium is indicated with arrows. Adapted from Yelon (2001).

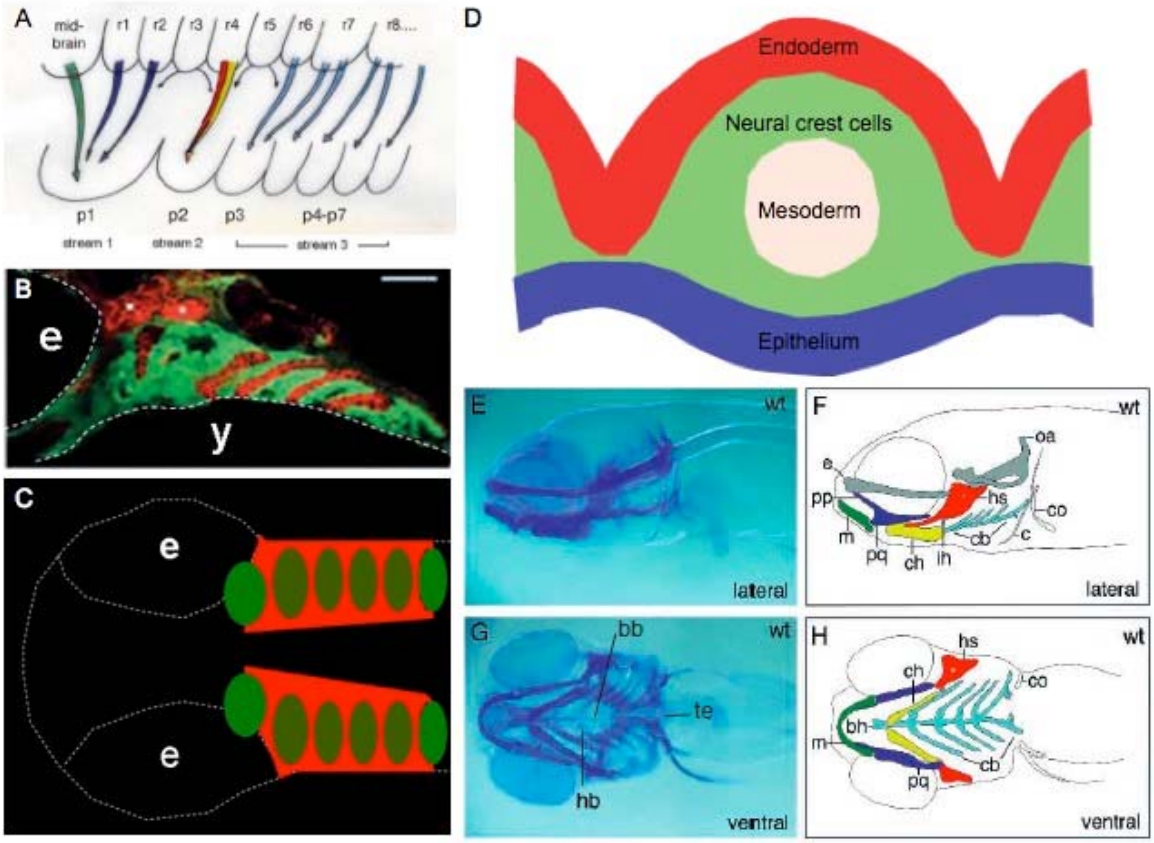

Figure 1.4 Zebrafish pharyngeal arch and cartilage patterning
(A) Schematic drawing showing the migration of neural crest cells in three different streams from the rhombomeres in the brain to the different pharyngeal arches. Adapted from Piotrowski et al. (2003). (B) Lateral view of 30 hpf zebrafish larva showing neural crest in green and pharyngeal endoderm in red. E denotes the eye and y the yolk. Adapted from Crump et al. (2004). (C) Schematic showing the ventral view of zebrafish larva shown in B. (D) Schematic showing cross-section of an individual pharyngeal arch with pharyngeal endoderm (red) on both sides. The arch is composed of a cylinder of neural crest cells (green) surrounding a mesodermal core (beige) with epithelium (blue) on the outside and endoderm on the inside (red). Lateral and ventral views of 5 dpf WT larva showing Alcian Blue staining (E, G) and corresponding schematic (F, H) Abbreviation used : bh, basihyal; ch, ceratohyal; cb, ceratobranchial; e, ethmoid plate; hs, hyosymplectic; m, Meckel's cartilage; pp, pterygoid process of the palatoquadrate; pq, palatoquadrate. Color code used : green, Meckel's; blue, platoquadrate; red, hyosymplectic; yellow, ceratohyal; light blue, interhyal; light green, arches 3-5; grey, neurocranium. Adapted from Piotrowski et al. (1996).

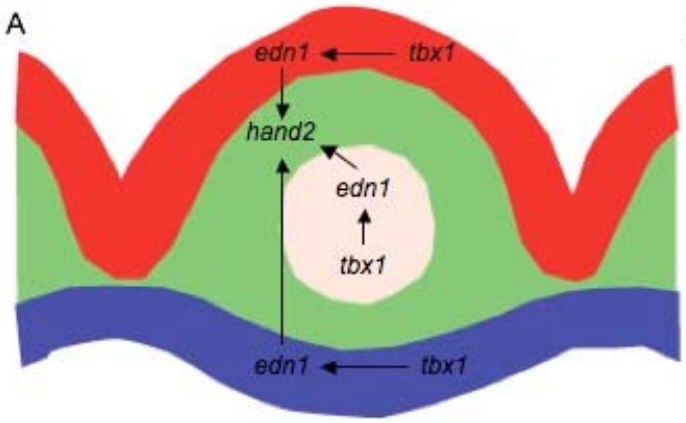

B

	tbx1	*edn1*	*hand2*
tbx1$^{-/-}$	–	↓	↓
edn1$^{-/-}$	normal	–	↓
hand2$^{-/-}$	normal	normal	–

Figure 1.5 The Tbx1 pathway regulating pharyngeal arch development
(A) The Tbx1 pathway is shown schematically within a cross-section of a pharyngeal arch. The mesodermal core is colored beige, neural crest green, endoderm red and epithelium as blue. (B) The expression of *tbx1*, *edn1* and *hand2* in the respective mutants in summarized in the table. Adapted from Piotrowski et al. (2003).

1.7 References

Arnold, J.S., Werling, U., Braunstein, E.M., Liao, J., Nowotschin, S., Edelmann, W., Hebert, J.M., Morrow, B.E., 2006. Inactivation of Tbx1 in the pharyngeal endoderm results in 22q11DS malformations. Development (Cambridge, England) 133, 977-987.

Auman, H.J., Coleman, H., Riley, H.E., Olale, F., Tsai, H.J., Yelon, D., 2007. Functional modulation of cardiac form through regionally confined cell shape changes. PLoS Biol 5, e53.

Beis, D., Bartman, T., Jin, S.W., Scott, I.C., D'Amico, L.A., Ober, E.A., Verkade, H., Frantsve, J., Field, H.A., Wehman, A., Baier, H., Tallafuss, A., Bally-Cuif, L., Chen, J.N., Stainier, D.Y., Jungblut, B., 2005. Genetic and cellular analyses of zebrafish atrioventricular cushion and valve development. Development 132, 4193-4204.

Belema Bedada, F., Technau, A., Ebelt, H., Schulze, M., Braun, T., 2005. Activation of myogenic differentiation pathways in adult bone marrow-derived stem cells. Mol Cell Biol 25, 9509-9519.

Bowen, M.A., Aruffo, A.A., Bajorath, J., 2000. Cell surface receptors and their ligands: in vitro analysis of CD6-CD166 interactions. Proteins 40, 420-428.

Brade, T., Manner, J., Kuhl, M., 2006. The role of Wnt signalling in cardiac development and tissue remodelling in the mature heart. Cardiovasc Res 72, 198-209.

Brand, T., 2003. Heart development: molecular insights into cardiac specification and early morphogenesis. Dev Biol 258, 1-19.

Brown, D.D., Martz, S.N., Binder, O., Goetz, S.C., Price, B.M., Smith, J.C., Conlon, F.L., 2005. Tbx5 and Tbx20 act synergistically to control vertebrate heart morphogenesis. Development 132, 553-563.

Burns, F.R., von Kannen, S., Guy, L., Raper, J.A., Kamholz, J., Chang, S., 1991. DM-GRASP, a novel immunoglobulin superfamily axonal surface protein that supports neurite extension. Neuron 7, 209-220.

Crump, J.G., Swartz, M.E., Kimmel, C.B., 2004. An integrin-dependent role of pouch endoderm in hyoid cartilage development. PLoS Biol 2, E244.

David, N.B., Saint-Etienne, L., Tsang, M., Schilling, T.F., Rosa, F.M., 2002. Requirement for endoderm and FGF3 in ventral head skeleton formation. Development 129, 4457-4468.

DeBernardo, A.P., Chang, S., 1996. Heterophilic interactions of DM-GRASP: GRASP-NgCAM interactions involved in neurite extension. J Cell Biol 133, 657-666.

Degen, W.G., van Kempen, L.C., Gijzen, E.G., van Groningen, J.J., van Kooyk, Y., Bloemers, H.P., Swart, G.W., 1998. MEMD, a new cell adhesion molecule in

metastasizing human melanoma cell lines, is identical to ALCAM (activated leukocyte cell adhesion molecule). Am J Pathol 152, 805-813.

Diekmann, H., Stuermer, C.A., 2009. Zebrafish neurolin-a and -b, orthologs of ALCAM, are involved in retinal ganglion cell differentiation and retinal axon pathfinding. J Comp Neurol 513, 38-50.

Eisenberg, C.A., Eisenberg, L.M., 1999. WNT11 promotes cardiac tissue formation of early mesoderm. Dev Dyn 216, 45-58.

Eisenberg, L.M., Eisenberg, C.A., 2006. Wnt signal transduction and the formation of the myocardium. Dev Biol 293, 305-315.

Ensenauer, R.E., Adeyinka, A., Flynn, H.C., Michels, V.V., Lindor, N.M., Dawson, D.B., Thorland, E.C., Lorentz, C.P., Goldstein, J.L., McDonald, M.T., Smith, W.E., Simon-Fayard, E., Alexander, A.A., Kulharya, A.S., Ketterling, R.P., Clark, R.D., Jalal, S.M., 2003. Microduplication 22q11.2, an emerging syndrome: clinical, cytogenetic, and molecular analysis of thirteen patients. American Journal of Human Genetics 73, 1027-1040.

Fashena, D., Westerfield, M., 1999. Secondary motoneuron axons localize DM-GRASP on their fasciculated segments. J Comp Neurol 406, 415-424.

Flaherty, M.P., Abdel-Latif, A., Li, Q., Hunt, G., Ranjan, S., Ou, Q., Tang, X.L., Johnson, R.K., Bolli, R., Dawn, B., 2008. Noncanonical Wnt11 signaling is sufficient to induce cardiomyogenic differentiation in unfractionated bone marrow mononuclear cells. Circulation 117, 2241-2252.

Garriock, R.J., D'Agostino, S.L., Pilcher, K.C., Krieg, P.A., 2005. Wnt11-R, a protein closely related to mammalian Wnt11, is required for heart morphogenesis in Xenopus. Dev Biol 279, 179-192.

Garrity, D.M., Childs, S., Fishman, M.C., 2002. The heartstrings mutation in zebrafish causes heart/fin Tbx5 deficiency syndrome. Development 129, 4635-4645.

Gessert, S., Maurus, D., Brade, T., Walther, P., Pandur, P., Kuhl, M., 2008. DM-GRASP/ALCAM/CD166 is required for cardiac morphogenesis and maintenance of cardiac identity in first heart field derived cells. Dev Biol 321, 150-161.

Goldmuntz, E., 2005. DiGeorge syndrome: new insights. Clinics in Perinatology 32, 963-978, ix-x.

Gong, W., Gottlieb, S., Collins, J., Blescia, A., Dietz, H., Goldmuntz, E., McDonald-McGinn, D.M., Zackai, E.H., Emanuel, B.S., Driscoll, D.A., Budarf, M.L., 2001. Mutation analysis of TBX1 in nondeleted patients with features of DGS/VCFS or isolated cardiovascular defects. Journal of Medical Genetics 38, E45.

Graham, A., 2003. Development of the pharyngeal arches. Am J Med Genet A 119A, 251-256.

Hami, D., Grimes, A.C., Tsai, H.J., Kirby, M.L., 2011. Zebrafish cardiac development requires a conserved secondary heart field. Development 138, 2389-2398.

Heffron, D.S., Golden, J.A., 2000. DM-GRASP is necessary for nonradial cell migration during chick diencephalic development. J Neurosci 20, 2287-2294.

Jerome, L.A., Papaioannou, V.E., 2001. DiGeorge syndrome phenotype in mice mutant for the T-box gene, Tbx1. Nature Genetics 27, 286-291.

Kelly, R.G., Buckingham, M.E., 2002. The anterior heart-forming field: voyage to the arterial pole of the heart. Trends Genet 18, 210-216.

Kimmel, C.B., Miller, C.T., Kruze, G., Ullmann, B., BreMiller, R.A., Larison, K.D., Snyder, H.C., 1998. The shaping of pharyngeal cartilages during early development of the zebrafish. Dev Biol 203, 245-263.

Liao, J., Kochilas, L., Nowotschin, S., Arnold, J.S., Aggarwal, V.S., Epstein, J.A., Brown, M.C., Adams, J., Morrow, B.E., 2004. Full spectrum of malformations in velo-cardio-facial syndrome/DiGeorge syndrome mouse models by altering Tbx1 dosage. Human Molecular Genetics 13, 1577-1585.

Lindsay, E.A., 2001. Chromosomal microdeletions: dissecting del22q11 syndrome. Nat Rev Genet 2, 858-868.

Lindsay, E.A., Botta, A., Jurecic, V., Carattini-Rivera, S., Cheah, Y.C., Rosenblatt, H.M., Bradley, A., Baldini, A., 1999. Congenital heart disease in mice deficient for the DiGeorge syndrome region. Nature 401, 379-383.

Lindsay, E.A., Vitelli, F., Su, H., Morishima, M., Huynh, T., Pramparo, T., Jurecic, V., Ogunrinu, G., Sutherland, H.F., Scambler, P.J., Bradley, A., Baldini, A., 2001. Tbx1 haploinsufficieny in the DiGeorge syndrome region causes aortic arch defects in mice. Nature 410, 97-101.

Merscher, S., Funke, B., Epstein, J.A., Heyer, J., Puech, A., Lu, M.M., Xavier, R.J., Demay, M.B., Russell, R.G., Factor, S., Tokooya, K., Jore, B.S., Lopez, M., Pandita, R.K., Lia, M., Carrion, D., Xu, H., Schorle, H., Kobler, J.B., Scambler, P., Wynshaw-Boris, A., Skoultchi, A.I., Morrow, B.E., Kucherlapati, R., 2001. TBX1 is responsible for cardiovascular defects in velo-cardio-facial/DiGeorge syndrome. Cell 104, 619-629.

Miller, C.T., Schilling, T.F., Lee, K., Parker, J., Kimmel, C.B., 2000. sucker encodes a zebrafish Endothelin-1 required for ventral pharyngeal arch development. Development 127, 3815-3828.

Morrow, B., Goldberg, R., Carlson, C., Das Gupta, R., Sirotkin, H., Collins, J., Dunham, I., O'Donnell, H., Scambler, P., Shprintzen, R., et al., 1995. Molecular definition of the

22q11 deletions in velo-cardio-facial syndrome. American Journal of Human Genetics 56, 1391-1403.

Ofori-Acquah, S.F., King, J.A., 2008. Activated leukocyte cell adhesion molecule: a new paradox in cancer. Transl Res 151, 122-128.

Oskarsdottir, S., Vujic, M., Fasth, A., 2004. Incidence and prevalence of the 22q11 deletion syndrome: a population-based study in Western Sweden. Arch Dis Child 89, 148-151.

Pandur, P., Lasche, M., Eisenberg, L.M., Kuhl, M., 2002. Wnt-11 activation of a noncanonical Wnt signalling pathway is required for cardiogenesis. Nature 418, 636-641.

Piotrowski, T., Ahn, D.G., Schilling, T.F., Nair, S., Ruvinsky, I., Geisler, R., Rauch, G.J., Haffter, P., Zon, L.I., Zhou, Y., Foott, H., Dawid, I.B., Ho, R.K., 2003. The zebrafish van gogh mutation disrupts tbx1, which is involved in the DiGeorge deletion syndrome in humans. Development (Cambridge, England) 130, 5043-5052.

Piotrowski, T., Nusslein-Volhard, C., 2000. The endoderm plays an important role in patterning the segmented pharyngeal region in zebrafish (Danio rerio). Dev Biol 225, 339-356.

Piotrowski, T., Schilling, T.F., Brand, M., Jiang, Y.J., Heisenberg, C.P., Beuchle, D., Grandel, H., van Eeden, F.J., Furutani-Seiki, M., Granato, M., Haffter, P., Hammerschmidt, M., Kane, D.A., Kelsh, R.N., Mullins, M.C., Odenthal, J., Warga, R.M., Nusslein-Volhard, C., 1996. Jaw and branchial arch mutants in zebrafish II: anterior arches and cartilage differentiation. Development 123, 345-356.

Puech, A., Saint-Jore, B., Merscher, S., Russell, R.G., Cherif, D., Sirotkin, H., Xu, H., Factor, S., Kucherlapati, R., Skoultchi, A.I., 2000. Normal cardiovascular development in mice deficient for 16 genes in 550 kb of the velocardiofacial/DiGeorge syndrome region. Proceedings of the National Academy of Sciences of the United States of America 97, 10090-10095.

Qu, X., Jia, H., Garrity, D.M., Tompkins, K., Batts, L., Appel, B., Zhong, T.P., Baldwin, H.S., 2008. Ndrg4 is required for normal myocyte proliferation during early cardiac development in zebrafish. Dev Biol 317, 486-496.

Ribeiro, I., Kawakami, Y., Buscher, D., Raya, A., Rodriguez-Leon, J., Morita, M., Rodriguez Esteban, C., Izpisua Belmonte, J.C., 2007. Tbx2 and Tbx3 regulate the dynamics of cell proliferation during heart remodeling. PLoS ONE 2, e398.

Ryan, K., Chin, A.J., 2003. T-box genes and cardiac development. Birth Defects Res C Embryo Today 69, 25-37.

Schneider, V.A., Mercola, M., 2001. Wnt antagonism initiates cardiogenesis in Xenopus laevis. Genes Dev 15, 304-315.

Smith, J., 1999. T-box genes: what they do and how they do it. Trends Genet 15, 154-158.

Ueno, S., Weidinger, G., Osugi, T., Kohn, A.D., Golob, J.L., Pabon, L., Reinecke, H., Moon, R.T., Murry, C.E., 2007. Biphasic role for Wnt/beta-catenin signaling in cardiac specification in zebrafish and embryonic stem cells. Proc Natl Acad Sci U S A 104, 9685-9690.

Vitelli, F., Morishima, M., Taddei, I., Lindsay, E.A., Baldini, A., 2002. Tbx1 mutation causes multiple cardiovascular defects and disrupts neural crest and cranial nerve migratory pathways. Human Molecular Genetics 11, 915-922.

Waldo, K.L., Kumiski, D.H., Wallis, K.T., Stadt, H.A., Hutson, M.R., Platt, D.H., Kirby, M.L., 2001. Conotruncal myocardium arises from a secondary heart field. Development 128, 3179-3188.

Weiner, J.A., Koo, S.J., Nicolas, S., Fraboulet, S., Pfaff, S.L., Pourquie, O., Sanes, J.R., 2004. Axon fasciculation defects and retinal dysplasias in mice lacking the immunoglobulin superfamily adhesion molecule BEN/ALCAM/SC1. Mol Cell Neurosci 27, 59-69.

Wurdak, H., Ittner, L.M., Sommer, L., 2006. DiGeorge syndrome and pharyngeal apparatus development. Bioessays 28, 1078-1086.

Yagi, H., Furutani, Y., Hamada, H., Sasaki, T., Asakawa, S., Minoshima, S., Ichida, F., Joo, K., Kimura, M., Imamura, S., Kamatani, N., Momma, K., Takao, A., Nakazawa, M., Shimizu, N., Matsuoka, R., 2003. Role of TBX1 in human del22q11.2 syndrome. Lancet 362, 1366-1373.

Yelon, D., 2001. Cardiac patterning and morphogenesis in zebrafish. Dev Dyn 222, 552-563.

Zhang, Z., Huynh, T., Baldini, A., 2006. Mesodermal expression of Tbx1 is necessary and sufficient for pharyngeal arch and cardiac outflow tract development. Development (Cambridge, England) 133, 3587-3595.

Zhou, W., Lin, L., Majumdar, A., Li, X., Zhang, X., Liu, W., Etheridge, L., Shi, Y., Martin, J., Van de Ven, W., Kaartinen, V., Wynshaw-Boris, A., McMahon, A.P., Rosenfeld, M.G., Evans, S.M., 2007. Modulation of morphogenesis by noncanonical Wnt signaling requires ATF/CREB family-mediated transcriptional activation of TGFbeta2. Nat Genet 39, 1225-1234.

Zimmerman, A.W., Joosten, B., Torensma, R., Parnes, J.R., van Leeuwen, F.N., Figdor, C.G., 2006. Long-term engagement of CD6 and ALCAM is essential for T-cell proliferation induced by dendritic cells. Blood 107, 3212-3220.

Zweier, C., Sticht, H., Aydin-Yaylagul, I., Campbell, C.E., Rauch, A., 2007. Human TBX1 missense mutations cause gain of function resulting in the same phenotype as 22q11.2 deletions. American Journal of Human Genetics 80, 510-517.

CHAPTER 2

DIGEORGE SYNDROME GENE *TBX1* FUNCTIONS THROUGH *WNT11R* TO REGULATE HEART MORPHOLOGY AND FUNCTION

Priya Choudhry[a], Joseph Yost[b], Nikolaus Trede[b]

a : Huntsman Cancer Institute, b: Department of Neurobiology and Anatomy, c: Department of Pediatrics, University of Utah, Salt Lake City, UT 84112, USA

priya.choudhry@hci.utah.edu

nikolaus.trede@hci.utah.edu

Corresponding author : Dr Nikolaus Trede

Investigator, The Huntsman Cancer Institute

University of Utah

2000, Circle of Hope

Salt Lake City, UT 84112, USA

Office: 1-801-585-0199

FAX: 1-801-581-8547

2.1 Abstract

DiGeorge syndrome (DGS), a debilitating syndrome characterized by congenital heart disease, craniofacial and immune system abnormalities, is the most common microdeletion syndrome with a rate of 1 in 4000 live births. The congenital cardiac defects in DGS patients predominantly include conotruncal and ventricular septal defects and may be caused by abnormal heart looping. DGS is caused by haploinsufficiency of the *TBX1* gene. However, the molecular pathways underpinning *TBX1*'s role in heart development are not fully understood. Previous work in zebrafish has identified a *tbx1*$^{-/-}$ mutant with craniofacial and immune defects similar to DGS patients, but the heart defects are not fully characterized. Here we show that zebrafish *tbx1*$^{-/-}$ mutants have defective heart morphology, looping and function. Failure of proper looping is accompanied by the lack of proper differentiation of cells derived from PHF and SHF. A severe reduction in proliferation and lack of heart cell shape change contribute to defective looping and heart cell differentiation. We show for the first time that *tbx1* regulates heart looping and differentiation via *wnt11r* (wnt11 related), a member of the noncanonical Wnt pathway. Moreover, we demonstrate that activated leukocyte cell adhesion molecule a (*alcama*) functions downstream of both *tbx1* and *wnt11r* in zebrafish heart development. Our data supports a model whereby heart looping and differentiation are regulated by *tbx1* in a linear pathway through *wnt11r* and *alcama*.

2.2 Keywords

tbx1, *wnt11r*, *alcama*, heart, DiGeorge

2.3 Introduction

DiGeorge syndrome (DGS) is the most common microdeletion syndrome occurring in 1/4000 live births (Oskarsdottir et al., 2004). Approximately 75-80% of patients have congenital heart disease with conotruncal defects (Tetralogy of Fallot, aortic arch defects, and truncus arteriosus) and ventricular septal defects. Other defects include thymic hypoplasia, palate defects and thyroid and parathyroid abnormalities. Cardiac defects are the leading cause of mortality, but the underlying molecular pathobiology is not well understood.

Most DGS patients have a 3Mb or a nested 1.5 Mb deletion of chromosome 22q11 2 which includes the *TBX1* gene. Genetically engineered mouse mutants have led to the identification of *Tbx1* as the gene responsible for cardiovascular and thymic defects (Jerome and Papaioannou, 2001; Lindsay et al., 2001; Merscher et al., 2001). Several patients without the chromosomal deletion harbor frame-shift and missense mutations in *TBX1*, strongly suggesting that DGS is caused by haploinsufficiency of *TBX1* (Gong et al., 2001; Yagi et al., 2003). *TBX1* is a member of a group of transcription factors that are characterized by the presence of a T-box, a highly conserved DNA-binding region that also has a conserved interaction domain for other transcription factors. T-box genes mediate transcriptional activation and/or repression and are important for embryonic development and differentiation of all three germ layers (Smith, 1997, 1999; Wilson and Conlon, 2002). In addition, T-box genes are extremely dose-sensitive and often act in a combinatorial or hierarchical fashion (Greulich et al., 2011). Dose-sensitivity of *Tbx1* has been tested using various mouse hypomorphic and null alleles and transgenics (Liao et al., 2004; Lindsay et al., 2001; Xu et al., 2004). While *Tbx1*+/- mice have a milder

phenotype, *Tbx1-/-* mice have a severe phenotype with single cardiac outflow tract (OFT), aortic and pharyngeal arch defects, thymus and parathyroid gland aplasia (Jerome and Papaioannou, 2001). Tissue-specific knockdown of *Tbx1* in the pharyngeal endoderm or mesoderm recapitulates the cardiac defects observed in *Tbx1-/-* mice and DGS patients, making it difficult to isolate the role of *Tbx1* in different tissues (Arnold et al., 2006; Zhang et al., 2006). Though several genes such as *Fgf10* have been implicated to be in the *Tbx1* pathway (Xu et al., 2004), validation and detailed description of their roles is lacking and the *Tbx1* pathway remains uncharacterized.

Several genes and pathways, such as Nkx2.5, GATA family and Bone Morphogenetic Protein pathway, regulate heart development (Brand, 2003). These pathways may be synergistic, hierarchical or antagonistic in function. For example, canonical *Wnt* and *Sonic hedgehog* signaling have been postulated to operate upstream of *Tbx1* (Huh and Ornitz, 2010; Liao et al., 2008). However, noncanonical *Wnt* signaling plays an important role in proper heart morphogenesis by inhibition of β-catenin signaling and by mediating its own signaling via protein kinase C and c-jun terminal kinase (Brade et al., 2006; Garriock et al., 2005; Gessert et al., 2008; Matsui et al., 2005). *Wnt11*, a noncanonical *Wnt* member, is required for heart specification and can induce expression of cardiac genes in *Xenopus* explants and noncardiac cells from humans and mouse (Belema Bedada et al., 2005; Eisenberg and Eisenberg, 1999; Flaherty et al., 2008; Garriock et al., 2005; Pandur et al., 2002; Schneider and Mercola, 2001; Ueno et al., 2007). Furthermore, mutations in *Wnt11* cause cardiac OFT defects such as truncus arteriosus, similar to those observed in *Tbx1-/-* mutants (Zhou et al., 2007). Knockdown of *Wnt11r*, an ortholog of *Wnt11* present in *Xenopus*, resulted in heart morphology

defects and cardia bifida in some cases (Garriock et al., 2005). While both *Tbx1* and *Wnt11* signaling have been shown to be important in heart morphogenesis, no link has been established to date.

The pattern of heart development is conserved through evolution. Development begins with specification of the bilateral Primary Heart Fields (PHF) in lateral plate mesoderm. Subsequent migration towards the midline results in the cardiac crescent and later the linear heart tube, at which point the heart starts beating. The tube then undergoes jogging, looping and morphogenetic movements to result in the four-chambered heart. This is a complex process involving ballooning of the chamber walls, addition of cardiomyocytes derived from the Secondary Heart Field (SHF) at the arterial pole and formation of septa and valves. Formation of heart chambers is accompanied by differential gene expression within the various parts of the heart (Brade et al., 2006; Brand, 2003). Cell tracing experiments in mice and chick have established that heart myocardium derives from PHF, while SHF contributes to the OFT (Buckingham et al., 2005). Interestingly, previous studies suggest that *Tbx1* is expressed in SHF and that *Tbx1* positively regulates SHF cell proliferation and contribution to the muscle layer of OFT (Chen et al., 2009; Liao et al., 2008; Xu et al., 2004).

The pattern of heart development is largely conserved in zebrafish. Similar to mice and chicken, fusion of PHFs results in a cardiac cone that tilts and elongates to form the linear heart tube. Moreover, presence of SHF and its contribution to OFT has been recently confirmed in zebrafish (Hami et al., 2011). Zebrafish have a simple two-chambered heart with a single inflow and outflow tract and looping results in an S-shaped heart instead of the four-chambered heart with multiple outlets. The OFT retains the

bulbous arteriosus (BA), an accessory chamber equivalent to the conus arteriosus of amphibians and reptiles. This structure has been replaced by the pulmonary and aortic trunk in mammals and birds. The simpler structure of the heart combined with transparency of embryos and availability of a *tbx1* mutant, make zebrafish the ideal system to study cardiac defects associated with DGS. Here we use the zebrafish *tbx1*$^{-/-}$ mutant (Piotrowski et al., 2003) to study cardiac defects associated with DGS and identify *Tbx1* target genes. We show that *tbx1* is required for proper heart looping and differentiation of myocardium derived from the PHF and SHF. In addition we provide evidence that *tbx1* mediates its function at least in part via *wnt11r*, and its downstream gene *alcama*.

2.4 Materials and methods

2.4.1 Fish stocks and maintenance

Fish were maintained at 28.5 ^{o}C under standard conditions (Westerfield, 2000) and were staged as described (Kimmel et al., 1995). The *vgo*^{tm208} (*tbx1*$^{-/-}$) line and *wnt11r* $^{fh224/+}$ (*wnt11r* $^{-/-}$) mutant lines were a kind gift from Dr Tatjana Piotrowski (Stowers Institute of Medical Research, Kansas City, MO) and Dr. Cecilia Moens (Fred Hutchinson Cancer Center, Seattle, WA). Homozygous mutants were obtained by inbreeding of heterozygous carriers. *Tg(cmlc2:EGFP)* fish that express green fluorescent protein (GFP) in the nuclei of cardiomyocytes under the control of *cardiac myocyte light chain* promoter, were a gift from Dr Joseph Yost (Department of Neurobiology, University of Utah).

2.4.2 Identification and genotyping of mutants

tbx1$^{-/-}$ mutants have an A-to-T missense mutation (Piotrowski et al., 2003). Mutant embryos were identified by high resolution melting analysis (Zhou et al., 2005). DNA was extracted from the tails of stained embryos and PCR was conducted using the primers 5'- CACAACTGAAAATCGCCAGCAATC-3' (forward, 0.2 μM), 5'- AATATGGTAAAACTCACCAGTCCT -3' (reverse, 1 μM) and 5'- TTTACCAAAGGCTTCAGAGACTGTAATCCC -3' (unlabelled probe complementary to reverse strand, 1 μM). After PCR, the samples were heated to 94 °C for 2 minutes and then cooled to 10 °C before melting. LCGreen dye (Idaho Technology) was included in the PCR mix and melting analysis was done on LightScanner™ (Idaho Technology). The *wnt11r*$^{-/-}$ mutant was generated by tilling, and has a G-to-T nonsense mutation that generates a stop codon at amino acid 94. *wnt11r* $^{-/-}$ mutants were identified in a similar fashion using the primers 5'- GGTCTGCCAAAAGACCTTCACAG-3' (forward, 0.2μM), 5'- TTGGAAATAAATGCGTTTAGACACGGTT-3' (reverse, 1μM) and 5'- TGTTCCCCTATTGATGGACCGAAACTCCT-3' (unlabelled probe complementary to reverse strand, 1 μM). All the identified WT and mutants were included in the analysis.

2.4.3 Cloning and RNA transcription

The *tbx1* gene cloned in pCS2+, and *wnt11r* gene cloned in pCMVSport6.1, were obtained from ZIRC (Zebrafish International Resource Center). To make sense RNA for injection, these plasmids were cut with *NotI* and *XhoI* respectively, and in vitro transcribed from Sp6 promoter using mMessage Machine kit (Ambion). RNA for *alcama* was made as previously described (Choudhry et al., 2010).

2.4.4 Morpholino antisense oligonucleotide and RNA injections

Morpholino and RNA were dissolved in molecular biology grade water and pressure injected into 1-4 cell zebrafish embryos. For RNA rescue experiments, 26 pg of *tbx1, wnt11r* or *alcama* RNA was injected per embryo. The previously described translation blocking morpholino for *alcama* was used at 1.1 ng per embryo (Choudhry et al., 2010).

2.4.5 Tissue labeling procedures

Whole mount RNA in situ hybridization (ISH) with digoxigenin was performed as previously described (Miller et al., 2000). The plasmids for *versican* and *eln2* were a gift from Dr Joseph Yost (Department of Neurobiology, University of Utah) and for *amhc* and *vmhc* from Dr Dean Li (Department of Human Genetics, University of Utah). Alcama protein was stained using Zn-5 antibody from ZIRC at 1:500 dilution. A goat anti-mouse secondary antibody conjugated with Alexa 555 (Invitrogen) was used for fluorescence labeling of cell boundaries. The Isl-1 antibody was a gift from Dr Richard Dorsky (Department of Neurobiology and Anatomy, University of Utah) and was used at 1:100 dilution. Labelling of bulbous arteriosus with DAF-2DA (VWR) was done as previously described (Grimes et al., 2006).

2.4.6 Imaging and quantification

Head-on photographs of 48 hours post fertilization (hpf) larvae were taken on Nikon SMZ1000. Dissected hearts and ISH embryos were photographed on a Nikon Y-

IDP microscope at 20x zoom using Spot software. Confocal images of dissected hearts were taken on Olympus FV1000 microscope at 40x zoom. Images of all larvae from the same experiment were taken using the same settings and exposure. Cell numbers were counted using Imaris software. Measurements for circularity, length and volume were done using ImageJ and angles were measured on Adobe Photoshop. Live embryos were mounted in 1% low melt agarose and movies of the beating heart were taken with the Nikon Y-IDP microscope.

2.4.7 Analysis of cardiac performance

Movies of beating hearts were imaged as above and analyzed as follows. Heart rate was calculated by counting the number of sequential contractions. The widths of ventricles/atria at diastole and systole were measured. Shortening fractions were calculated as width [(diastole – systole) / diastole]. Stroke volume was determined as previously described (Fritsche et al., 2000). The perimeter of the ventricle during diastole and systole was outlined on ImageJ and analyzed with a "fit-to-ellipse" algorithm, giving the major and minor axes. Volume was calculated using $V = 4/3 * \pi * a * b^2$, and the stroke volume was obtained by subtracting the volume at systole from volume at diastole.

2.4.8 Paraffin embedding and sectioning

Seventy two hpf larvae were fixed in 4% paraformaldehyde for 2 days, dehydrated in ethanol series and transferred directly to xylene. They were allowed to equilibrate for 90 min and then placed in paraffin. Embryos were embedded in disposable plastic molds and cooled before sectioning at 5 μm on a Leica RM2155 microtome. Glass

slides were heated to 60^{o}C overnight, placed in xylenes for 5 min, rehydrated through an ethanol series to water, stained with 0.1% toluidine blue, and coverslipped using Cytoseal 60 (Fisher Scientific).

2.5 Results

2.5.1 *tbx1* is required for proper cardiac looping and morphogenesis in zebrafish

In zebrafish, *tbx1* expression starts between 6 to 10 somites in the lateral plate mesoderm containing the cardiac progenitors (Fig. 2S1A and (Piotrowski et al., 2003), and continues to be expressed in the myocardium as the heart develops (Fig. 2S1B-D). By 48 hpf, expression is stronger in the ventricle as compared to the atrium and especially strong in the AVC (Fig. 2S4A). TBX1 is a key transcription factor necessary for correct cardiac morphogenesis in humans and mice. We tested whether *tbx1* plays a role in cardiac morphogenesis in zebrafish by using *cmlc2* ISH to visualize the cardiomyocytes at various developmental stages in the *tbx1*$^{-/-}$ mutant. The cardiac progenitors are correctly specified from the lateral plate mesoderm at 14 somites, migrate towards the midline to fuse (21 somites) and form the linear heart tube at 24 hpf in *tbx1*$^{-/-}$ mutants. Jogging of ventricle (30-36 hpf) and looping of the heart (36-48 hpf), leads to an S-shaped heart in WT embryos (Fig. 2.1A). Defective jogging and looping in *tbx1*$^{-/-}$ mutants yields a straight heart (Fig. 2.1A) with variation in severity between larvae. In order to quantify this defect, we measured the angle between the longitudinal axes of ventricle and atrium. Our data show a marked difference in the angle between WT (22^{o})

and *tbx1*$^{-/-}$ mutants (10^{o}) (Fig. 2.1A, B), demonstrating that *tbx1* is necessary for heart looping.

In addition to the looping defect, *tbx1*$^{-/-}$ mutants have other cardiac morphological defects. Mutant ventricles are significantly shorter at 48 hpf (Fig. 2.1C), while atrial length is similar between mutants and WT. The ventricle at its widest point is significantly wider in the mutant when compared to WT at 48 hpf, (Fig. 2.1D) and 72 hpf (Fig. 2S1G). Atrium width differences between mutants and WT are significant at 72 hpf (Fig. 2.1E), but not at 48 hpf (Fig. 2S1H). In addition, sections of the heart at 72 hpf, reveal that mutant hearts have thinner ventricular walls and fewer cells and larger intercellular spaces (Fig. 2S1E, F). Overall our data indicate that *tbx1* is necessary for heart looping and morphogenesis of both chambers, with a stronger effect in the ventricles.

2.5.2 *tbx1* is necessary for proper OFT formation and differentiation

DGS patients and *Tbx1-/-* mutant mice have defects in OFT such as persistent truncus arteriosus and interrupted aortic arch. Hence we studied the OFT in the zebrafish *tbx1*$^{-/-}$ mutants. The zebrafish ventricle ends in a constriction leading to the BA, an accessory chamber present in lower vertebrates that is composed of smooth muscle. While the width of BA is unaffected (Fig. 2.2A, E, I), it is shorter in *tbx1*$^{-/-}$ mutants versus WT siblings (Fig. 2.2A, E, J). Our analysis revealed that BA smooth muscle in *tbx1*$^{-/-}$ mutants is defective as evidenced by negative staining with the fluorescent nitric oxide sensor DAF-2DA (Grimes et al., 2006) (Fig. 2.2B, F). *tbx1*$^{-/-}$ mutants also fail to express the BA-specific marker *tropoelastin2* (*eln2*) at 72 hpf (Fig. 2.2G). These findings

suggest that the BA is improperly formed and undifferentiated in *tbx1*$^{-/-}$ mutants. Since *cmlc2* staining revealed normal cardiac specification of the PHF, we analyzed the SHF that also contributes to the muscle wall of the OFT. Islet-1 (Isl-1) antibody staining reveals that *tbx1*$^{-/-}$ mutants have normal specification of SHF cells (Fig. 2.2H) at 14-somites. Our results suggest that in the absence of *tbx1* signal, SHF cells form but fail to differentiate into smooth muscle of the BA.

2.5.3 *tbx1*$^{-/-}$ mutants have defects in cardiac performance

Since cardiac defects are the leading cause of mortality in DGS patients, we analyzed cardiac function in *tbx1*$^{-/-}$ mutants. We analyzed movies of beating hearts in live embryos at 31 hpf, 48 hpf and 72 hpf. Cardiac contractility was assessed using the ventricular and atrial shortening fractions. Mean ventricular shortening fraction was unaffected at 48 hpf but was significantly lower at 72 hpf in *tbx1*$^{-/-}$ mutants (0.160 $\pm$ 0.012) compared to WT (0.197 $\pm$ 0.014) (Fig. 2.3A). Mean atrial shortening fraction was unaffected at 48 hpf and 72 hpf (Fig. 2.3B), in keeping with the weaker morphological defect in atria. Cardiac output was analyzed as stroke volume. The stroke volume was 10-20% lower in *tbx1*$^{-/-}$ mutants but this difference is not significant (p-value > 0.05) (Fig. 2.3C). This result is surprising considering the severe ventricular morphological defect. Heart rate was lower in *tbx1*$^{-/-}$ mutants. At 48 hpf the mean heart rate decreased to 75% in *tbx1*$^{-/-}$ mutants (108 $\pm$ 2 beats per minute) as compared to WT siblings (143 $\pm$ 2 beats per minute). At 72 hpf the mutant heart rate (167 $\pm$ 2) partially recovered to 86% of WT (195 $\pm$ 4) (Fig. 2.3D). This is in contrast to DGS patients where the heart beats faster to

compensate for OFT obstructions. In conclusion, the ventricle in *tbx1*$^{-/-}$ mutants has defects in contractility and heart rate.

2.5.4 *tbx1* expression is necessary for subspecification of heart regions

At 48 hpf the heart becomes subspecified to form the various regions: inflow tract (IFT), atrium, atrioventricular canal (AVC), ventricle and OFT. In zebrafish, heart looping defects are highly correlated with defects in subspecification of the heart, suggesting that these regional changes in expression pattern are important for the looping process (Auman et al., 2007; Chi et al., 2008; Garrity et al., 2002; Qu et al., 2008; Ribeiro et al., 2007; Tu et al., 2009). We performed ISH analysis in *tbx1*$^{-/-}$ mutants at 52 hpf to evaluate if subspecification and differentiation occurs normally. The ventral marker *vmhc* and atrial marker *amhc* are expressed normally in *tbx1*$^{-/-}$ mutants, suggesting that atrial and ventricular specification occurs normally in *tbx1*$^{-/-}$ mutants (Fig. 2S2). *Bone morphogenetic protein 4* (*bmp4*) is expressed in the IFT, AVC and OFT in WT siblings (Fig. 2.4A). Similarly, *versican* and *notch1b* are expressed in the AVC myocardium and endocardium, respectively (Fig. 2.4B, C). *tbx1*$^{-/-}$ mutants fail to express these markers in the AVC at this stage (Fig. 2.4E-G). In order to determine if these defects are heart specific, we examined *versican* expression in the otoliths. *tbx1*$^{-/-}$ mutant otoliths express *versican* (inset Fig. 2.4G), indicating that the defect is heart-specific. Expression of *atrial natriuretic factor* (*anf*) is restricted to the outer curvature of the ventricle and atrium. However *anf* expression is expanded to the inner curvature in the ventricle and to a lesser degree in the atrium in *tbx1*$^{-/-}$ mutants. The abovementioned markers are expressed normally at 30 hpf (data not shown) in the mutants, indicating that the differentiation

defect arises during the looping process. In addition, penetrance of these defects is variable in *tbx1*$^{-/-}$ mutant larvae (Fig. 2.4M-P). *notch1b* showed the highest penetrance and we will henceforth use it as a marker for subspecification. Failure of *tbx1*$^{-/-}$ mutants to restrict *anf* expression, taken together with absence of *bmp4*, *notch1b*, and *anf*, suggests that *tbx1* is necessary for looping, subspecification and differentiation of heart regions.

2.5.5 *tbx1* regulates cardiomyocyte proliferation and shape

The spatiotemporal pattern of cell proliferation is a major contributor to inflation of the chambers giving rise to the final looped structure of the heart (Ribeiro et al., 2007). Hence a defect in the timing, region or amount of proliferation may lead to looping defects. We used *Tg*(*cmcl2:EGFP*) larvae to count total cell numbers in hearts, and phosphohistone 3 staining to determine the percentage of cells undergoing mitosis (Fig. 2.5A,B). Total cardiomyocyte number was unchanged at 33 hpf, but was decreased 1.3 fold at 48 hpf (post-looping and morphological defects) (Fig. 2.5C). This correlates with the lower cell density and larger intercellular spaces observed in sections of *tbx1*$^{-/-}$ mutant hearts (Fig. 2S1F). Analysis of phosphohistone 3 staining reveals that the mean number of proliferating cells per heart is reduced 1.6 times at 33 hpf (15 in WT siblings versus 9 in *tbx1*$^{-/-}$ mutants, Fig. 2.5D), suggesting that the decrease in cell number is due to decreased proliferation. In addition to the number, we analyzed the spatial distribution of proliferating cells. By 33hpf, proliferating cells become restricted to the chambers exclusively, as opposed to even distribution along the heart tube at 24 hpf. We detected no defect in this restriction of proliferating cells in mutants (data not shown), suggesting

that *tbx1* regulates the number but not the spatial distribution of proliferating cells during the later stages of heart development (after 30 hpf).

Cardiomyocyte shape changes are another important element of proper heart looping. The cells transition from small and rounded morphology in the linear heart tube (24-28 hpf) to flattened and elongated structures in the outer curvature at the expanded chamber stage (48-58 hpf) (Auman et al., 2007). We stained 48 hpf *Tg(cmlc2:EGFP)* larvae with Alcama antibody to visualize the cell boundary, and analyze cell shape. In WT siblings the cells in the outer curvature are elongated with their longitudinal axes pointing towards the AVC (white, Fig. 2.5E), while cells in the inner curvature continue to be small and rounded (yellow, Fig. 2.5E). However, *tbx1*$^{-/-}$ mutant cells in the outer and inner curvatures retain the small and rounded morphology (Fig. 2.5F). We assessed this defect by calculating the circularity of 10 cells from the inner and outer chambers of 7 larvae. Cells from *tbx1*$^{-/-}$ mutants in the outer curvature have 1.2-1.3 fold higher circularity (are rounder) as compared to WT siblings (Fig. 2.5G), while cells in the inner curvature are equally round in between the mutant and WT (Fig. 2.5H). In summary, our data suggests that *tbx1* is required for maintenance of cardiomyocyte proliferation and regulation of cell shape, and thus reduced proliferation and failure to change shape causes the looping defect in *tbx1*$^{-/-}$ mutants.

2.5.6 *lox* and *pdpk1a* are new candidates for Tbx1 target genes

To look for downstream targets and/or interactors of Tbx1 that may mediate heart looping defects, we performed a microarray screen. *tbx1*$^{-/-}$ mutants were identified from *Tg(cmlc2:EGFP)* fish based on the looping phenotype at 52 hpf and their hearts were

isolated for RNA extraction. WT sibling hearts were used as controls. Fig. 2.6A shows the results from gene ontology analysis of the microarray. As expected, *tbx1* functions as both a transcriptional activator and repressor. The results for several genes like *fibroblast growth factor 10* (*fgf10*) and *six1* that are implicated in the *tbx1* pathway (Guo et al., 2011; Xu et al., 2004) are shown in Fig. 2.6B. From our microarray results, we tested *lysyl oxidase* (*lox*) and *3-phosphoinositide dependent protein kinase-1a* (*pdpk1a*) as they were highly down-regulated and were expressed in the heart. We verified that *lox* and *pdpk1a* are down-regulated in *tbx1*$^{-/-}$ mutants by ISH analysis (Fig. 2.6C), validating our microarray.

2.5.7 *tbx1* and *wnt11r* function in the same pathway to regulate heart looping and subspecification

We extended our survey of new Tbx1 target genes by a candidate approach. T-Box proteins frequently interact and several among them such as *tbx2a*, *tbx3b* (Ribeiro et al., 2007), *tbx5* (Garrity et al., 2002), and *tbx20* (Brown et al., 2005) have been implicated in heart looping. *wnt11r*, a member of the noncanonical Wnt pathway, has also been implicated in regulating expression of cardiac markers and heart looping in *Xenopus* (Gessert et al., 2008). While zebrafish *wnt11r* is homologous to *Xenopus wnt11r*, its role in zebrafish heart development and looping has not been studied so far. In order to discriminate which looping pathways are affected in *tbx1*$^{-/-}$ mutants, we analyzed the microarray and performed ISH analysis for these genes. Microarray analysis revealed that *wnt11r* and *tbx3b* were down-regulated, *tbx20* was up-regulated, while *tbx2a* and *tbx5* were unaffected. By ISH analysis, all these genes are expressed stronger in the

ventricle as compared to the atrium at 52 hpf in WT embryos. While all the *tbx* genes were unaffected in *tbx1*$^{-/-}$ mutants (Fig. 2.7A-D, F-I), *wnt11r* expression was down-regulated in *tbx1*$^{-/-}$ mutants (Fig. 2.7E, J). This result was corroborated by quantitative RT-PCR, which indicates that *wnt11r* RNA is down-regulated by 37% in hearts of *tbx1*$^{-/-}$ mutants (not shown). These data led us to hypothesize that *tbx1* regulates heart looping via *wnt11r*.

To test the hypothesis that *tbx1* regulates heart looping and subspecification of heart regions via *wnt11r*, we first analyzed *wnt11r* expression in zebrafish larvae. The expression and role of *wnt11r* in heart development in zebrafish is unknown. ISH revealed that *wnt11r* is expressed for the first time in cardiac mesoderm just prior to fusion (21 somites, Fig. 2S3A). *wnt11r* continues to be expressed in cardiomyocytes as the heart forms and loops, though expression becomes weaker (Fig. 2S3B, C). Next, we analyzed the zebrafish *wnt11r* $^{-/-}$ mutant (Banerjee et al., 2011). *cmcl2* ISH revealed that the *wnt11r* $^{-/-}$ mutants also have defective heart looping (Fig. 2.8A, B) with the angle between the ventricular and atrial axes significantly reduced to 10^{o} from 19^{o} in WT siblings. Next we tested whether *wnt11r* $^{-/-}$ mutants have subspecification defects similar to *tbx1*$^{-/-}$ mutants. ISH analysis revealed that *wnt11r* $^{-/-}$ mutants have down-regulated *bmp4*, *versican* and *notch1b* and mis-expressed *anf* (Fig. 2.8C). DAF-2DA and *eln2* ISH reveal that *wnt11r* $^{-/-}$ mutants do not have BA defects (Fig. 2S3D, E), suggesting that the heart looping and subspecification defects are independent of BA defects. The subspecification defect combined with the looping defect observed in *wnt11r* $^{-/-}$ mutants, supports our hypothesis that *tbx1* and *wnt11r* function in the same pathway to regulate heart looping and subspecification.

To further explore this hypothesis we conducted nonallelic noncomplementation assays. We crossed *tbx1*$^{+/-}$ and *wnt11r* $^{+/-}$ mutants and analyzed the double heterozygous larvae for looping and subspecification defects. Our analysis reveals that *tbx1*$^{+/-}$*/wnt11r* $^{+/-}$ larvae have incomplete looping and fail to express *notch1b* in significantly more larvae as compared to *tbx1* $^{+/-}$ or *wnt11r* $^{+/-}$ larvae (Fig. 2.8D). These data suggest that *tbx1* and *wnt11r* function in the same pathway to regulate heart looping and subspecification.

2.5.8 *tbx1* regulates heart looping and subspecification via *wnt11r* and *alcama*

Our data suggests that *tbx1* and *wnt11r* function in the same pathway and down-regulation of *wnt11r* in *tbx1*$^{-/-}$ mutants (Fig. 2.7J) suggests that *wnt11r* may be downstream of *tbx1*. We tested this by analyzing *tbx1* expression in *wnt11r* $^{-/-}$ mutants. By ISH *tbx1* expression is unchanged in *wnt11r* $^{-/-}$ mutants as compared to WT siblings (Fig. 2S4A, C). The nonallelic noncomplementation assay in conjunction with expression analysis indicate that *wnt11r* functions downstream of *tbx1* in regulating heart looping and subspecification.

Previous work identified *Xenopus alcama* as a downstream target of *wnt11r* during differentiation of cardiomyocytes and heart looping (Gessert et al., 2008). This led us to extend our hypothesis: *tbx1* regulates *wnt11r*, *wnt11r* regulates *alcama*, which in turn regulates heart looping and subspecification. We first probed our hypothesis by analysis of *alcama* ISH during heart development. *alcama* expression starts in the heart progenitors at 21 somites and continues on until 4 dpf (Beis et al., 2005; Rohr et al., 2008). Similar to *tbx1* expression, *alcama* expression is stronger in the ventricle than

atrium and is especially strong in the AVC in WT embryos. AT 48 hpf, *alcama* expression is down-regulated in both *tbx1*$^{-/-}$ and *wnt11r* $^{-/-}$ mutants (Fig. 2S4D, F), supporting our hypothesis that *wnt11r* and *alcama* are downstream of *tbx1*. The observed down-regulation is stronger in the ventricle while the atrium seems unaffected. To test the specific function of *alcama* during zebrafish heart morphogenesis, we injected a morpholino directed against *alcama* (Choudhry et al., 2010) into zebrafish at the 1-cell stage and assessed heart looping and subspecification at 48 hpf. *alcama* morphants have defective heart looping of varying severity (Fig. 2S5B-D), a finding that may be explained by dosage differences in morpholino injections. In addition to looping defects, *alcama* morphants have defects in subspecification of the heart as assessed by *notch1b* ISH (Fig. 2S5F). Hence, we have shown that *alcama* is down-regulated in *tbx1*$^{-/-}$ and *wnt11r* $^{-/-}$ mutants, and that *alcama* is needed for normal heart looping and subspecification.

We further tested whether *alcama* and *wnt11r* function downstream of *tbx1* by injecting *wnt11r* and *alcama* RNA into *tbx1*$^{-/-}$ mutants at the 1-cell stage. Injected mutants were assessed for rescue of heart looping (*cmlc2* ISH, Fig. 2.9B) and subspecification (*notch1b* ISH, Fig. 2.9E) at 52 hpf. *tbx1* RNA was injected as a positive control for rescue. Injection of either *wnt11r* RNA or *alcama* RNA increases the angle between the ventricular and atrial axes to nearly WT levels (18^{o} in RNA injected *tbx1*$^{-/-}$ mutants versus 9^{o} in uninjected *tbx1*$^{-/-}$ mutants and 23^{o} in WT) (Fig. 2.9C). Similarly, injection of either RNA decreased the percentage of larvae with absent *notch1b* staining (Fig. 2.9F). Partial rescue by RNA injection substantiates our model whereby *tbx1*

regulates *wnt11r*, *wnt11r* regulates *alcama*, which in turn regulates heart looping and subspecification (Fig. 2.9G).

2.6 Discussion

2.6.1 *tbx1*$^{-/-}$ mutants have defects in heart morphology and differentiation

Tbx1 has been identified as the gene responsible for causing DGS. However, the cardiac defects in the zebrafish *tbx1*$^{-/-}$ mutant have not been characterized so far. Using the *tbx1*$^{-/-}$ mutant, we have demonstrated that *tbx1* is required for normal heart development, as has been demonstrated in mice. Though *tbx1* is expressed in cardiac mesodermal progenitors at 14 somites from the commitment stage, cardiogenesis proceeds normally in *tbx1*$^{-/-}$ mutants until the onset of looping. This observation is consistent with mouse data, suggesting that *tbx1* is not required at the very early stages of heart development. Hence we conclude that *tbx1* is required for differentiation of cardiomyocytes, rather than for their commitment or specification.

Defective heart looping in *tbx1*$^{-/-}$ mutants is associated with other morphological abnormalities, including a wider and shorter heart with a shortened and undifferentiated BA. *tbx1*$^{-/-}$ mutant hearts also display weaker ventricular contractions and slower heart rate. At 33 hpf, the onset of jogging, the number of cardiomyocytes is the same in WT and *tbx1*$^{-/-}$ mutants indicating that proliferation and expansion of cardiomyocytes occurs normally until this stage. However, proliferation is decreased in the mutants at this stage causing a reduction in the number of cardiomyocytes by 48 hpf. While *tbx1* has been shown to regulate cell proliferation in mouse SHF (Guo et al., 2011; Xu et al., 2004;

Zhang et al., 2006), we are the first to demonstrate its role in regulating cell proliferation in PHF. Similarly, cardiomyocytes assume a different shape during heart development, and this contributes to looping. In *tbx1*$^{-/-}$ mutants, the cells in the outer curvature fail to assume elongated morphology, remaining small and rounded, similar to cells in the linear heart tube. These data indicate that *tbx1* is required for induction of morphological, proliferative and shape changes that contribute to heart looping.

Other zebrafish mutants/morphants with looping defects share the observed defect in cell proliferation and shape (Auman et al., 2007; Qu et al., 2008; Ribeiro et al., 2007). Failure of the cardiomyocytes to change shape taken together with reduction in cell number may contribute to looping defects by changing cell-cell interaction behavior. Indeed, cross-sections of *tbx1*$^{-/-}$ mutant hearts reveal an increase in extracellular spaces compared to WT siblings. This observation is important, as increased extracellular spaces have been observed in *wnt11r* and *alcama* morphants in *Xenopus* (Garriock et al., 2005; Gessert et al., 2008). These extracellular spaces might lead to altered cell polarity or might be causing the observed lack of change in cell shape or lack of differentiation or *vice versa*. Alternatively, the lack of looping might be causing the defect in cell proliferation and shape.

tbx1$^{-/-}$ mutants have defects in subspecification of the various heart regions. ISH stainings for *cmcl2*, *vmhc* and *amhc*, and antibody stainings for S46 and MF20 are normal in *tbx1*$^{-/-}$ mutants, indicating that atrial and ventricular fates are assigned properly in the *tbx1*$^{-/-}$ mutant. However, *bmp4*, *versican* and *notch1b* are down-regulated and *anf* is mis-expressed in the *tbx1*$^{-/-}$ mutants, indicating that cardiomyocytes fail to differentiate into the specific regions of the heart such as the OFT. Absent expression of *bmp4*, *versican*

and *notch1b* in *tbx1*$^{-/-}$ mutants is in striking contrast to other looping mutants, where these markers fail to get localized to their respective domains (Auman et al., 2007; Qu et al., 2008; Ribeiro et al., 2007; Tu et al., 2009). Hence we propose that *tbx1* has distinct functions from other genes involved in heart morphology, such as *tbx2a*, and *nkx2.5*. An unresolved question is whether subspecification of the heart regions causes looping or vice versa.

T-box genes generally act in combination or in the same pathway (Ryan and Chin, 2003; Smith, 1999). The presence of heart looping defects in multiple morphants of T-box genes such as *tbx5* and *tbx20* suggests that *tbx1* might function in conjunction with other T-box genes. While our ISH analysis does not support the possibility of these genes functioning downstream of *tbx1*, it is possible that they act combinatorially, in parallel or upstream of *tbx1*. Future analysis of *wnt11r* and *alcama* expression in *tbx* gene depleted embryos will help to elucidate *tbx* gene interations during heart development.

2.6.2 *tbx1* regulates differentiation of the SHF and BA

DGS patients and *Tbx1-/-* mice have OFT defects such as persistent truncus arteriosus. Moreover, *Tbx1* is expressed in the SHF and regulates SHF contribution to the OFT (Xu et al., 2004). In accordance with mouse data, our data suggest that *tbx1*$^{-/-}$ mutants have a smaller BA. In addition, absent *eln2* expression and DAF-2DA staining indicates that smooth muscle in the BA is undifferentiated. At 14 somites, Isl1-positive SHF cells seem unaffected in *tbx1*$^{-/-}$ mutants, suggesting that SHF is formed properly in *tbx1*$^{-/-}$ mutants, but then fails to differentiate into smooth muscle of the BA. While our investigation of the BA defect in *tbx1*$^{-/-}$ mutants was ongoing, another study identified

that absence of *tbx1* led to reduced incorporation of SHF-derived arterial pole cells into the BA (Hami et al., 2011). These results are in agreement with our data, indicating that *tbx1* is not required for formation of SHF cells but is required for their incorporation into the BA and subsequent differentiation of smooth muscle cells.

2.6.3 *wnt11r* functions downstream of *tbx1*

Though *Wnt11* signaling has been shown to be important for specification of cardiac fate and *Wnt11-/-* mutants have OFT defects, *Tbx1* and *Wnt11* signaling has not been linked as yet (Eisenberg and Eisenberg, 1999; Pandur et al., 2002; Zhou et al., 2007). Unlike mouse and chicken embryos, *Xenopus* and zebrafish embryos do not express *wnt11* in the developing heart (Garriock et al., 2005). *wnt11r*, a second *wnt11* gene in *Xenopus* and zebrafish, with high homology to human and chicken *Wnt11*, mediates noncanonical *Wnt* signaling and is necessary for normal heart morphogenesis. In *Xenopus*, *wnt11r* starts to be expressed just prior to fusion of cardiac progenitors and subsequently continues to be expressed in the heart tissue. It was later discovered that *alcama* regulates cardiac looping and functions downstream of *wnt11r* in *Xenopus* (Gessert et al., 2008).

In spite of previous work in *Xenopus*, the role of *wnt11r* in zebrafish heart morphogenesis has not been previously characterized. We have shown that similarly to *Xenopus*, zebrafish *wnt11r* is first expressed at 21somites just prior to cardiac progenitor fusion and continues to be expressed as the heart develops. Our data show that *wnt11r* is down-regulated in *tbx1*$^{-/-}$ mutant hearts, and that *wnt11r* $^{-/-}$ mutants have similar looping and subspecification defects as observed in *tbx1*$^{-/-}$ mutants. Furthermore, our nonallelic

noncomplementation assay indicates that *tbx1* and *wnt11r* function in the same pathway. Moreover, knockdown of *alcama*, a gene demonstrated to be downstream of *wnt11r*, also presents with looping and subspecification defects. Importantly, we were able to rescue the looping and subspecification defects in *tbx1*$^{-/-}$ mutants by injection of *wnt11r* and/or *alcama* RNA. All these data lead us to our working model: *tbx1* regulates *wnt11r*, *wnt11r* regulates *alcama*, which in turn regulates heart looping and subspecification (Fig. 2.9G). We were unable to obtain complete rescue with *wnt11r* and *alcama* mRNA injections. This might indicate that *tbx1* regulates genes other than *wnt11r* and *alcama*. This interpretation is supported by the fact that *wnt11r* $^{-/-}$ mutants do not possess defects in BA, suggesting that *tbx1* regulates BA morphogenesis via an independent mechanism.

2.7 Conclusion

In summary, this study demonstrates that zebrafish *tbx1-/-* mutants have defects in heart looping and function. This is the first demonstration that *tbx1* regulates differentiation of cardiomyocytes derived from both the PHF and SHF. In addition, it is the first description implicating *tbx1*'s role in regulating PHF cardiomyocyte proliferation and shape. Importantly, we have identified *wnt11r* and *alcama* as a novel members of the *tbx1* pathway. We show for the first time that *wnt11r*$^{-/-}$ mutants and *alcama* morphants have heart looping and differentiation defects similar to *tbx1*$^{-/-}$ mutants. Moreover, these defects can be rescued by overexpression of *wnt11r* and/or *alcama* in *tbx1*$^{-/-}$ mutants, suggesting that they function downstream of *tbx1*. Our data supports our model, whereby *tbx1* regulates heart looping and differentiation via *wnt11r* and *alcama*.

2.8 Acknowledgments

The authors wish to thank Sarah Hutchinson and Joseph Yost for intellectual contributions. We wish to thank Tatjana Piotrowski for *vgo*^{tm208} (*tbx1*$^{-/-}$) mutant zebrafish and Joseph Yost for *Tg(cmlc2:EGFP)* fish. The wnt11r$^{fh224/+}$ mutant line was obtained from the Moens lab TILLING project, which is supported by NIH grant HG002995. Several plasmid for ISH probes were kind gifts from Sheila Samson and Josh Wythe. This work was supported in part by R01 HD047863-01 and by the Huntsman Cancer Foundation. Huntsman Cancer Institute core facilities, supported by grant P30 CA042014, also facilitated this work.

Figure 2.1. Heart shape and looping defects in *tbx1*$^{-/-}$ larvae.
(A) *cmlc2* ISH in *tbx1*$^{-/-}$ mutants and WT siblings at various stages. Cardiac progenitors are specified and fuse to form the linear heart tube by 24hpf. By 30-36 hpf jogging of the ventricle towards the midline is delayed in *tbx1*$^{-/-}$ larvae. By 48hpf the heart has finished looping in WT forming an acute angle between the axes (green lines), but in *tbx1*$^{-/-}$ mutants the axes are nearly parallel. White arrows indicate the AVC; a, atrium; v, ventricle. The plot in B shows the decreased angles between the ventricular and atrial axes in *tbx1*$^{-/-}$ mutants. The plot in C shows the decreased lengths of the ventricle and atrium in *tbx1*$^{-/-}$ mutants. The plots in D and E show the widths of the ventricles at 48 hpf and atriums at 72 hpf in *tbx1*$^{-/-}$ mutants and WT siblings in the expanded and contracted states. WT siblings are represented in green and *tbx1*$^{-/-}$ mutants in pink. N depicts the total number of larvae represented in the plot. Scale bar: 50 μm.

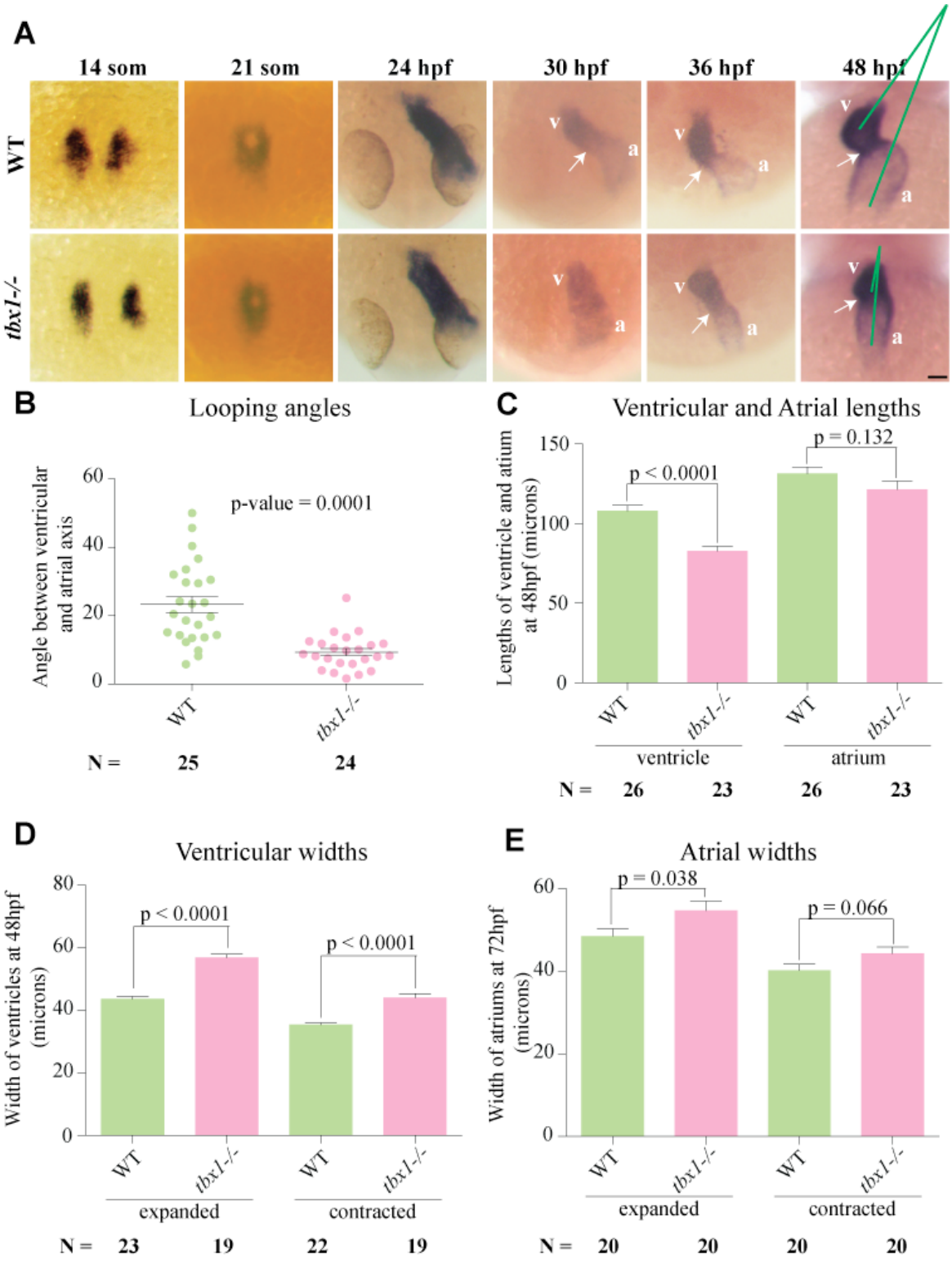
A
14 som
21 som
24 hpf
30 hpf
36 hpf
48 hpf
WT
tbx1-/-
v
a
B
Looping angles
Angle between ventricular and atrial axis
p-value = 0.0001
WT
tbx1-/-
N = 25 24
C
Ventricular and Atrial lengths
Lengths of ventricle and atium at 48hpf (microns)
p < 0.0001
p = 0.132
ventricle
atrium
N = 26 23 26 23
D
Ventricular widths
Width of ventricles at 48hpf (microns)
p < 0.0001
p < 0.0001
expanded
contracted
N = 23 19 22 19
E
Atrial widths
Width of atriums at 72hpf (microns)
p = 0.038
p = 0.066
expanded
contracted
N = 20 20 20 20

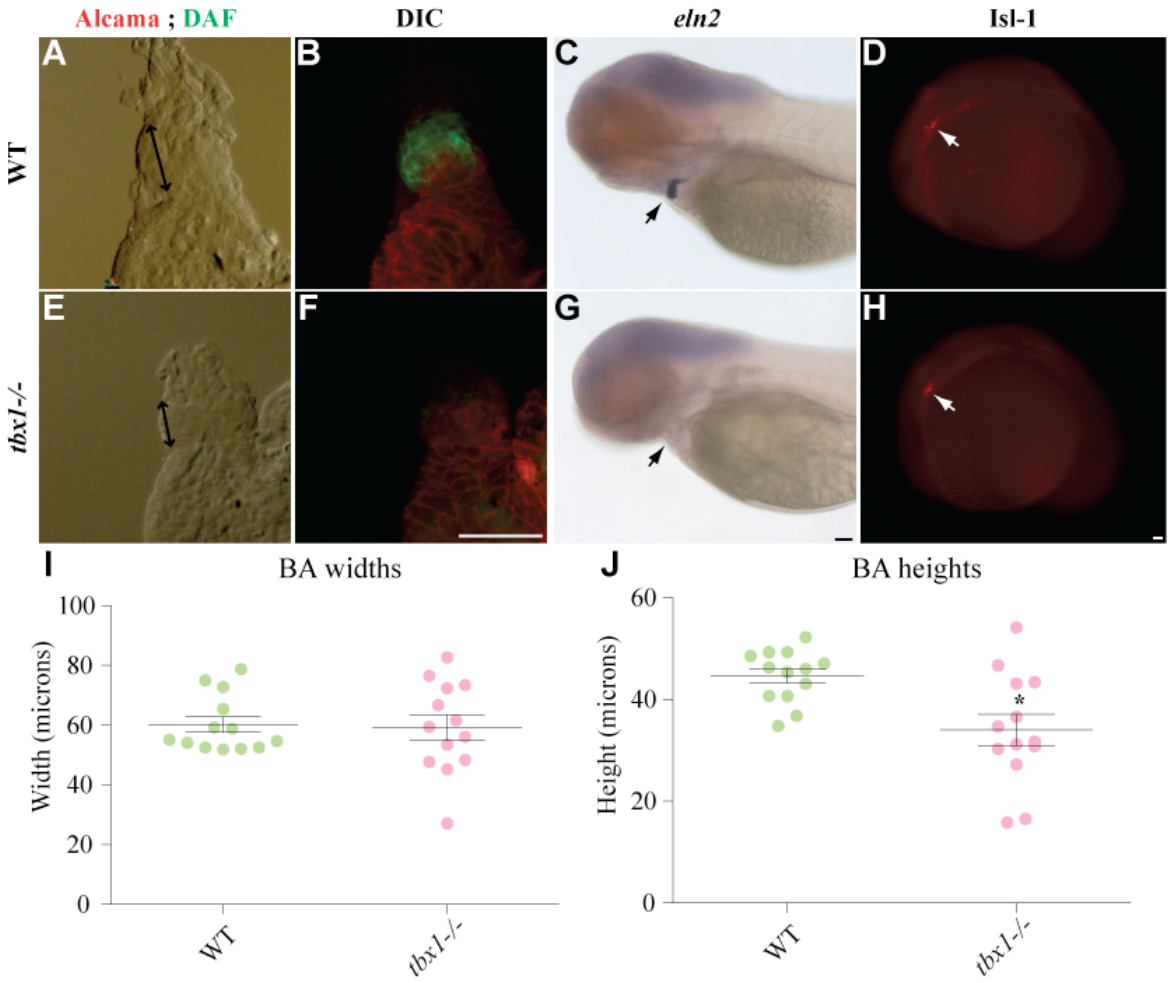

Figure 2.2. Bulbous arteriosus defects in *tbx1*$^{-/-}$ larvae.
Dissected hearts from 72 hpf larvae showing the BA region (A, E) and the corresponding image showing staining for Alcama antibody (red) and DAF-2DA (green)(B, F). (C, G) *tbx1*$^{-/-}$ mutants at the same stage have absent *eln2* expression. (D, H) 14 somite embyos stained with Isl-1 antibody indicate the presence of secondary heart field progenitors in *tbx1*$^{-/-}$ mutants. Black arrows indicate the BA and white arrows the secondary heart field progenitors. The plot in I shows that the BA is unobstructed, but its length is reduced in *tbx1*$^{-/-}$ mutants (J); * p-value = 0.0045. N = 13 for all measurements. Bidirectional arrowheads (B, F) show the length of the BA. Scale bars: 25 μm.

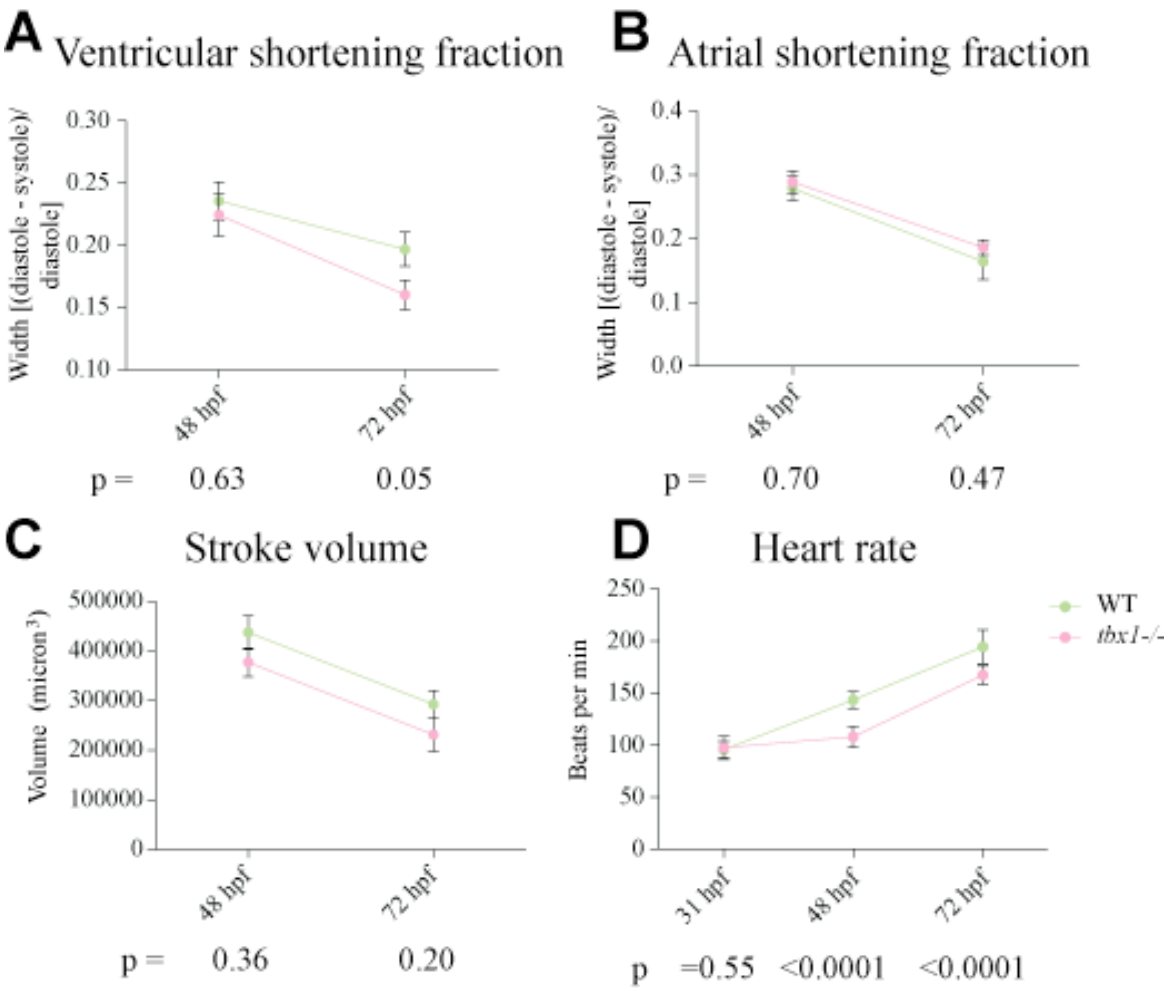

Figure 2.3. *tbx1*$^{-/-}$ larvae have defects in heart performance.
The plot in A shows the defect in ventricular contractility measured as shortening fraction [(width at diastole – width at systole)/ width at diastole]. The plot in B shows that atrium contractility is unaffected in *tbx1*$^{-/-}$ larvae. The stroke volume (ventricular volume [diastole – systole]) plotted in C is unaffected in *tbx1*$^{-/-}$ larvae, though the heart rate is decreased, shown in D. N = 19 in all experiments. WT siblings are represented in green and *tbx1*$^{-/-}$ mutants in pink. p-values are reported under each measurement.

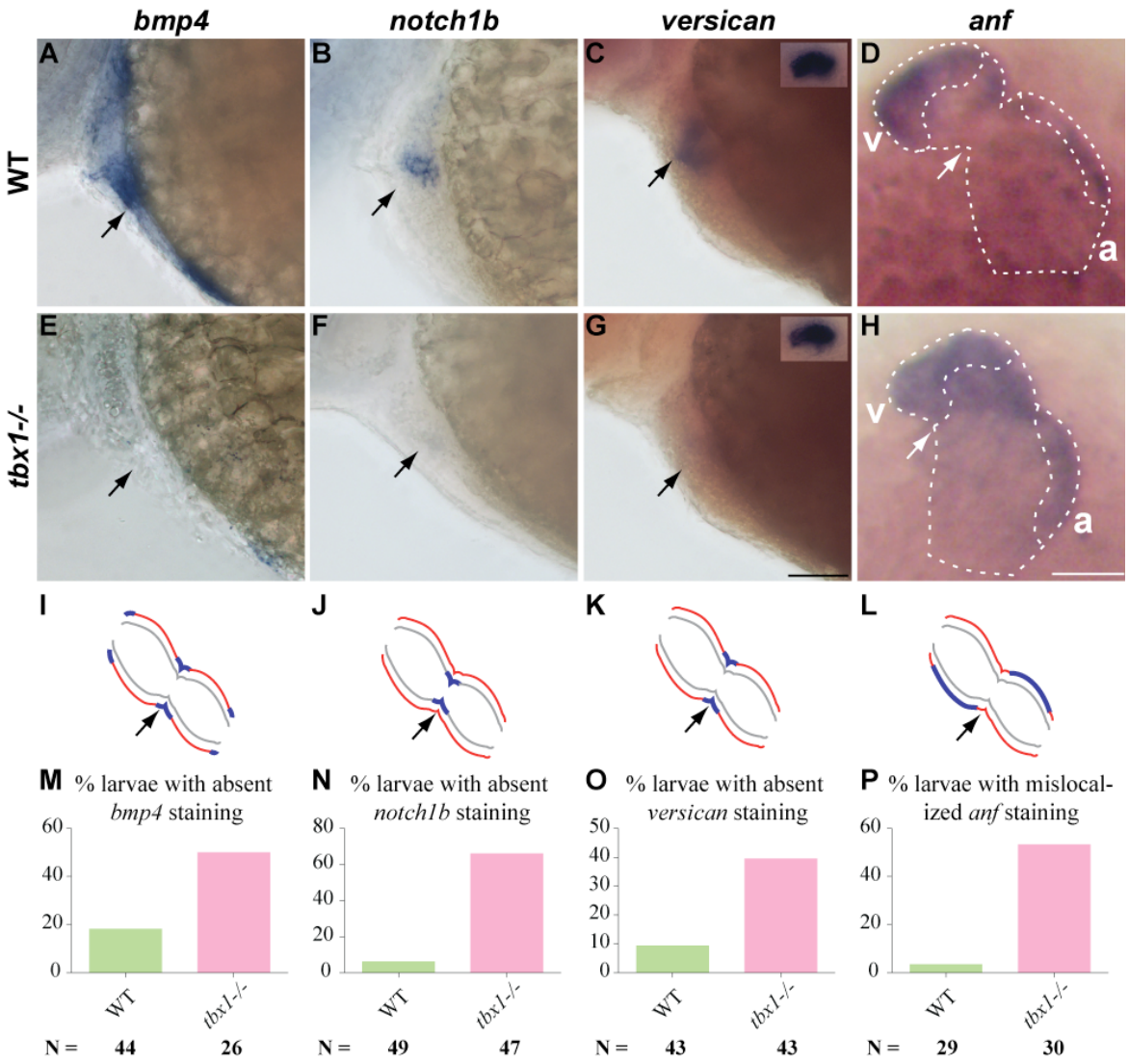

Figure 2.4. Subspecification defects in *tbx1*$^{-/-}$ mutants.
48 hpf larvae stained for region-specific markers (A-H) and their schematic representation (I-L). Red lines indicate myocardium, grey lines indicate endocardium and blue lines indicate gene expression. *bmp4* (OFT, AVC and IFT), *notch1b* (AVC endocardium) and *versican* (AVC myocardium) expression is downregulated in *tbx1*$^{-/-}$ mutants (E-G) as compared to WT siblings (A-C). The insets in C and G show *versican* expression in the ear as a control for ISH. *anf* expression is localized to the outer chambers of the myocardium in WT (D), but is broadly expressed in the ventricle and atrium in *tbx1*$^{-/-}$ mutants (H). Arrows point to the AVC in all panels; v, ventricle; a, atrium. The plots in M-P show the penetrance of the phenotype as percentage larvae with absent/mislocalized expression of the respective gene. N depicts the total number of larvae represented in the plot. Scale bars: 50 μm.

Figure 2.5. Proliferation and Cell shape defects in *tbx1*$^{-/-}$ mutants.
(A, B) Confocal projections of hearts from *cmlc2:gfp* (all heart cells are green) larvae at 33hpf stained with phospho-histone 3 antibody (proliferating cells are pink). The heart is wider and shorter in the mutant (B) with fewer numbers of proliferating cells (B). C, Plot showing that the total number of cells is equal in WT and *tbx1*$^{-/-}$ mutants at 33 hpf (C), but is decreased at 48 hpf. The decrease in proliferating cell number is at 33hpf is quantified in Plot D. N is the total number of larvae represented in the plots. (E, F) Confocal projections of hearts from *cmlc2:gfp* larvae at 48 hpf stained with Alcama antibody (red) to demarcate cell boundaries. Cells in the outer chamber (white) are elongated and their long axes point towards the AVC in WT (E). However, cells in the outer chamber of *tbx1*$^{-/-}$ mutants continue to be small and rounded (F), much like the cells in the inner chamber (shown in yellow). The plot in G shows that cells in the outer chamber of *tbx1*$^{-/-}$ mutants are rounder (circularity tending towards 1) as compared to WT. The plot in H shows that the cell shape is unchanged in the inner chamber of *tbx1*$^{-/-}$ mutants. Each bar in plots G and H represents data from 70 cells collected from 7 larvae. Arrows point to the AVC; v, ventricle; a, atrium. Scale bars: 25 μm.

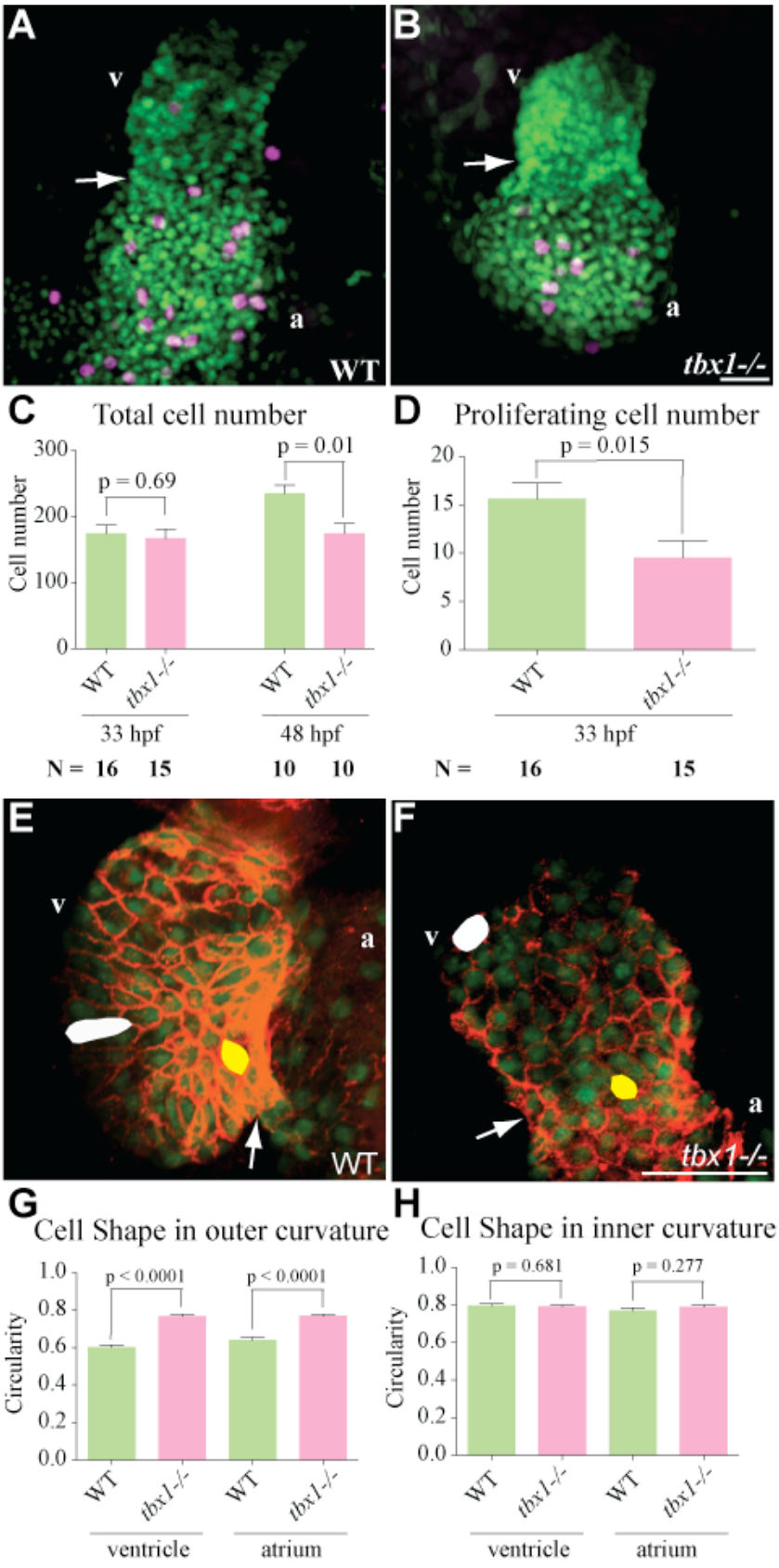
A
v
a
WT
B
v
a
tbx1-/-
C
Total cell number
Cell number
300
200
100
0
p = 0.69
p = 0.01
WT
tbx1-/-
WT
tbx1-/-
33 hpf
48 hpf
N = 16 15 10 10
D
Proliferating cell number
Cell number
20
15
10
5
0
p = 0.015
WT
tbx1-/-
33 hpf
N = 16 15
E
v
a
WT
F
v
a
tbx1-/-
G
Cell Shape in outer curvature
Circularity
1.0
0.8
0.6
0.4
0.2
0.0
p < 0.0001
p < 0.0001
WT
tbx1-/-
WT
tbx1-/-
ventricle
atrium
H
Cell Shape in inner curvature
Circularity
1.0
0.8
0.6
0.4
0.2
0.0
p = 0.681
p = 0.277
WT
tbx1-/-
WT
tbx1-/-
ventricle
atrium

Figure 2.6. Microarray of *tbx1*$^{-/-}$ mutant hearts reveals new tbx1 targets.
(A) Gene ontology results for a microarray of *tbx1*$^{-/-}$ mutant hearts versus WT sibling hearts. (B) Results of the microarray for genes implicated in the *tbx1* pathway from previous literature. *lox* and *pdpk* were chosen by us as new candidate genes from the microarray. (C) Lateral views of ISH analysis for *lox* and *pdpk* at 48 hpf, showing they are downregulated in hearts of *tbx1*$^{-/-}$ mutants. Arrows point to the AVC. Scale bar: 50 μm.

A

Activity	z-score upregulated	z-score downregulated
Binding	-0.43	1.91
Catalytic	-1.04	2.24
Transcription regulator	5.22	1.05
Molecular transducer	-0.02	0.92
Nucleic acid binding	2.47	1.05
Transporter	-1.18	1.56
Structural molecule	0.47	-0.46

B

Gene	Fold downregulated
pitx2	1.15
fgf8	1.22
fgf10	1.46
six1	1.44
eya1	1.51
lox	3.54
pdpk	3.64

C

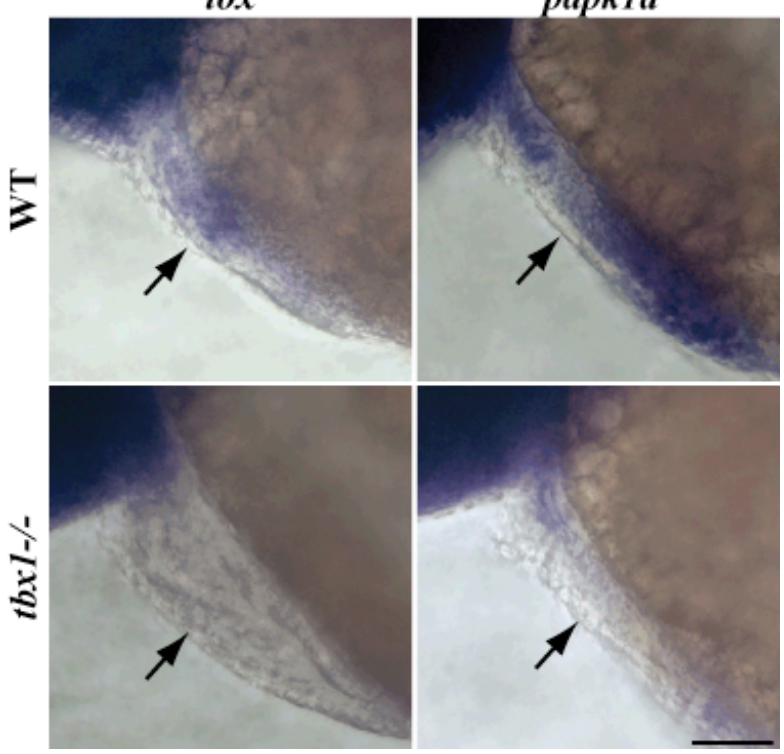

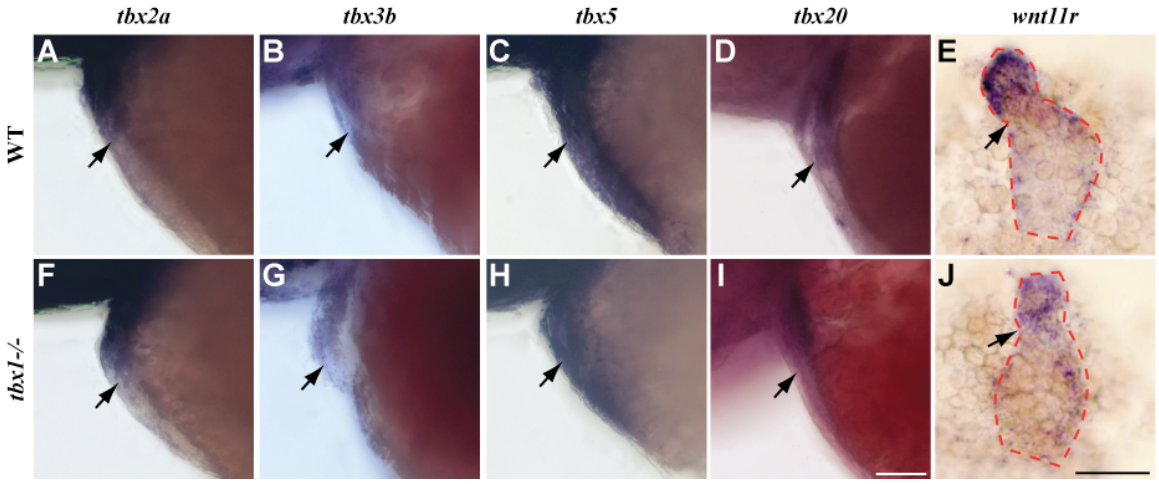

Figure 2.7. Candidate gene analysis for *tbx1*$^{-/-}$ mutants.
(A-D and F-I), Whole mount lateral views of 48 hpf larvae stained for known genes that affect heart looping. Expression of *tbx2a* (A, F), *tbx3b* (B, G), *tbx5* (C, H) and *tbx20* (D, I) was unaffected between WT siblings and *tbx1*$^{-/-}$ mutants. Dissected hearts from 48 hpf larvae show down-regulated expression of *wnt11r* in the mutant (J) versus WT (E). The heart boundary is shown by the red dotted line. Arrows point to the AVC. Scale bars: 50 μm.

Figure 2.8. Looping and subspecification defects in *wnt11r* $^{-/-}$ mutants.
A, *cmlc2* ISH showing the looping defect in *wnt11r* $^{-/-}$ mutants at 48 hpf. The plot in B shows the decreased angles between the ventricular and atrial axes in *wnt11r* $^{-/-}$ mutants. C shows defect in subspecification of heart regions in *wnt11r* $^{-/-}$ mutants similar to those seen in *tbx1*$^{-/-}$ mutants. The plots in D and E show the increased penetrance of looping and subspecification defects in double heterozygotes as compared to single heterozygotes of *tbx1* and *wnt11r*. Arrows point to the AVC; v, ventricle; a, atrium. Scale bars: 50 μm. N depicts the total number of larvae from 3 experiments.

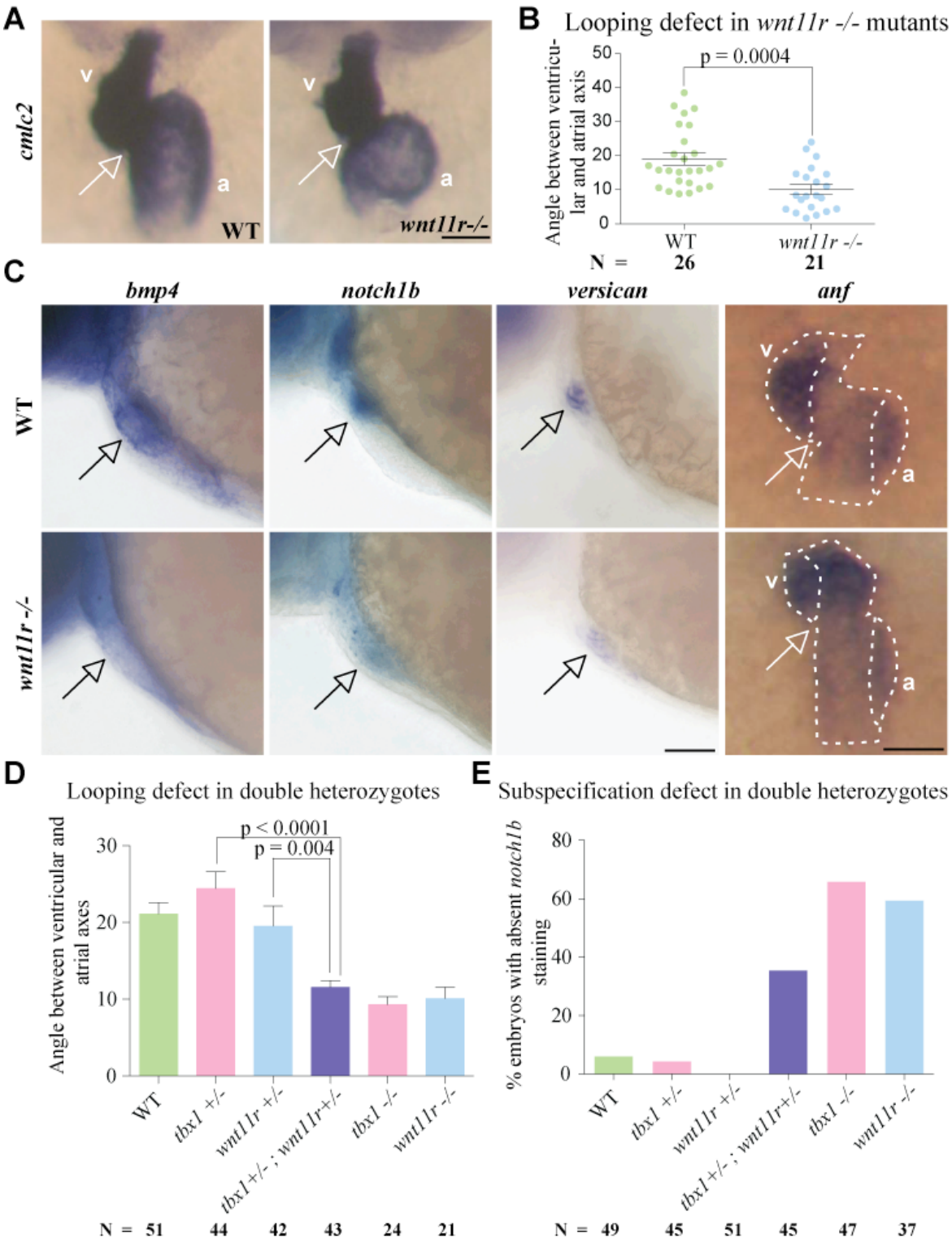
A
cmlc2
v
a
WT
wnt11r-/-
B
Looping defect in wnt11r -/- mutants
Angle between ventricular and atrial axis
p = 0.0004
WT
wnt11r -/-
N = 26 21
C
bmp4
notch1b
versican
anf
WT
wnt11r -/-
D
Looping defect in double heterozygotes
Angle between ventricular and atrial axes
p < 0.0001
p = 0.004
WT
tbx1 +/-
wnt11r +/-
tbx1+/- ; wnt11r+/-
tbx1 -/-
wnt11r -/-
N = 51 44 42 43 24 21
E
Subspecification defect in double heterozygotes
% embryos with absent notch1b staining
N = 49 45 51 45 47 37

Figure 2.9. *tbx1* functions through *wnt11r* to regulate heart looping and subspecification. ISH for *cmlc2* (A, B) and *notch1b* (D, E) showing rescue of looping (B) and subspecification defect (E) at 48hpf after injection of 26 pf *wnt11r* RNA at the 1-cell stage. Plots in C and D quantify the rescue of looping and subspecification defect after the indicated injections. WT siblings are represented in green and uninjected *tbx1*$^{-/-}$ mutants in pink, with injected mutants in dark pink or red. Scale bars: 50 μm. N depicts the total number of larvae from 3 experiments. The schematic in G shows our working model, where *tbx1* regulates *wnt11r*; *wnt11r* regulates *alcama*, which in turn regulates heart looping and subspecification. *tbx1* regulates migration/differentiation of SHF cells by an independent mechanism.

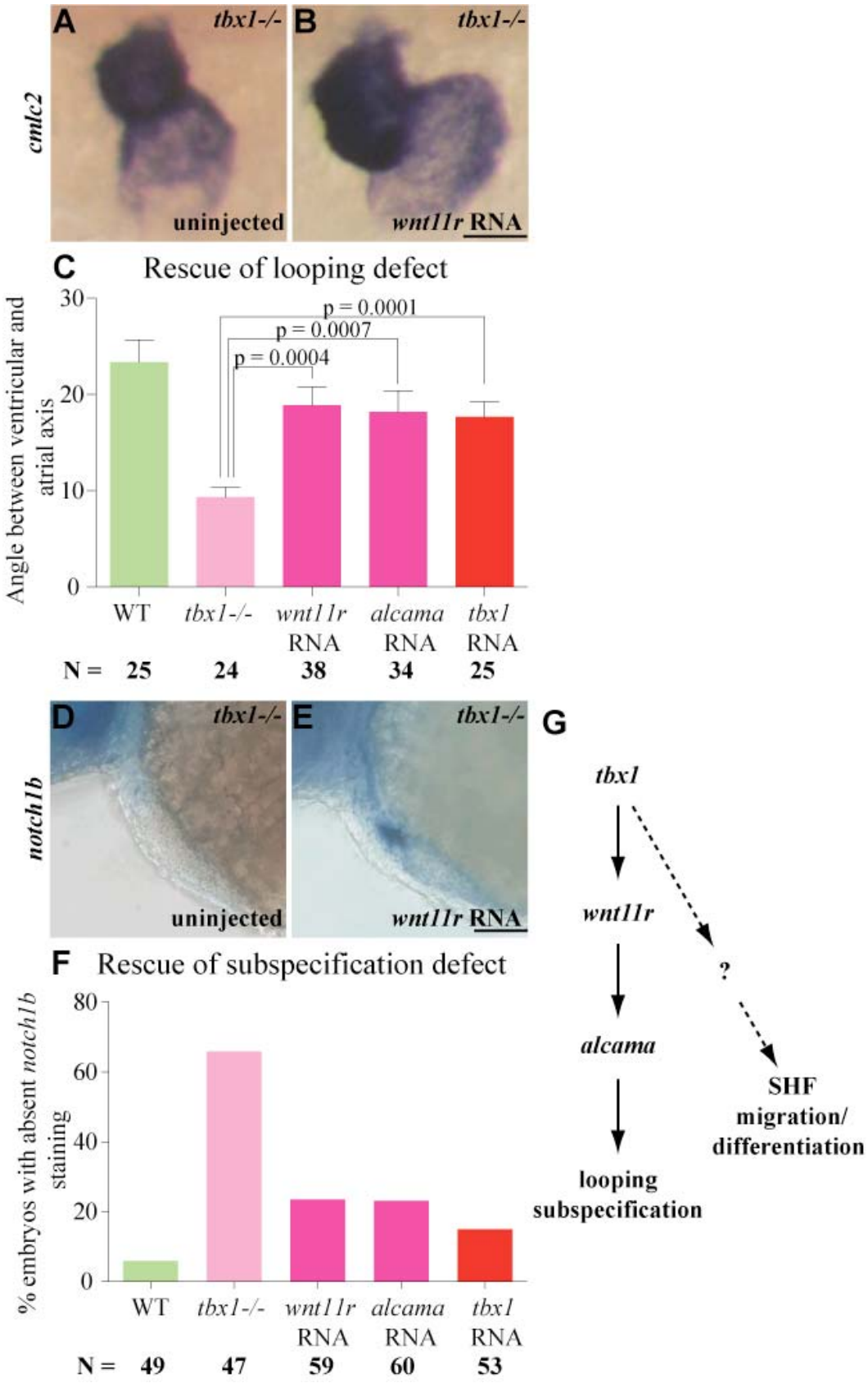
A
tbx1-/-
uninjected
cmlc2
B
tbx1-/-
wnt11r RNA
C
Rescue of looping defect
Angle between ventricular and atrial axis
30
20
10
0
p = 0.0001
p = 0.0007
p = 0.0004
WT
tbx1-/-
wnt11r RNA
alcama RNA
tbx1 RNA
N = 25 24 38 34 25
D
tbx1-/-
uninjected
notch1b
E
tbx1-/-
wnt11r RNA
F
Rescue of subspecification defect
% embryos with absent notch1b staining
80
60
40
20
0
WT
tbx1-/-
wnt11r RNA
alcama RNA
tbx1 RNA
N = 49 47 59 60 53
G
tbx1
wnt11r
alcama
?
SHF migration/ differentiation
looping subspecification

Figure 2S1. *tbx1* expression and phenotype of *tbx1*$^{-/-}$ 1arvae.
ISH for *tbx1* in WT larvae showing expression in the lateral plate mesoderm (14 somites, A), the fusing heart fields (21 somites, B), linear heart tube (24 hpf, C) and the looped heart (48 hpf, D). (E,F) 5 micron sections of the hearts from 72 hpf larvae, showing absence of looping, wider ventricle and atrium and thinner heart walls in *tbx1*$^{-/-}$ mutant (F) as compared to WT sibling (E). The plot in G shows that the ventricle continues to be wider in *tbx1*$^{-/-}$ larvae at 72 hpf, while the atrium is unaffected at 48 hpf (H) and becomes wider only at 72 hpf. Scale bars: 50 μm.

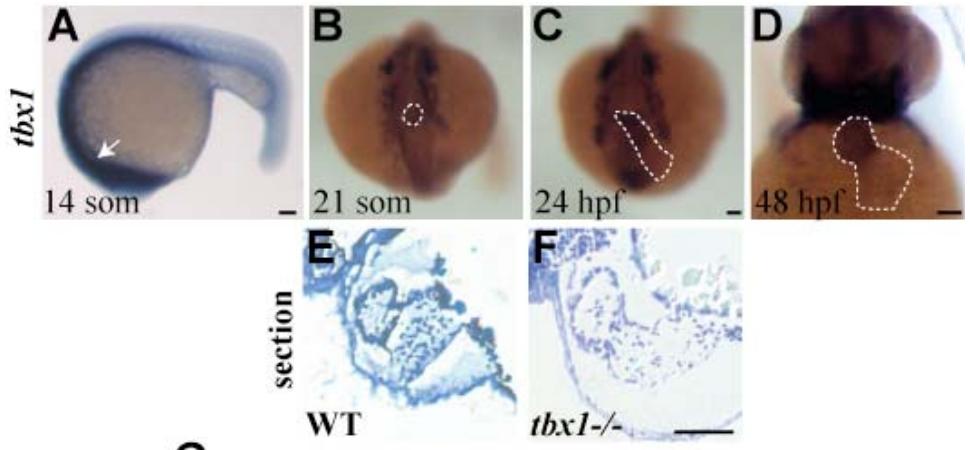
A
B
C
D
tbx1
14 som
21 som
24 hpf
48 hpf
E
F
section
WT
tbx1-/-

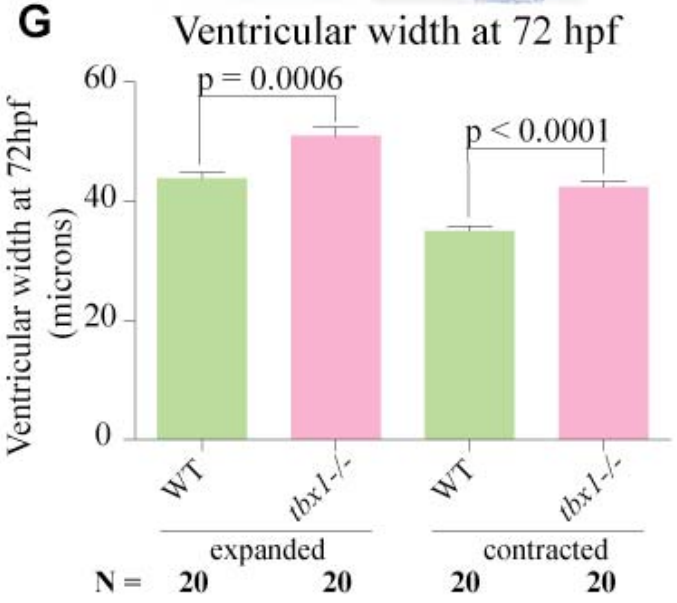
G
Ventricular width at 72 hpf
Ventricular width at 72hpf (microns)
60
40
20
0
p = 0.0006
p < 0.0001
WT
tbx1-/-
WT
tbx1-/-
expanded
contracted
N = 20 20 20 20

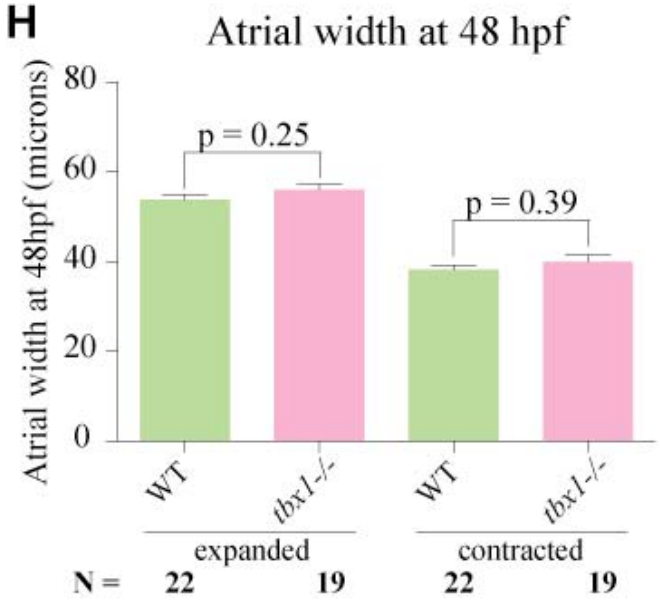
H
Atrial width at 48 hpf
Atrial width at 48hpf (microns)
80
60
40
20
0
p = 0.25
p = 0.39
WT
tbx1-/-
WT
tbx1-/-
expanded
contracted
N = 22 19 22 19

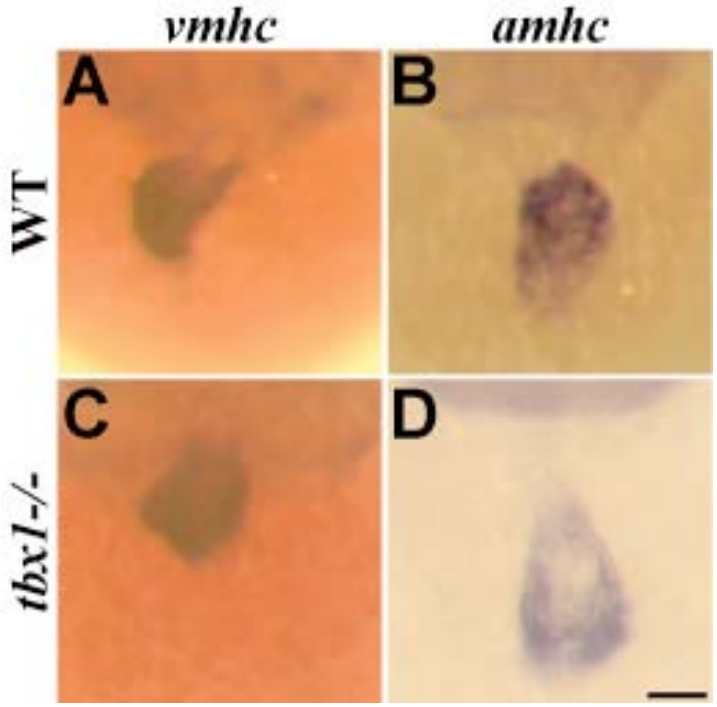

Figure 2S2. Chambers are specified correctly in *tbx1*$^{-/-}$ mutants.
ISH analysis at 48 hpf for *vmhc* (A, C) and *amhc* (B, D) shows that the chambers are correctly specified in *tbx1*$^{-/-}$mutants.

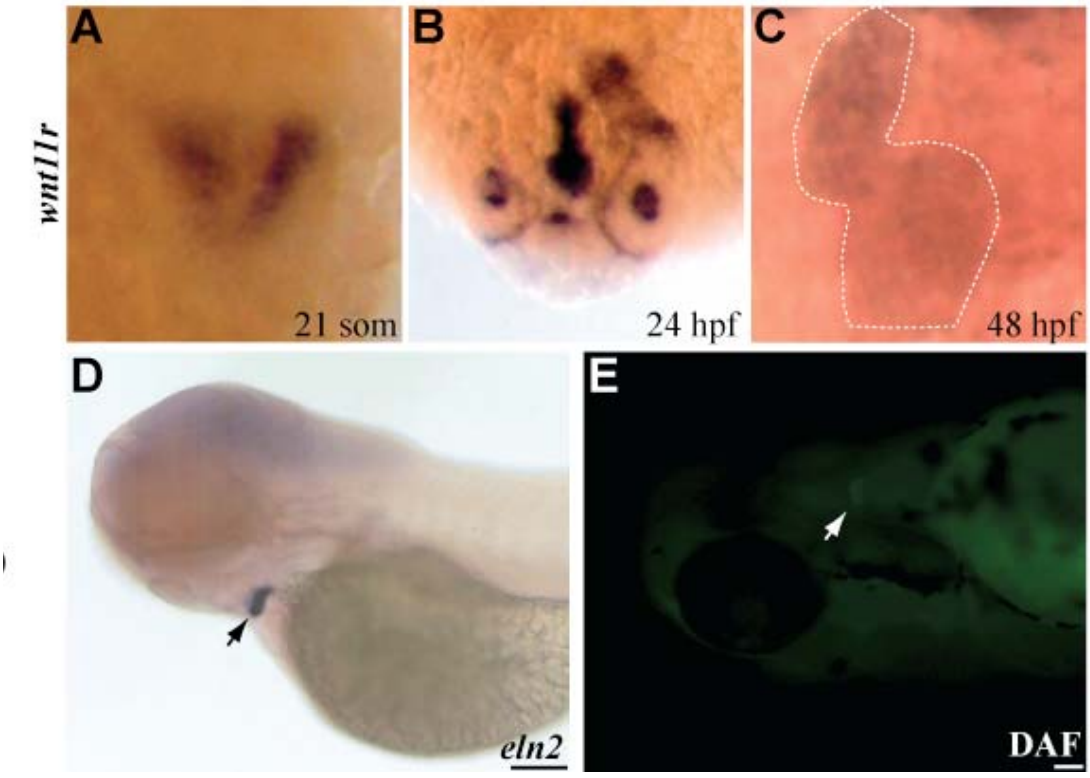

Figure 2S3. *wnt11r* expression and unaffected bulbous arteriosus in *wnt11r* $^{-/-}$ mutants. (A-C) *wnt11r* ISH showing expression in the fusing heart fields (21 somites, A), linear heart tube (24 hpf, B) and fully looped heart (48 hpf, C). (D,E) Lateral and ventral views of 72 hpf larva showing normal *eln2* and DAF-2DA staining respectively in *wnt11r* $^{-/-}$ mutants.

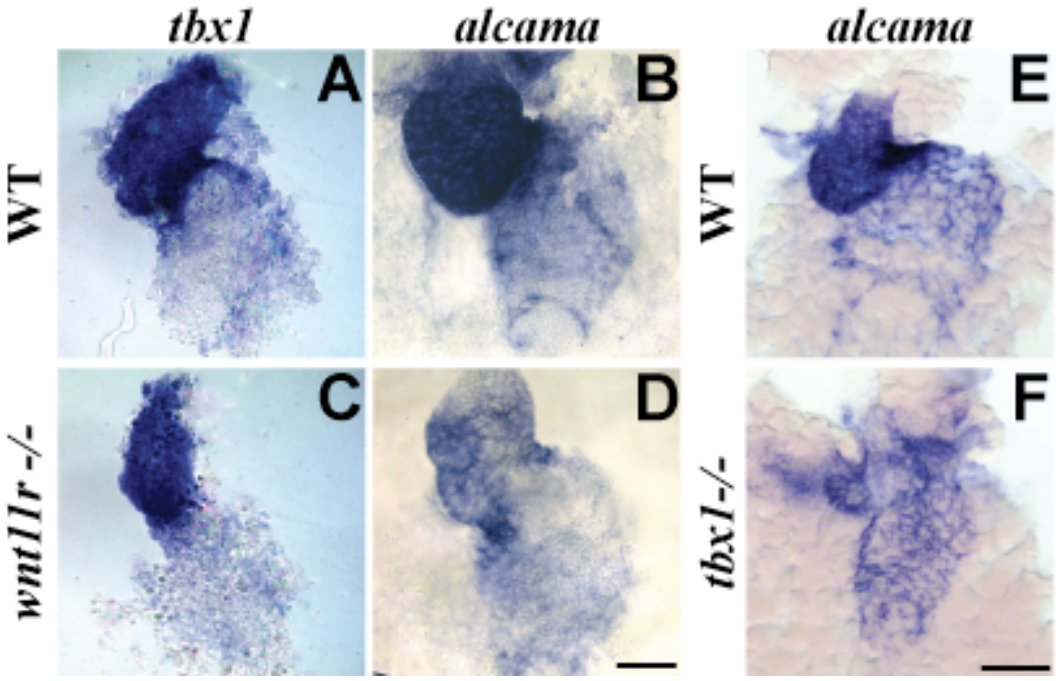

Figure 2S4. *tbx1* regulates *alcama* levels via *wnt11r*.
(A-F) ISH analysis on 48 hpf larvae showing that *wnt11r* $^{-/-}$ mutants have unaffected *tbx1* expression (C) but downregulated *alcama* expression (D) when compared to WT siblings (A, B). In addition *alcama* is downregulated in *tbx1*$^{-/-}$ mutants (F).

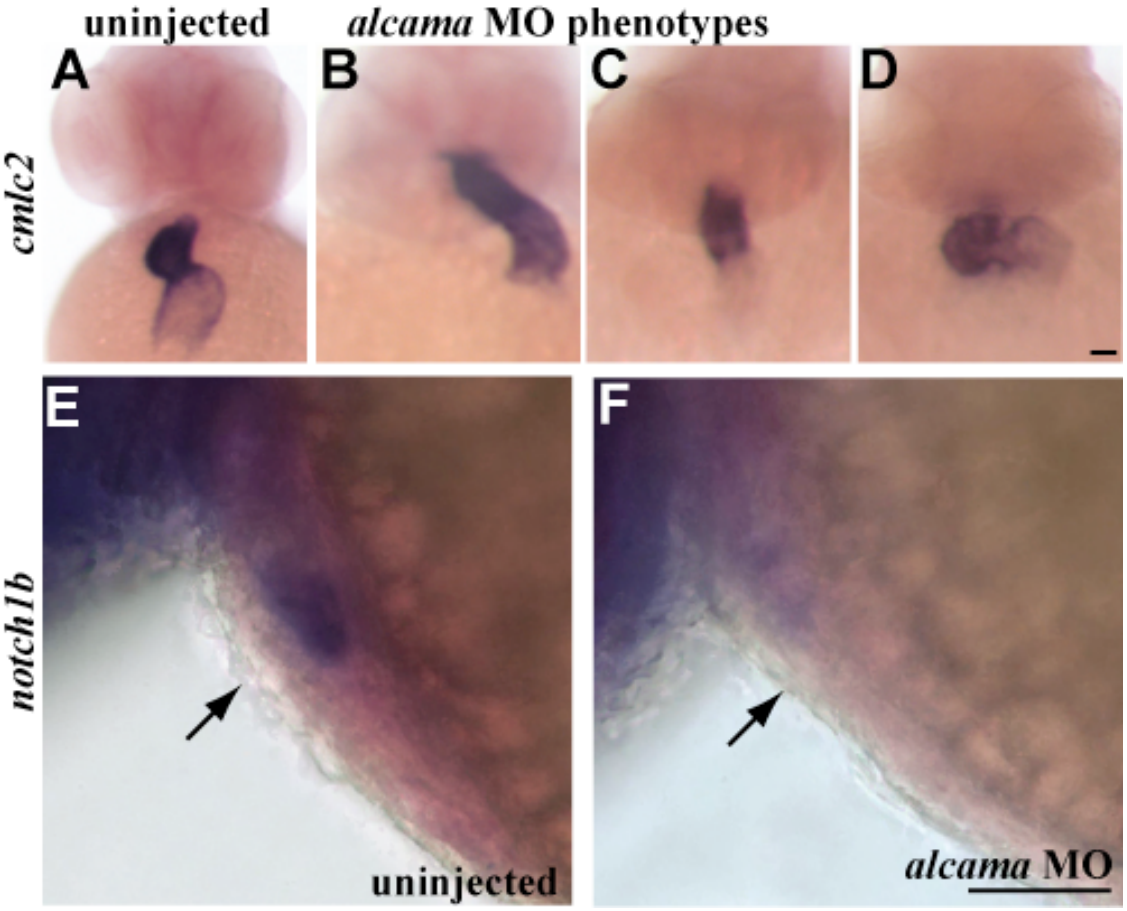

Figure 2S5. *alcama* morphants have heart looping and subspecification defects. *cmlc2* ISH on 48hpf larvae showing the various looping phenotypes observed in alcama morphants (B-D) and proper looping in an uninjected larva (A). *notch1b* is expressed in the AVC endocardium in an uninjected larva at 48 hpf (E), but is downregulated in alcama morphant (F). Arrows point to the AVC. Scale bars: 50 μm.

2.9 References

Arnold, J.S., Werling, U., Braunstein, E.M., Liao, J., Nowotschin, S., Edelmann, W., Hebert, J.M., Morrow, B.E., 2006. Inactivation of Tbx1 in the pharyngeal endoderm results in 22q11DS malformations. Development (Cambridge, England) 133, 977-987.

Auman, H.J., Coleman, H., Riley, H.E., Olale, F., Tsai, H.J., Yelon, D., 2007. Functional modulation of cardiac form through regionally confined cell shape changes. PLoS Biol 5, e53.

Banerjee, S., Gordon, L., Berti, C., Donn, T., Moens, C.B., Burden, S.J., Granato, M., 2011. A novel role for unplugged/MuSK and noncanonical Wnt signaling during segmental neural crest cell migration. , Development 138(15):3287-96.

Beis, D., Bartman, T., Jin, S.W., Scott, I.C., D'Amico, L.A., Ober, E.A., Verkade, H., Frantsve, J., Field, H.A., Wehman, A., Baier, H., Tallafuss, A., Bally-Cuif, L., Chen, J.N., Stainier, D.Y., Jungblut, B., 2005. Genetic and cellular analyses of zebrafish atrioventricular cushion and valve development. Development 132, 4193-4204.

Belema Bedada, F., Technau, A., Ebelt, H., Schulze, M., Braun, T., 2005. Activation of myogenic differentiation pathways in adult bone marrow-derived stem cells. Mol Cell Biol 25, 9509-9519.

Brade, T., Manner, J., Kuhl, M., 2006. The role of Wnt signalling in cardiac development and tissue remodelling in the mature heart. Cardiovasc Res 72, 198-209.

Brand, T., 2003. Heart development: molecular insights into cardiac specification and early morphogenesis. Dev Biol 258, 1-19.

Brown, D.D., Martz, S.N., Binder, O., Goetz, S.C., Price, B.M., Smith, J.C., Conlon, F.L., 2005. Tbx5 and Tbx20 act synergistically to control vertebrate heart morphogenesis. Development 132, 553-563.

Buckingham, M., Meilhac, S., Zaffran, S., 2005. Building the mammalian heart from two sources of myocardial cells. Nat Rev Genet 6, 826-835.

Chen, L., Fulcoli, F.G., Tang, S., Baldini, A., 2009. Tbx1 regulates proliferation and differentiation of multipotent heart progenitors. Circ Res 105, 842-851.

Chi, N.C., Shaw, R.M., De Val, S., Kang, G., Jan, L.Y., Black, B.L., Stainier, D.Y., 2008. Foxn4 directly regulates tbx2b expression and atrioventricular canal formation. Genes Dev 22, 734-739.

Choudhry, P., Joshi, D., Funke, B., Trede, N., 2010. Alcama mediates Edn1 signaling during zebrafish cartilage morphogenesis. Dev Biol 349, 483-493.

Eisenberg, C.A., Eisenberg, L.M., 1999. WNT11 promotes cardiac tissue formation of early mesoderm. Dev Dyn 216, 45-58.

Flaherty, M.P., Abdel-Latif, A., Li, Q., Hunt, G., Ranjan, S., Ou, Q., Tang, X.L., Johnson, R.K., Bolli, R., Dawn, B., 2008. Noncanonical Wnt11 signaling is sufficient to induce cardiomyogenic differentiation in unfractionated bone marrow mononuclear cells. Circulation 117, 2241-2252.

Fritsche, R., Schwerte, T., Pelster, B., 2000. Nitric oxide and vascular reactivity in developing zebrafish, Danio rerio. Am J Physiol Regul Integr Comp Physiol 279, R2200-2207.

Garriock, R.J., D'Agostino, S.L., Pilcher, K.C., Krieg, P.A., 2005. Wnt11-R, a protein closely related to mammalian Wnt11, is required for heart morphogenesis in Xenopus. Dev Biol 279, 179-192.

Garrity, D.M., Childs, S., Fishman, M.C., 2002. The heartstrings mutation in zebrafish causes heart/fin Tbx5 deficiency syndrome. Development 129, 4635-4645.

Gessert, S., Maurus, D., Brade, T., Walther, P., Pandur, P., Kuhl, M., 2008. DM-GRASP/ALCAM/CD166 is required for cardiac morphogenesis and maintenance of cardiac identity in first heart field derived cells. Dev Biol 321, 150-161.

Gong, W., Gottlieb, S., Collins, J., Blescia, A., Dietz, H., Goldmuntz, E., McDonald-McGinn, D.M., Zackai, E.H., Emanuel, B.S., Driscoll, D.A., Budarf, M.L., 2001. Mutation analysis of TBX1 in non-deleted patients with features of DGS/VCFS or isolated cardiovascular defects. Journal of Medical Genetics 38, E45.

Grimes, A.C., Stadt, H.A., Shepherd, I.T., Kirby, M.L., 2006. Solving an enigma: arterial pole development in the zebrafish heart. Dev Biol 290, 265-276.

Guo, C., Sun, Y., Zhou, B., Adam, R.M., Li, X., Pu, W.T., Morrow, B.E., Moon, A., 2011. A Tbx1-Six1/Eya1-Fgf8 genetic pathway controls mammalian cardiovascular and craniofacial morphogenesis. J Clin Invest 121, 1585-1595.

Hami, D., Grimes, A.C., Tsai, H.J., Kirby, M.L., 2011. Zebrafish cardiac development requires a conserved secondary heart field. Development 138, 2389-2398.

Huh, S.H., Ornitz, D.M., 2010. Beta-catenin deficiency causes DiGeorge syndrome-like phenotypes through regulation of Tbx1. Development (Cambridge, England) 137, 1137-1147.

Jerome, L.A., Papaioannou, V.E., 2001. DiGeorge syndrome phenotype in mice mutant for the T-box gene, Tbx1. Nature Genetics 27, 286-291.

Kimmel, C.B., Ballard, W.W., Kimmel, S.R., Ullmann, B., Schilling, T.F., 1995. Stages of embryonic development of the zebrafish. Dev Dyn 203, 253-310.

Liao, J., Aggarwal, V.S., Nowotschin, S., Bondarev, A., Lipner, S., Morrow, B.E., 2008. Identification of downstream genetic pathways of Tbx1 in the second heart field. Dev Biol 316, 524-537.

Liao, J., Kochilas, L., Nowotschin, S., Arnold, J.S., Aggarwal, V.S., Epstein, J.A., Brown, M.C., Adams, J., Morrow, B.E., 2004. Full spectrum of malformations in velo-cardio-facial syndrome/DiGeorge syndrome mouse models by altering Tbx1 dosage. Human Molecular Genetics 13, 1577-1585.

Lindsay, E.A., Vitelli, F., Su, H., Morishima, M., Huynh, T., Pramparo, T., Jurecic, V., Ogunrinu, G., Sutherland, H.F., Scambler, P.J., Bradley, A., Baldini, A., 2001. Tbx1 haploinsufficieny in the DiGeorge syndrome region causes aortic arch defects in mice. Nature 410, 97-101.

Matsui, T., Raya, A., Kawakami, Y., Callol-Massot, C., Capdevila, J., Rodriguez-Esteban, C., Izpisua Belmonte, J.C., 2005. Noncanonical Wnt signaling regulates midline convergence of organ primordia during zebrafish development. Genes Dev 19, 164-175.

Merscher, S., Funke, B., Epstein, J.A., Heyer, J., Puech, A., Lu, M.M., Xavier, R.J., Demay, M.B., Russell, R.G., Factor, S., Tokooya, K., Jore, B.S., Lopez, M., Pandita, R.K., Lia, M., Carrion, D., Xu, H., Schorle, H., Kobler, J.B., Scambler, P., Wynshaw-Boris, A., Skoultchi, A.I., Morrow, B.E., Kucherlapati, R., 2001. TBX1 is responsible for cardiovascular defects in velo-cardio-facial/DiGeorge syndrome. Cell 104, 619-629.

Miller, C.T., Schilling, T.F., Lee, K., Parker, J., Kimmel, C.B., 2000. sucker encodes a zebrafish Endothelin-1 required for ventral pharyngeal arch development. Development 127, 3815-3828.

Oskarsdottir, S., Vujic, M., Fasth, A., 2004. Incidence and prevalence of the 22q11 deletion syndrome: a population-based study in Western Sweden. Arch Dis Child 89, 148-151.

Pandur, P., Lasche, M., Eisenberg, L.M., Kuhl, M., 2002. Wnt-11 activation of a noncanonical Wnt signalling pathway is required for cardiogenesis. Nature 418, 636-641.

Piotrowski, T., Ahn, D.G., Schilling, T.F., Nair, S., Ruvinsky, I., Geisler, R., Rauch, G.J., Haffter, P., Zon, L.I., Zhou, Y., Foott, H., Dawid, I.B., Ho, R.K., 2003. The zebrafish van gogh mutation disrupts tbx1, which is involved in the DiGeorge deletion syndrome in humans. Development (Cambridge, England) 130, 5043-5052.

Qu, X., Jia, H., Garrity, D.M., Tompkins, K., Batts, L., Appel, B., Zhong, T.P., Baldwin, H.S., 2008. Ndrg4 is required for normal myocyte proliferation during early cardiac development in zebrafish. Dev Biol 317, 486-496.

Ribeiro, I., Kawakami, Y., Buscher, D., Raya, A., Rodriguez-Leon, J., Morita, M., Rodriguez Esteban, C., Izpisua Belmonte, J.C., 2007. Tbx2 and Tbx3 regulate the dynamics of cell proliferation during heart remodeling. PLoS ONE 2, e398.

Rohr, S., Otten, C., Abdelilah-Seyfried, S., 2008. Asymmetric involution of the myocardial field drives heart tube formation in zebrafish. Circ Res 102, e12-19.

Ryan, K., Chin, A.J., 2003. T-box genes and cardiac development. Birth Defects Res C Embryo Today 69, 25-37.

Schneider, V.A., Mercola, M., 2001. Wnt antagonism initiates cardiogenesis in Xenopus laevis. Genes Dev 15, 304-315.

Smith, J., 1997. Brachyury and the T-box genes. Curr Opin Genet Dev 7, 474-480.

Smith, J., 1999. T-box genes: what they do and how they do it. Trends Genet 15, 154-158.

Tu, C.T., Yang, T.C., Tsai, H.J., 2009. Nkx2.7 and Nkx2.5 function redundantly and are required for cardiac morphogenesis of zebrafish embryos. PLoS One 4, e4249.

Ueno, S., Weidinger, G., Osugi, T., Kohn, A.D., Golob, J.L., Pabon, L., Reinecke, H., Moon, R.T., Murry, C.E., 2007. Biphasic role for Wnt/beta-catenin signaling in cardiac specification in zebrafish and embryonic stem cells. Proc Natl Acad Sci U S A 104, 9685-9690.

Westerfield, M., 2000. The zebrafish book. A guide for the laboratory use of zebrafish (Danio rerio). 4th ed. ed. University of Oregon Press, Eugene, Eugene, OR.

Wilson, V., Conlon, F.L., 2002. The T-box family. Genome Biol 3, REVIEWS3008.

Xu, H., Morishima, M., Wylie, J.N., Schwartz, R.J., Bruneau, B.G., Lindsay, E.A., Baldini, A., 2004. Tbx1 has a dual role in the morphogenesis of the cardiac outflow tract. Development (Cambridge, England) 131, 3217-3227.

Yagi, H., Furutani, Y., Hamada, H., Sasaki, T., Asakawa, S., Minoshima, S., Ichida, F., Joo, K., Kimura, M., Imamura, S., Kamatani, N., Momma, K., Takao, A., Nakazawa, M., Shimizu, N., Matsuoka, R., 2003. Role of TBX1 in human del22q11.2 syndrome. Lancet 362, 1366-1373.

Zhang, Z., Huynh, T., Baldini, A., 2006. Mesodermal expression of Tbx1 is necessary and sufficient for pharyngeal arch and cardiac outflow tract development. Development (Cambridge, England) 133, 3587-3595.

Zhou, L., Wang, L., Palais, R., Pryor, R., Wittwer, C.T., 2005. High-resolution DNA melting analysis for simultaneous mutation scanning and genotyping in solution. Clin Chem 51, 1770-1777.

Zhou, W., Lin, L., Majumdar, A., Li, X., Zhang, X., Liu, W., Etheridge, L., Shi, Y., Martin, J., Van de Ven, W., Kaartinen, V., Wynshaw-Boris, A., McMahon, A.P., Rosenfeld, M.G., Evans, S.M., 2007. Modulation of morphogenesis by noncanonical Wnt signaling requires ATF/CREB family-mediated transcriptional activation of TGFbeta2. Nat Genet 39, 1225-1234.

CHAPTER 3

ALCAMA REGULATION OF CARTILAGE MORPHOGENESIS

Alcama mediates Edn1 signaling during zebrafish

cartilage morphogenesis

Reprinted with permission from *Developmental Biology*

349 (2011) 483-493

Developmental Biology 349 (2011) 483–493

Contents lists available at ScienceDirect

Developmental Biology

journal homepage: www.elsevier.com/developmentalbiology

Alcama mediates Edn1 signaling during zebrafish cartilage morphogenesis

Priya Choudhry [a], Deepa Joshi [a], Birgit Funke [b], Nikolaus Trede [a,c,*]

[a] Huntsman Cancer Institute, University of Utah, Salt Lake City, UT 84112, USA
[b] Laboratory for Molecular Medicine (LMM), Harvard Medical School, Cambridge, MA 02139, USA
[c] Department of Pediatrics, University of Utah, Salt Lake City, UT 84112, USA

ARTICLE INFO

Article history:
Received for publication 9 September 2010
Revised 1 November 2010
Accepted 3 November 2010
Available online 10 November 2010

Keywords:
Alcama
Edn1
Cartilage
Endoderm
Neural crest

ABSTRACT

The zebrafish pharyngeal cartilage is derived from the pharyngeal apparatus, a vertebrate-specific structure derived from all three germ layers. Developmental aberrations of the pharyngeal apparatus lead to birth defects such as Treacher-Collins and DiGeorge syndromes. While interactions between endoderm and neural crest (NC) are known to be important for cartilage formation, the full complement of molecular players involved and their roles remain to be elucidated. Activated leukocyte cell adhesion molecule a (*alcama*), a member of the immunoglobulin (Ig) superfamily, is among the prominent markers of pharyngeal pouch endoderm, but to date no role has been assigned to this adhesion molecule in the development of the pharyngeal apparatus. Here we show that *alcama* plays a crucial, non-autonomous role in pharyngeal endoderm during zebrafish cartilage morphogenesis. *alcama* knockdown leads to defects in NC differentiation, without affecting NC specification or migration. These defects are reminiscent of the phenotypes observed when Endothelin 1 (Edn1) signaling, a key regulator of cartilage development is disrupted. Using gene expression analysis and rescue experiments we show that Alcama functions downstream of Edn1 signaling to regulate NC differentiation and cartilage morphogenesis. In addition, we also identify a role for *neural adhesion molecule 1.1* (*nadl1.1*), a known interacting partner of Alcama expressed in neural crest, in NC differentiation. Our data shows that *nadl1.1* is required for *alcama* rescue of NC differentiation in *edn1*$^{-/-}$ mutants and that Alcama interacts with Nadl1.1 during chondrogenesis. Collectively our results support a model by which Alcama on the endoderm interacts with Nadl1.1 on NC to mediate Edn1 signaling and NC differentiation during chondrogenesis.

Introduction

Formation of the pharyngeal apparatus is a crucial part of vertebrate development because it gives rise to the cartilage, connective tissue, sensory neurons, thyroid, parathyroid and thymus. Defects in this process results in human birth defects such as DiGeorge and Treacher-Collins syndromes. Generation of this tissue is highly complex, involving extensive cell migration and signaling between cells derived from all three germ layers. NC cells migrate from the dorsal neural tube in three distinct streams into a series of pharyngeal arches and eventually give rise to cartilages and bones of the head. Each pharyngeal arch is composed of a cylinder of NC surrounding a mesodermal core. The NC is covered by ectoderm on the outside and endoderm on the inside. Between the arches, endoderm meets ectoderm forming the pharyngeal pouches, which later develop into gill clefts and the epithelial lining of the pharynx, thyroid, parathyroid and thymus (Graham, 2003).

Though NC cells carry intrinsic cues for patterning (Noden, 1983), they receive extrinsic cues from the surrounding cells and extracellular matrix as they migrate. Recently, the endoderm has been found to contribute significantly to NC development. Ablation and extirpation experiments in chicken have revealed that the endoderm carries patterning information for the NC in segments along the antero-posterior and medio-lateral axis (Couly et al., 2002; Ruhin et al., 2003). In addition, genetic mutants in zebrafish have also revealed the requirement of endoderm in formation of cartilage. The *sox32*-deficient *casanova* mutant lacks endodermal pouches and cartilages that are rescued by wild-type endodermal transplants (David et al., 2002). Likewise, the *tbx1*-deficient *van gogh* mutant fails to form segmented endodermal pouches resulting in fusion of the pharyngeal cartilages (Piotrowski and Nusslein-Volhard, 2000). Similarly, the zebrafish mutant for *integrinα5* lacks the first endodermal pouch and the anterior part of the hyoid cartilage (Crump et al., 2004). Although these data demonstrate that endoderm is essential for cartilage development, the cellular and molecular interactions between the NC and endodermal cells are not fully understood.

One major signaling factor that provides an extrinsic cue regulating NC differentiation is *endothelin-1* (*edn1*). *edn1* is expressed in the mesodermal cores, ectoderm and endoderm of the pharyngeal arches, but not in NC. Edn1 signals the NC and induces ventralization

* Corresponding author. The Huntsman Cancer Institute, University of Utah, 2000, Circle of Hope, Salt Lake City, UT 84112, USA. Fax: +1 801 581 8547.
E-mail addresses: priya.choudhry@hci.utah.edu (P. Choudhry), nikolaus.trede@hci.utah.edu (N. Trede).

0012-1606/$ – see front matter © 2010 Elsevier Inc. All rights reserved.
doi:10.1016/j.ydbio.2010.11.006

of pharyngeal arch cartilage (Miller et al., 2000). Mutations in *edn1*, Edn1 cleaving enzymes and other genes in the Edn1 signaling cascade (*sucker, schmerle, hoover* and *sturgeon*) cause similar cartilage defects, and have been placed in the same class (Kimmel et al., 2001; Piotrowski et al., 1996). Typically, the ventral domains of the first two arches are reduced in size, changed in orientation, and fused with the dorsal domains, while the posterior arches are mostly unaffected. Hence, Edn1 is an important signaling factor that is required non-autonomously for NC differentiation into cartilage.

Other molecular players that may signal from endoderm to NC remain elusive. While Alcama is commonly used as a marker for pharyngeal endoderm in zebrafish (Crump et al., 2004; Piotrowski and Nusslein-Volhard, 2000), its role in this tissue has not been elucidated thus far. In zebrafish, Alcama has been studied primarily for its role in neurogenesis (Diekmann and Stuermer, 2009; Fashena and Westerfield, 1999). Initially identified in chicken for its role in neurite extension (Burns et al., 1991), ALCAMA has now been shown to be involved in axonal pathfinding and axonal fasciculation (Diekmann and Stuermer, 2009; Weiner et al., 2004). Its non-neuronal roles include T-cell activation (Bowen et al., 2000; Fashena and Westerfield, 1999; Ofori-Acquah and King, 2008; Zimmerman et al., 2006), metastasis (Degen et al., 1998; Ofori-Acquah and King, 2008) and cell migration (Heffron and Golden, 2000). Human ALCAM is a transmembrane glycoprotein having five Ig domains, a transmembrane domain and a short cytoplasmic tail. It mediates cell-cell clustering through homophilic (ALCAM-ALCAM) as well as heterophilic (ALCAM-NgCAM and ALCAM-CD6) interactions (DeBernardo and Chang, 1996; Degen et al., 1998). While ALCAM can activate signal transduction pathways in neighbouring cells through heterophilic interactions (Ibanez et al., 2006), a non-autonomous role of ALCAM has not been defined thus far. In this paper we demonstrate that zebrafish Alcama, expressed in the pharyngeal endoderm, is an important non-autonomous molecule for NC differentiation. In addition, we provide evidence that Alcama mediates Edn1 signaling from the endoderm to the NC by interacting with Nadl1.1 (NgCAM in chicken) on the NC cells. These data for the first time link Alcama to Edn1 signaling and identify a role for the molecular interaction between Alcama and Nadl1.1 in cartilage formation.

Materials and methods

Fish stocks and maintenance

Fish were maintained at 28.5 °C under standard conditions (Westerfield, 2000) and were staged as described (Kimmel et al., 1995). The *sucker*^{tf216b} mutant (*edn1*$^{-/-}$) line was obtained from Zebrafish International Resource Center (Miller et al., 2000). Homozygous mutants were obtained by inbreeding of heterozygous carriers. *Tg(fli1:EGFP)* fish have been previously described (Lawson and Weinstein, 2002). Alcian Blue stained larvae of *furina*$^{-/-}$ mutants at 5 days post fertilization (dpf) were a kind gift from Chuck Kimmel (Institute of Neuroscience, University of Oregon).

Identification and genotyping of edn1$^{-/-}$ *mutants*

edn1$^{-/-}$ mutants have an A-to-T missense mutation (Miller et al., 2000). The mutants were identified by Derived Cleaved Amplified Polymorphic Sequences assay (Neff et al., 1998). DNA was extracted from the tails of stained embryos and PCR was conducted using the primers 5'-AGATGCTCCTGCGCAAGTTTTCTAG-3' and 5'-CTGACTTACTCTGGTGTGTTCACCC-3'. The mismatch in the primer which introduces a *XbaI* site in the wild-type (WT) but not in the mutant is underlined. The 93 bp PCR product, when digested with *Xba*I, gives a 68 bp product in WT. The 93 and 68 bp products were resolved on a 4% Metaphor agarose gel (Lonza). All the identified WT and mutants were included in the analysis.

Cloning and RNA transcription

RNA extracted from 48 h post fertilization (hpf) Tü larvae was used for cDNA synthesis. PCR for *alcama* was performed using the forward primer 5'-ggatccgccaccATGCATTCGGTTATCTGCCTTTTCG-3' with a *BamHI* and Kozak overhang and the reverse primer 5'-ctcgagTTAGACATCTGCTTTATGATTGTTCTCCTCC-3' with a *XhoI* overhang. The overhangs are shown in lower case. The PCR product was cloned into pCMV-Script using TOPO TA kit (Invitrogen). The *edn1* cDNA clone in pBK-CMV was obtained from ZIRC.

To make sense RNA for injection, the *edn1* and *alcama* plasmids were cut with *KpnI* and in vitro transcription was driven from the T3 promoter using mMessage Machine kit (Ambion). *ednrb1* was cloned from cDNA into TOPO TA using the primers 5'-ATGCGTTTCCAAATTATTATGGAAACAAGATGCG-3' (forward) and 5'-TCAGTGCCTAATTTGAAGTATACTTGTTGGAGAC-3' (reverse) and this plasmid was used to make ISH probe.

Morpholino anti-sense oligonucleotide and RNA injections

Translation blocking (TB) and splice site blocking (SB) Morpholinos (MOs) were designed to bind 143 bp upstream of the transcription start site and at the donor site of exon 6 *alcama* mRNA, respectively. *alcama* blocking and control MO were purchased from Gene Tools, Inc. The sequences are TB MO: 5'-GTTCTCCTTTATACAGTCCGGCGAC-3'; SB MO: 5'-GCAGTCCCTCACCTTAATGTTAAAG-3'; control MO: 5'-TGATCACCTGCAGATGGACGCTGCG-3'. The optimal doses were determined to be 1.1 ng for the TB MO and 2.2 ng for the SB MO. The control MO was injected at 1.1 ng per embryo. The TB MO for *nadl1.1*: 5-'CAGGCTGACTCTGCACTGGAGGCAT-3' has been previously described (Wolman et al., 2007) and was injected at 4.4 ng per embryo. 26 pg of *alcama* or *edn1* RNA was injected per embryo. MOs and RNA were dissolved in molecular biology grade water and pressure injected into one to four cell zebrafish embryos. For suboptimal doses, the *alcama* TB MO was used at 0.5 ng and the *nadl* MO at 1.1 ng per embryo.

Treatment with proteasome inhibitor MG-132

MG-132 was dissolved in DMSO at a stock concentration of 500 mM. Embryos were dechorionated at 5 hpf and transferred to E2 with 50 μM MG-132 (Bretaud et al., 2007) or with 1% dimethyl sulfoxide (DMSO). MG-132- and DMSO-treated control larvae were fixed at 30 hpf and stained.

Tissue labeling procedures

Alcian Blue cartilage staining and dissection were performed as described (Kimmel et al., 1998). Whole mount RNA in situ hybridization (ISH) with digoxigenin was performed as described (Miller et al., 2000). The plasmids for *dlx2a*, *dlx3b*, *dlx5a* were a kind gift from Gage DeKoeyer Crump (Keck School of Medicine, University of Southern California). The plasmid for nadl1.1 was a gift from Gavin J Wright (Cell Surface Signalling Laboratory, Wellcome Trust Sanger Institute). Alcama protein was stained using Zn-5 antibody from ZIRC at 1:500 dilution. A goat anti-mouse secondary antibody conjugated with Alexa 555 (Invitrogen) was used for fluorescence quantification purposes. DAPI staining was used for counting the number of cells in the pouches.

Imaging and quantification

Skeletons and ISH embryos were photographed on a Nikon Y-IDP microscope at 20× zoom using Spot software. Confocal images of antibody stained embryos were taken on Olympus FV1000 microscope. Images of all larvae from the same experiment were taken

using the same settings and exposure. Cell numbers were counted using Imaris software and fluorescence intensity of each z-section was measured using ImageJ. For immunohistochemistry coupled to ISH, the secondary antibody conjugated to alkaline phosphatase (Bio-Rad) was used with Fast Red for detection (Sigma-Aldrich). Fluorescent ISH was performed following immunohistochemistry as described (Welten et al., 2006).

Results

alcama is necessary for ventral cartilage formation

We tested whether *alcama* plays a role in cartilage morphogenesis by injection of two different MOs: one blocking translation (TB MO), and the other blocking splicing of exon 6 (SB MO; Fig. 1A). Staining with Zn-5 antibody, which recognizes Alcama, revealed effective knockdown of Alcama protein by both MOs (Fig. 1C–E). 5 dpf *alcama* morphants are characterized by a protruding lower jaw, cardiac edema and absence of swim bladder (Fig. 1G). The jaw is shorter in the antero-posterior (A-P) direction and the ventral elements of the anterior arches, Meckels (mc) and ceratohyal (ch), are bent ventrally leading to the protruding lower jaw (Fig. 1I). Injection of the TB MO consistently leads to a more pronounced phenotype than the SB MO. Therefore, in subsequent experiments we use the TB MO exclusively and refer to it as *alcama* MO.

To eliminate the possibility that the jaw defect is caused by non-specific MO-induced p53-activation (Robu et al., 2007), *alcama* MO was injected into the *p53* (I166T) mutant line (Parant et al., 2010). Alcian blue staining of 5 dpf larvae revealed that the percentage of individuals with affected cartilage was equivalent in wild-type (WT) and the $p53^{-/-}$ mutant lines (Fig. S1). The specificity of the phenotype was also tested by co-injection of *alcama* MO and *alcama* RNA. *alcama* RNA can rescue the ventral cartilage defect caused by *alcama* knockdown (Fig. S1). This indicates that the cartilage defect is caused by *alcama* knockdown and not by off-target MO effects and that *alcama* is required for the proper formation of anterior ventral cartilages in zebrafish.

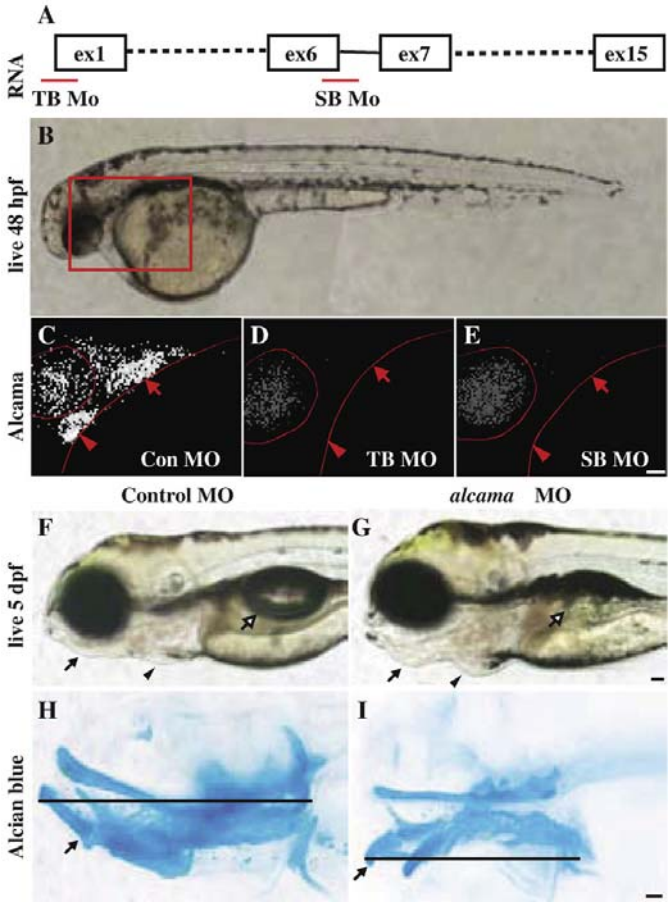

Fig. 1. *alcama* morphants have defects in facial skeletal patterning. (A) Graphic representation of *alcama* RNA illustrating the position of TB and SB MOs. (B) Nomarski image of a 48 hpf WT larva with the box indicating the region shown in (C)–(E). 48 hpf control (C), *alcama* TB (D), and *alcama* SB (E) morphants stained with Zn-5 antibody. Both MOs effectively knock down *alcama* expression in the heart (arrowheads) and pouches (arrows). (F, G) Lateral views of 5 dpf larvae injected with control and *alcama* TB MOs. *alcama* morphants have a protruding jaw (arrows), cardiac edema (arrowheads) and an absent swim bladder (open arrows). Lateral views of Alcian blue-stained control (H) and *alcama* (I) morphants at 5 dpf. The line indicates the length of the pharyngeal cartilage, which is shortened in *alcama* morphants. The arrow points to Meckels cartilage, which is bent ventrally in *alcama* morphants. Scale bars: 50 μm.

Cartilage defects in alcama morphants are reminiscent of the edn1-class of mutants

In *alcama* morphants the pharyngeal skeleton is shorter in the antero-posterior direction and the anterior arch ventral cartilages (mc and ch) point ventrally rather than anteriorly (Fig. 1H, I). In addition, mc and ch are fused to their respective dorsal elements, palatoquadrate (pq) and hyosymplectic (hm) (Fig. 2A, C). The posterior arches are shorter in the antero-posterior direction, but are otherwise unaffected (Fig. 1I). To identify the pathway affected in *alcama* morphants, we compared the jaw phenotype in *alcama* morphants to previously described cartilage mutants. The three characteristic phenotypes of the ventral cartilages in *alcama* morphants; shortening, change of orientation and fusion to dorsal cartilages, are typical of the *edn1*-class of mutants (Piotrowski et al., 1996; Walker et al., 2006, 2007). Particularly striking is the similarity of *alcama* morphants to *furinA*$^{-/-}$ mutants (Fig. 2C, E). This observation suggests that *alcama* and *edn1* may be in the same genetic pathway.

edn1 regulates alcama protein levels in the pharyngeal pouches

In order to test if an epistatic relationship exists between *alcama* and *edn1*, we analyzed *edn1* expression in *alcama* morphants. While *alcama* is also expressed in the heart, retina and the brain (Fig. S2A), expression of *edn1* and *alcama* coincides in the ventral pharyngeal area from 18 to 36 hpf (Thisse and Thisse, 2004, 2005). By 30 hpf *edn1* expression is clearly demarcated in the mesodermal cores and surface ectoderm of pharyngeal arches in addition to the pharyngeal pouches (Miller et al., 2000). At that stage, *alcama* is expressed in pharyngeal pouch endoderm (Kopinke et al., 2006). *edn1* expression is unchanged between control and *alcama* morphants, suggesting that *edn1* may act upstream of *alcama* (Fig. 3A, B).

To test this possibility, we analyzed Alcama protein expression in pharyngeal pouches of *edn1*$^{-/-}$ mutants. 30 hpf larvae were co-stained with Zn-5 Alcama antibody and DAPI (Fig. 3C, D). Confocal images were cropped to individual endodermal pouches and analyzed. Alcama intensity in individual pouches of *edn1*$^{-/-}$ mutants was down-regulated to less than 40% of the WT individuals (Fig. 3E). The total number of Alcama-expressing cells in each pouch (determined by DAPI staining) is comparable between WT and *edn1*$^{-/-}$ mutants (Fig. 3F), indicating that endodermal pouch tissue is present in *edn1*$^{-/-}$ mutants, but it expresses reduced amounts of Alcama. This observation suggests that *edn1* possibly regulates Alcama levels in pharyngeal pouches.

Edn1 is produced as a proprotein, which is cleaved twice to produce a diffusible 21-amino acid peptide. The peptide acts by binding to endothelin receptors (Ednr) coupled to G proteins. In zebrafish, two Ednrs exist; EdnrA and EdnrB. Previous ISH studies

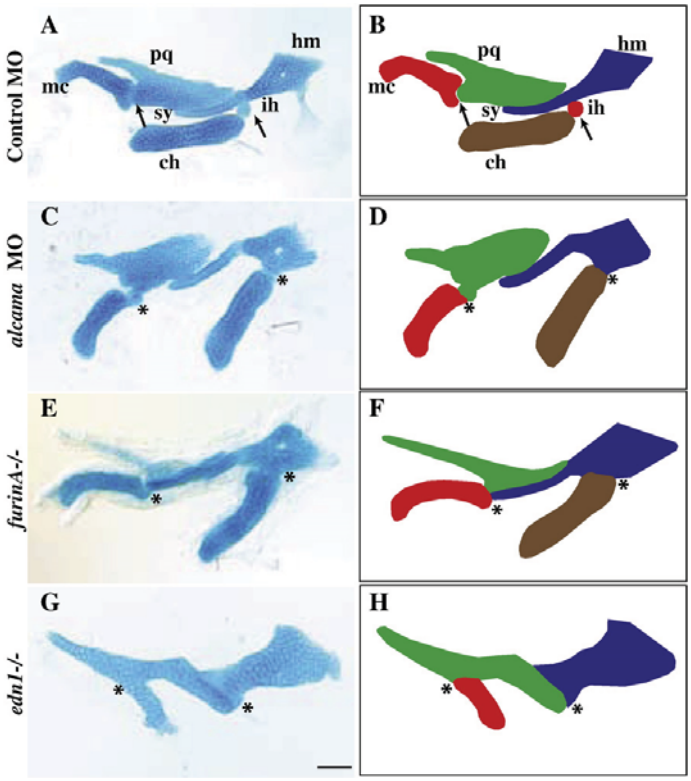

Fig. 2. *alcama* morphants have cartilage defects similar to the *edn1* class of mutants. Flatmounts of mandibular and hyoid cartilage from 5 dpf Alcian Blue-stained larvae (A, C, E, G); corresponding schematics (B, D, F, H). The joint between Meckel's and palatoquadrate is fused in *alcama* morphants and *furinA*$^{-/-}$ and *edn1*$^{-/-}$ mutants. Similarly, the interhyal is absent in *alcama* morphants and *furinA*$^{-/-}$ mutants leading to a fusion of the ceratohyal and hyosymplectic cartilages. *alcama* morphants and *furinA*$^{-/-}$ mutants have misshapen Meckel's cartilage and ceratohyal, but *edn1*$^{-/-}$ mutants have the most severe defect with a lack of ceratohyal and severely misshapen Meckel's cartilage. DV joint regions are indicated with arrows in A and B. Fusions at joints are indicated with asterisks in (C)–(H). Cartilages are labeled as followed: pq (palatoquadrate), mc (Meckel's cartilage), hm (hyomandibula), ch (ceratohyal), sy (symplectic), and ih (interhyal). Scale bar: 50 μm.

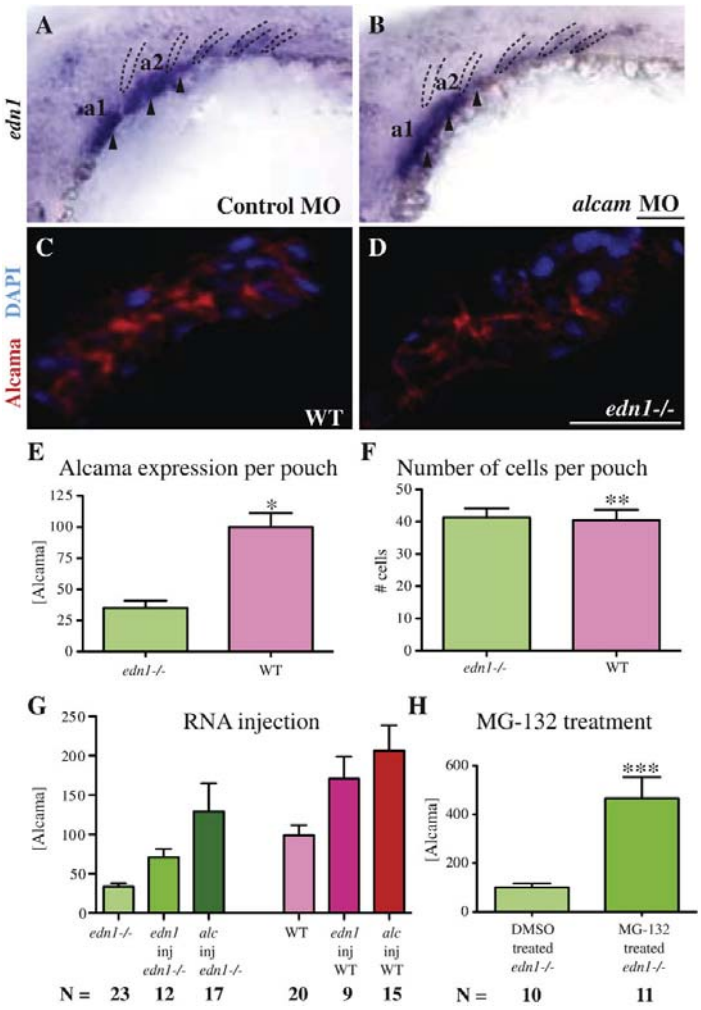

Fig. 3. Edn1 regulates Alcama levels. *edn1* is expressed in the mesodermal cores (arrowheads) of the first three arches and in pharyngeal pouches 2–4 (dotted lines) (A). Its expression is unchanged in *alcama* morphants (B). Cropped image of a single pharyngeal pouch from 30 hpf WT sibling (C) and *edn1*$^{-/-}$ mutant (D) stained with Zn-5 (anti-Alcama) antibody in red and DAPI in blue. (E) Bar graph showing the difference in total Alcama protein in a pouch (second or third pouch), represented as measured fluorescence intensity normalized to WT; $^{*}p$-value < 0.0001 by a two-tailed *t*-test. The bar graph in (F) shows the total number of cells per pouch is unchanged in WT and *edn1*$^{-/-}$ mutants; $^{**}p$-value = 0.08495 by a two-tailed *t*-test. $n = 14$ for WT; $n = 11$ for *edn1*$^{-/-}$ mutants for this experiment which was repeated with similar results. (G) *edn1* regulates the Alcama levels in pouches. The bar graph shows the sum of Alcama intensity in the first three pouches of 30 hpf *edn1*$^{-/-}$ (green) and WT (red) larvae after the indicated injections (p-value < 0.0001 by one-way analysis of variance). (H) Bar graph showing the sum of Alcama intensity in the first three pouches of 30 hpf *edn1*$^{-/-}$ larvae after treatment with DMSO or the proteasome inhibitor MG-132; $^{***}p$-value = 0.0009 by a two-tailed *t*-test. *N* is the number of larvae in a single experiment, which was repeated with similar results. a1 and a2 label pharyngeal arches 1 and 2. Scale bars: 50 μm.

have revealed that *ednrA1* and *ednrA2* are expressed almost exclusively in the NC of pharyngeal arches (Nair et al., 2007). We cloned *ednrb1* and validated that this receptor is expressed diffusely throughout the endoderm and NC (Fig. S2B). *ednrb1* expression in the endoderm is compatible with our hypothesis that Edn1 signals to the endoderm to regulate Alcam levels.

To corroborate our hypothesis that *edn1* regulates Alcama levels, we tested whether *edn1* over-expression could rescue Alcama levels in *edn1*$^{-/-}$ mutants. *edn1* RNA was injected into *edn1*$^{-/-}$ embryos at the 1-cell stage and Alcama protein levels were quantified at 30 hpf as discussed previously with one modification. The fluorescence intensity of Zn-5 staining in the pharyngeal area from the first to the third pouch, instead of single pouches, was measured and normalized to uninjected WT (Fig. S3). *alcama* RNA was injected as a positive control. *edn1* RNA injection results in more than 50% increase in Alcama protein in WT and *edn1*$^{-/-}$ mutants (Fig. 3G), suggesting that *edn1* regulates Alcama levels in the endoderm.

Additionally, we investigated the mechanism by which Edn1 regulates Alcama. ISH studies revealed that *alcama* RNA levels, while slightly down-regulated in *edn1*$^{-/-}$ mutants (Fig. S2C, D), do not explain the severe down-regulation observed in Alcama protein levels (Fig. 3D, E). This observation suggests that *edn1* does not regulate Alcama levels via regulating transcription. Previous studies have indicated that *edn1* may lead to Snail and β-catenin protein

stabilization by regulating the proteasome pathway (Rosano et al., 2005; Sato-Jin et al., 2008). To test whether Edn1 stabilizes Alcama protein by interfering with its degradation by the proteasome, we treated *edn1*$^{-/-}$ larvae with the proteasome inhibitor MG132 and measured Alcama levels. The fluorescence intensity was normalized to DMSO-treated *edn1*$^{-/-}$ mutants. Alcama levels in the pharyngeal pouches increased by more than 300% upon treatment with MG-132 (Fig. 3H), indicating that inhibition of proteasomal degradation is involved in Edn1-induced regulation of Alcama. While *edn1* RNA injection increases Alcama levels in the pharyngeal pouches, Alcama levels are unchanged in the heart and retina, where Edn1 signaling is not active (data not shown). These experiments indicate that Edn1 stabilizes Alcama levels specifically in the pharyngeal endodermal pouches by inhibiting some component of the proteasome pathway.

alcama is required for edn1-dependent differentiation of NC

We have determined that *alcama* morphants have defects in ventral cartilages. Since cartilage is formed from NC in the pharyngeal arches, we investigated whether *alcama* knockdown caused a defect in the patterning or specification of NC. We injected *alcama* MO into *Tg(fli*:EGFP*)* line which labels NC cells. Analysis of larvae at 30 hpf, a stage at which the cranial NC has already populated the arches, revealed that NC migration is unaffected in *alcama* morphants (Fig. S4B). This observation was corroborated by ISH with the NC marker *distalless 2a* (*dlx2a*) at the same developmental stage, showing normal patterning of NC (Fig. S4D). In addition *nkx2.3* expression in endoderm (Fig. S4F), and *edn1* expression in mesodermal cores and endodermal pouches (Fig. 3B) is unaffected in *alcama* morphants, suggesting that NC, endoderm and mesoderm are all patterned and specified correctly in the pharyngeal region of *alcama* morphants. This result implies that similarly to genes in the Edn1 pathway, Alcama is not required for NC migration or specification, but is involved in a later stage of cartilage morphogenesis.

Our data suggest that Alcama functions downstream of Edn1 in cartilage formation. To assess the functional importance of *alcama* in the Edn1 signaling pathway, we analyzed the expression of genes downstream of *edn1* in *alcama* morphants. Edn1 signaling is required for the expression of Dlx and Hand2 transcription factors in NC (Miller et al., 2000; Walker et al., 2006). Like Edn1, Hand2 is required for ventral cartilage formation and Dlx factors pattern the dorso-ventral axis of pharyngeal arches (Depew et al., 2002; Miller et al., 2003). In *alcama* morphants, the expression of *hand2*, *dlx3b*, *dlx5a* and *dlx6a* is strongly reduced in the first and the posterior arches, and mildly reduced in the second arch at 30 hpf (Fig. 4B, E, H, K). Although *hand2* expression recovers by 48 hpf, *dlx* genes continue to be down-regulated (Fig. S5). At 30 hpf, *hand2* expression is down-regulated in NC, but unaffected in the heart of *alcama* morphants (Fig. 4B) and *edn1*$^{-/-}$ mutants (Fig. 4C), indicating that Alcama is required specifically for *edn1*-dependent expression of NC genes.

edn1-dependent *bapx1* expression in the intermediate region of the precartilage arch is required for cartilage joint formation (Miller et al., 2003). Consistent with the joint fusion observed in *alcama* morphants, *bapx1* expression in the intermediate region of arch1 is down-regulated in *alcama* morphants (Fig. 4N). Down-regulation of Edn1-dependent genes in *alcama* morphants is similar to, but less severe than that observed in *edn1* mutants (Fig. 4C, F, I, L, O). This observation is consistent with the less severe jaw defect observed in *alcama* morphants when compared to *edn1* mutants. Taken together these data suggest that Alcama is required for Edn1-dependent NC differentiation and the proper formation of ventral cartilage and jaw joint.

Our data suggests that NC is patterned and specified correctly in *alcama* morphants (Fig. S3). Hence, the failure of NC to express *edn1*-dependent genes that come on later in development, suggests that *alcama* knockdown causes a defect in NC differentiation. In subsequent experiments, *dlx5a* expression is used as a marker for NC differentiation due to its robust expression. The specificity of MO-induced NC differentiation defect was tested by co-injection of *alcama* MO with *alcama* RNA, and by *alcama* MO injection in *p53*$^{-/-}$ mutants (Robu et al., 2007). *dlx5a* expression was categorized as strong (all arches stained), partial (all arches stained but weaker) and absent (most arches missing staining and some with very weak staining) (Fig. S6A–C). Co-injection of *alcama* RNA with *alcama* MO decreases the number of affected individuals (absent *dlx5a* staining) to WT levels (Fig. S6D), suggesting that the NC differentiation defect is caused specifically by *alcama* knockdown. The percentage of affected larvae is similar in WT and *p53*$^{-/-}$ mutants (Fig. S6D), indicating that similar to the cartilage defect, the NC differentiation defect is caused by *alcama* knockdown and is not dependent on off-target MO effects.

alcama over-expression can rescue NC differentiation defect in edn1$^{-/-}$ *mutants*

Our data suggests that *edn1* regulates Alcama levels and knockdown of either gene results in a NC differentiation defect. We tested our hypothesis that *edn1* affects NC differentiation via Alcama, by over-expressing *alcama* in *edn1*$^{-/-}$ mutants followed by analysis of NC differentiation. We injected *alcama* RNA into *edn1*$^{-/-}$ mutants at the one-cell stage and assessed *dlx5a* expression at 30 hpf as a marker for NC differentiation. *dlx5a* staining was classified as absent, partial and strong (Fig. 5A–C) and the number of larvae in each category were counted. *edn1* over-expression was used as a positive control, resulting in a 300% increase in the number of *edn1*$^{-/-}$ mutants with *dlx5a* staining (sum of strong and partial) (Fig. 5D). *alcama* RNA induces similar increases of rescued *edn1*$^{-/-}$ mutants as *edn1* RNA, although full rescue of *dlx5a* expression was not achieved. This indicates that Alcama functions downstream of Edn1 to regulate NC differentiation. To bolster this hypothesis, we asked if *edn1* rescue of *edn1*$^{-/-}$ mutants could be abrogated by *alcama* knockdown. Indeed, co-injection of *alcama* MO abrogates the ability of *edn1* RNA to rescue *dlx5a* staining in *edn1*$^{-/-}$ mutants (Fig. 5D), supporting our previous finding that *alcama* expression is necessary for Edn1 function. Injection of either *edn1* or *alcama* RNA was unable to rescue the cartilage defect of *edn* mutants at 5 dpf, possibly due to dilution of RNA in rapidly dividing cells.

As opposed to *edn1*$^{-/-}$ mutants, less than 5% of WT larvae have absent *dlx5a* expression. *alcama* or *edn1* RNA injections into WT embryos do not affect *dlx5a* expression (Fig. 5E), demonstrating that these genes do not negatively affect NC differentiation when they are over-expressed. Co-injection of *edn1* RNA with *alcama* MO results in a similar percentage of larvae with absent *dlx5a* staining to that observed in *alcama* morphants (Fig. 5E). However, there are more larvae with strong *dlx5a* expression, suggesting that *edn1* may regulate NC differentiation by another parallel pathway independent of *alcama*. In aggregate, these data provide evidence that Alcama functions downstream of Edn1 in regulation of NC differentiation.

Nadl1.1 mediates Alcama differentiation signal to the NC

Since Alcama is expressed in the endoderm, we investigated the possibility that it interacts with another protein to mediate Edn1-signaling to the adjacent NC. *Nadl1* (Ng-CAM in chick) has been shown to interact with Alcama in the chick brain to promote neurite extension (DeBernardo and Chang, 1996). Zebrafish have two orthologs of Ng-CAM, *nadl1.1* and *nadl1.2*, but only *nadl1.1* is expressed in the NC (Figs. 6A and 7A). To test if *nadl1.1* is involved in cartilage development, we used a previously described TB MO targeting *nadl1.1* (Wolman et al., 2007). Phenotypically, *nadl1.1* morphants are similar to *alcama* morphants: by 5 dpf they have a protruding lower jaw, cardiac edema and absent swim bladder (data not shown). Similar to *alcama* MO, *nadl1.1* MO affects *edn1*-dependent

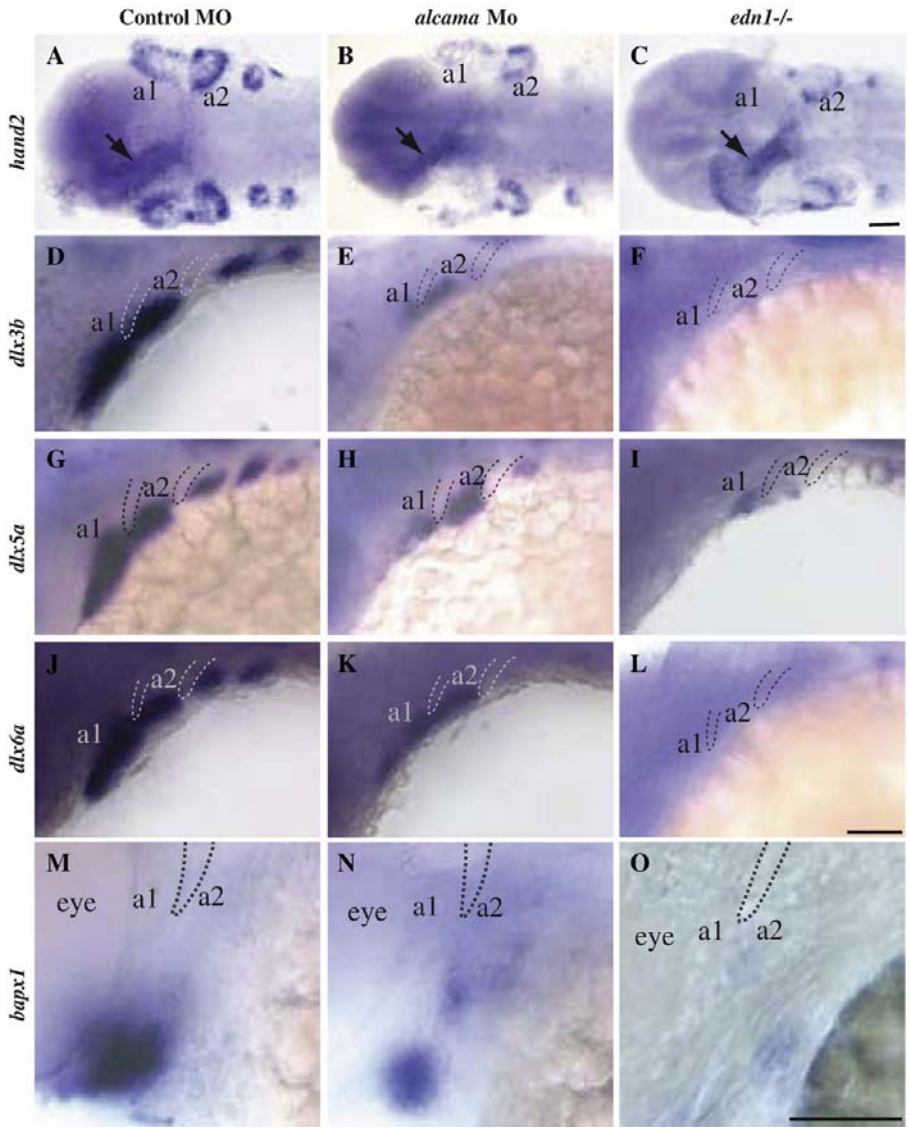

Fig. 4. *alcama* is required for *edn1*-dependent gene expression. Ventral views of larvae at 30 hpf (A–C), and lateral views at 30 hpf (D–L) and at 48 hpf (M–O) respectively. ISH for *hand2* (A–C), *dlx3b* (D–F), *dlx5a* (G–I), *dlx6a* (J–L), and *bapx1* (M–O) in control and *alcama* morphants and in *edn1*$^{-/-}$ mutants. *hand2, dlx3b, dlx5a* and *dlx6a* expression is strongly reduced in the first and branchial arches and moderately reduced in the second arch in *alcama* morphants. Their expression is strongly reduced in all arches in the *edn1*$^{-/-}$ mutants. *bapx1* expression in the first arch intermediate domain is moderately reduced in *alcama* morphants and strongly reduced in *edn1*$^{-/-}$ mutants. a1 and a2 label pharyngeal arches 1 and 2. Dotted lines highlight pharyngeal pouches 1 and 2. Scale bars: 50 μm.

gene expression: *hand2* and *dlx5a* expression is strongly reduced in the arches with a more pronounced effect on the posterior arches (Fig. 6B–E). Alcian blue staining reveals cartilage defects reminiscent of *alcama* morphants: mc and ch are changed in orientation and are fused to pq and hm, respectively (Fig. 6G–H'). Injection of *nadl1.1* MO into *p53*$^{-/-}$ mutants yields similar percentages of larvae with *dlx5a* down-regulation and jaw abnormalities (Fig. 6F, I), indicating that the observed effect is specific to *nadl1.1* knockdown. These data suggest that *nadl1.1* may be another player in the Edn1 signaling pathway that regulates ventral cartilage formation.

We investigated the possibility that *nadl1.1* is another downstream effector of Edn1-mediated NC differentiation and cartilage morphogenesis that functions independently of Alcama. *nadl1.1* expression is not down-regulated in *edn1*$^{-/-}$ mutants as compared to WT at 30 hpf (Fig. S2E, F), indicating that *edn1* does not regulate *nadl1.1* at the transcriptional level. Hence, it is unlikely that *nadl1.1* functions in the

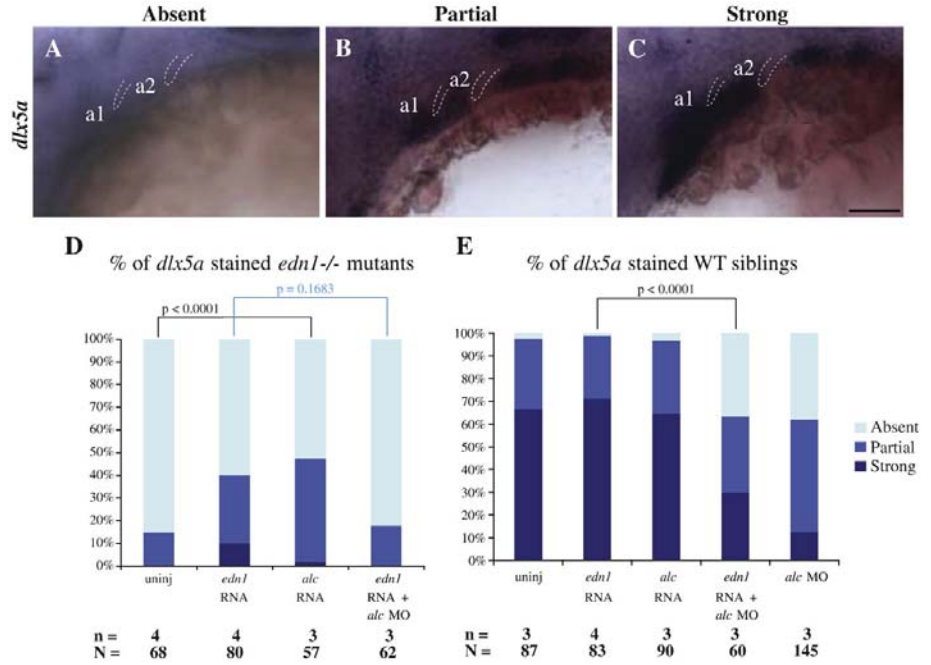

Fig. 5. *alcama* rescues NC differentiation defect in *edn1*$^{-/-}$ mutants. Lateral views of 30 hpf larvae with representative absent (A), partial (B) or strong (C) staining for *dlx5a*. Bar graphs show the percentage *dlx5a* expressing larvae in *edn1*$^{-/-}$ mutants (D) and WT (E) following the stated injections. *edn1* or *alcama* RNA was injected with or without *alcama* MO. *alcama* RNA decreases the percentage of affected individuals (absent *dlx5a* staining) by nearly 30% in *edn1*$^{-/-}$ mutants and co-injection of *alcam* Mo abrogates the ability of *edn1* RNA to rescue *dlx5a* expression in *edn1*$^{-/-}$ mutants. Indicated *p*-values are calculated by Fishers exact test. n depicts the number of experiments and N depicts the total number of larvae represented in the columns of the plot (*p*-value<0.0001 for both D and E by χ^2 analysis). a1 and a2 label pharyngeal arches 1 and 2. Dotted lines highlight pharyngeal pouches 1 and 2. Scale bar: 50 μm.

edn1-pathway independently of Alcama. These data show that loss of *alcama* and *nadl1.1* causes very similar defects in cartilage morphogenesis and NC differentiation, supporting our hypothesis that the two adhesion molecules might interact.

alcama and *nadl1.1* are expressed adjacent to each other in the endoderm and NC respectively (Fig. 7A), supporting our hypothesis that Nadl1.1 may propagate Alcama differentiation signal from the endoderm to NC. To bolster this hypothesis, we first asked if *alcama*-mediated rescue of *dlx5a* expression in *edn1*$^{-/-}$ mutants (Fig. 5) is abrogated by *nadl1.1* knockdown. Co-injection of *nadl1.1* MO with *alcama* RNA indeed blocked rescue of *dlx5a* expression in *edn1*$^{-/-}$ mutants (Fig. 7B), suggesting that Nadl1.1 expression is necessary for transmission of Edn1 signal through Alcama to NC.

To corroborate this observation we next tested possible interaction of Alcama and Nadl1.1 in synergy experiments by co-injecting suboptimal doses of *alcama* MO and *nadl1.1* MO into WT embryos. The read-out consisted of assessment of NC differentiation (*dlx5a* expression) and cartilage morphogenesis. While suboptimal doses of *alcama* and *nadl1.1* MOs alone do not cause significant changes in *dlx5a* expression or cartilage shape, co-injection resulted in synergistic increase in the number of larvae with down-regulated *dlx5a* expression and cartilage defects (Fig. 7C, D). This indicates that Alcama and Nadl1.1 interact during cartilage morphogenesis. Taken together with the ability of *nadl1.1* MO to block rescue of NC differentiation by Alcama over-expression in *edn1*$^{-/-}$ mutants, these data suggest that Alcama affects cartilage and NC differentiation by interacting with Nadl1.1.

Discussion

Our data shows for the first time that endodermally expressed Alcama is required for differentiation of NC and ventral pharyngeal cartilage morphogenesis. The *alcama*-deficient cartilage defect resembles that seen in *edn1*-class of mutants. In addition, *edn1* regulates Alcama protein levels in the pharyngeal endoderm. Moreover, similar to genes involved in Edn1 signaling, *alcama* is dispensible for NC patterning and migration, but is required for NC differentiation. Additionally, *alcama* over-expression partially rescues the NC differentiation defect in *edn1*$^{-/-}$ mutants, indicating that Alcama mediates Edn1 signaling to NC. Finally, we identify that Nadl1.1, an interacting partner of Alcama, is crucial for transmitting Alcama differentiation signal to NC and promoting ventral cartilage morphogenesis. These data lead us to propose a model (Fig. 8), whereby Edn1 signaling turns on *dlx* genes in the NC by two independent pathways. Edn1 binds to its receptor on NC to activate NC genes directly. In parallel, Edn1 binds to its receptor on the endoderm to stabilize Alcama protein, which in turn binds to Nadl1.1 on NC and further activates NC genes. Activation of both pathways is required for normal differentiation of NC and cartilage morphogenesis.

edn1 signals to NC by two parallel pathways

Edn1 is synthesized as a proprotein, which is cleaved twice by Furin and endothelin-converting enzyme resulting in a short, active Edn1 peptide. This short, active Edn1 peptide binds to the G protein-

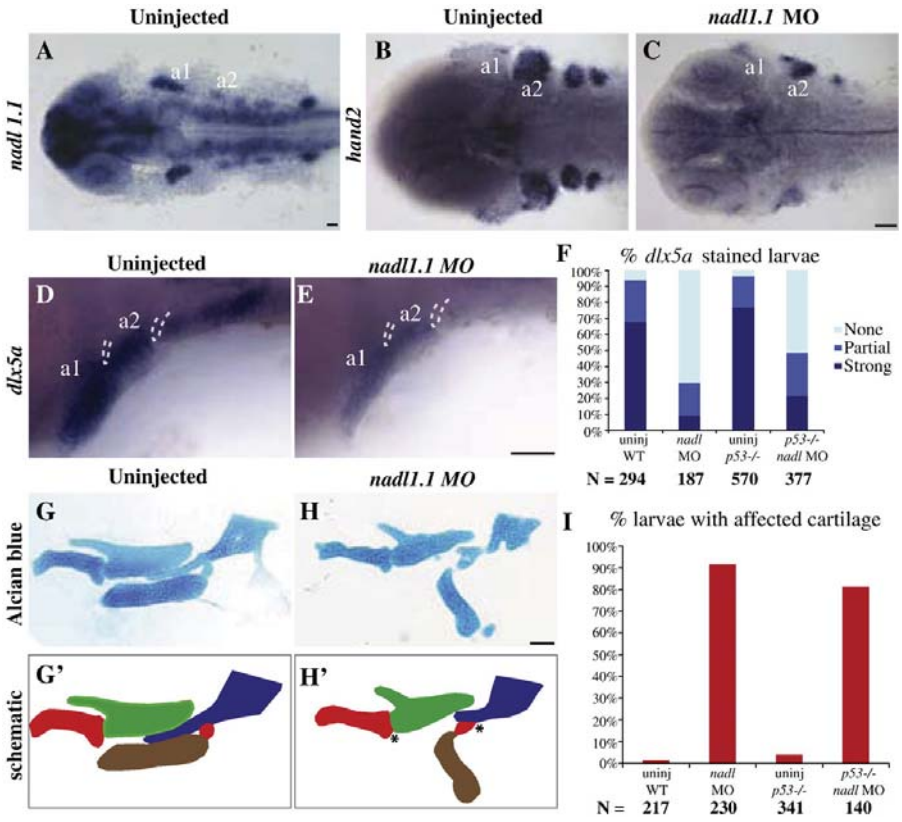

Fig. 6. *nadl1.1* morphants phenocopy *alcama* morphant cartilage defects. Dorsal views (A–C) and lateral views (D, E) of 30 hpf larvae. *nadl1.1* is expressed in the pharyngeal arches, diencephalon, telencephalon, hindbrain neurons, neural tube and pectoral fin in 30 hpf WT larvae (A). 30 hpf *nadl 1.1* morphants have down-regulated *hand2* (C) and *dlx5a* (E) expression as compared to uninjected WT (B, D). (F) Bar graph showing that the percentage of larvae with down-regulated (absent) *dlx5a* expression remains unchanged in the $p53^{-/-}$ background (*p*-value = 1.000 by Fishers exact test, indicating that WT and $p53^{-/-}$ mutants are not significantly different). Dissected mandibular and hyoid elements from 5 dpf WT and *nadl1.1* morphant larvae stained with Alcian blue (G, H) and their corresponding schematics (G', H'). The joint fusions in *nadl1.1* morphants (H, H') marked by * resemble those seen in *alcama* morphants. (I) Bar graph comparing the percentage of larvae with affected cartilage in *alcama* morphants in WT versus $p53^{-/-}$ mutants (*p*-value = 0.1941 by Fishers exact test, indicating that WT and $p53^{-/-}$ mutants are not significantly different). *N* is the total number of larvae from three experiments. Scale bars: 50 μm.

coupled Edn1 receptor. Phospholipase C enzyme further transmits the signal by producing inositol trisphosphate and diacylglycerol. Mouse mutants for Edn1, Ednra and the G-protein share skeletal defects with zebrafish mutants for *edn1*, *furinA* and *phospholipase C beta 3 (plcβ3)*; the ventral domains of the lower jaw are reduced in size and fused to the dorsal domains in both species (Clouthier et al., 1998, 2000; Dettlaff-Swiercz et al., 2005; Kurihara et al., 1994; Miller et al., 2000; Walker et al., 2006, 2007). Thus Edn1 signaling has been conserved during evolution to regulate ventral cartilage morphology.

Zebrafish $edn1^{-/-}$ and $plcβ3^{-/-}$ mutants have more severe ventral cartilage reductions and joint fusions than *alcama* morphants. The milder cartilage defect in *alcama* morphants correlates with the less pronounced reduction of *dlx*, *hand2* and *bapx1* gene expression in NC. We propose that this milder defect is due to two concomitant, additive pathways for *edn1* signaling; the first acts directly in the NC through the Edn1 receptor and the second activates Alcama signaling from the endoderm to the NC (Fig. 8). While both pathways are affected in *edn1* and *plcβ3* mutants, in *alcama* morphants direct signaling from the Edn1 receptor is still intact and can partially activate *dlx* gene expression in the NC, resulting in a milder phenotype.

Edn1 regulates alcama protein levels in pharyngeal endoderm

Previous data has implicated Edn1 as a regulator of the proteasome pathway (Rosano et al., 2005; Sato-Jin et al., 2008). Our data suggest that *edn1* stabilizes Alcama protein by inhibiting the proteasome pathway because inhibiting the proteasome pathway in $edn1^{-/-}$ mutants results in increased Alcama levels. It is still unknown whether Edn1 stabilizes Alcama by inducing a structural change that prevents polyubiquitination, or indirectly by regulating transcription of proteasome subunits or by activation of de-ubiquitinases. Alternatively, Alcama may not be a direct target of the proteasome pathway; instead a chaperone protein that stabilizes Alcama might be the target of proteasome pathway. An alternative possibility is that Edn1 signals to NC and thus induces Alcama stabilization indirectly. Further investigation into this mechanism will broaden our understanding of the process of NC differentiation.

Further inquiry is also needed into other proteins/signals regulating *alcama* expression. Although *edn1* RNA injections and MG132 treatment led to higher Alcama expression, in both cases expression was mostly restricted to the endoderm and not the NC. This data

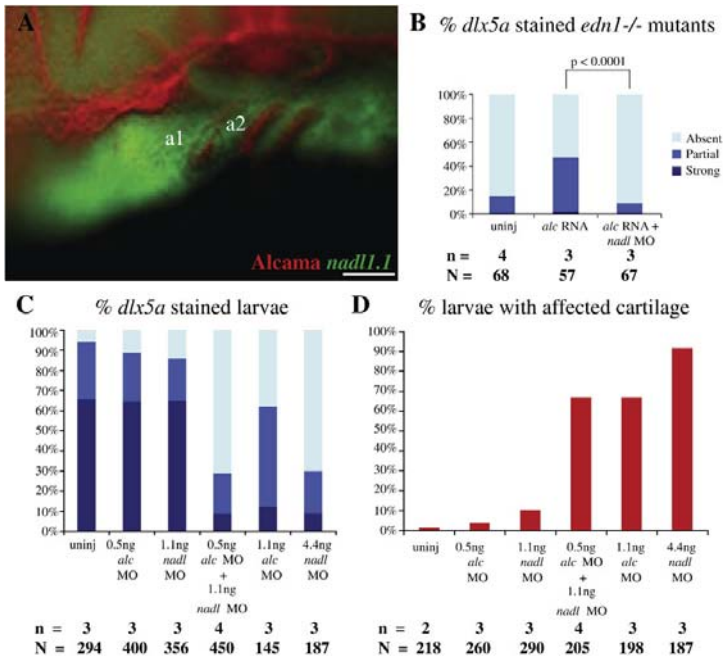

Fig. 7. *alcama* and *nadl1.1* interact during cartilage formation. (A) Lateral view of a 30 hpf WT larva stained with Zn-5 antibody (Fast Red) and anti-sense *nadl1.1* RNA (Fluorescein), revealing that *nadl1.1* is expressed in the NC adjacent to *alcama* in the endoderm. The bar graphs display the percentage of 30 hpf *edn1*$^{-/-}$ (B) and WT (C) larvae with *dlx5a* staining after the indicated injections. (B) shows that *nadl1.1* is required for *alcama* rescue of *dlx5a* expression in *edn1*$^{-/-}$ mutants (p-value<0.0001 by Fishers exact test). (C) and (D) show that *alcama* and *nadl1.1* interact during *dlx5a* expression and cartilage morphogenesis. (D) Bar graph displaying the percentage of 5 dpf larvae with affected cartilage after the indicated injections (p-value<0.0001 by χ^2 analysis). n indicates the number of experiments and N the total number of larvae. Scale bar: 50 μm.

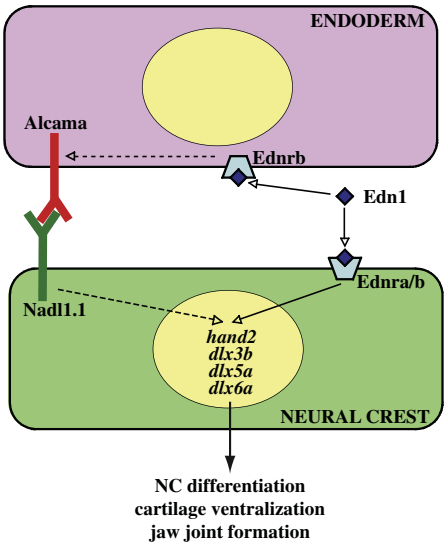

Fig. 8. Model demonstrating how Alcama mediates Edn1 signaling and NC differentiation. Previous data has supported the model that Edn1 peptide binds to its G-protein-coupled receptor on NC to turn on transcription of NC genes. We propose a parallel pathway by which Edn1 signaling stabilizes Alcama protein in endodermal cells. Alcama, in turn, binds to Nadl1.1 in NC and regulates NC differentiation.

points to an endoderm-specific role of Alcama in cartilage formation. Similarly, *edn1* and *alcama* RNA injections into the one-cell stage induced rescue of *dlx5a* expression, specifically in NC. Further investigation of these mechanisms, that restrict Alcama expression to endoderm and *dlx* genes to NC, is needed to gain a more complete understanding of the process of chondrogenesis.

Alcama interacts with Nadl1.1 on the NC to mediate differentiation signals

We established that Nadl1.1, a known interacting partner of Alcama expressed in NC, is important for cartilage morphogenesis and its knockdown results in similar cartilage defects to *alcama* knockdown. We also demonstrated that *nadl1.1* is necessary for Alcama-mediated rescue of NC differentiation in *edn1*$^{-/-}$ mutants and that Alcama and Nadl1.1 interact during cartilage formation, either directly or indirectly. Hence we concluded that Nadl1.1 possibly transmits Alcama-mediated Edn1 signaling to the NC. Future studies will focus on how Nadl1.1 activates *dlx* genes in the NC.

One possible function for Alcama and Nadl1.1 interaction during NC differentiation and cartilage morphogenesis may be to simply maintain cell–cell contacts between the endoderm and NC. Support for this hypothesis is provided by the *integrinα5* mutant and the Eph-ephrin system. Integrins are required for cell adhesion and migration in many tissues (Benoit et al., 2009; Brakebusch and Fassler, 2005). The zebrafish *integrinα5* mutant has defects in formation of the first pouch, resulting in defective compaction and survival of NC cells adjacent to the first pouch, giving rise to a deformed hyoid cartilage (Crump et al., 2004). Eph genes encode tyrosine kinase receptors for ephrin ligands. Eph-ephrin mediated repulsion establishes polarity and boundaries during development (Holder and Klein, 1999; Robinson et al., 1997). Since EphA3 is expressed

in ventral NC, it is also postulated that Eph-ephrin repulsion may play a role in separating the dorsal and ventral cartilages, giving rise to the joint between them (Kimmel et al., 2001). Hence, both adhesive (integrins) and repulsive forces (ephrins) play a role in NC differentiation. By analogy it is conceivable that Alcama-Nadl1.1 mediated adhesion between the endoderm and NC may play a similar role in chondrogenesis.

Conclusion

In summary, this is the first demonstration that Alcama, a commonly used marker for endoderm, plays a critical role in NC differentiation and cartilage morphogenesis. We show that Edn1 regulates Alcama levels in vivo and that Alcama functions downstream of Edn1 during cartilage formation. In addition, we provide support for a mechanism by which Alcama mediates Edn1-signaling by interacting with Nadl1.1 on NC cells.

Supplementary materials related to this article can be found online at doi:10.1016/j.ydbio.2010.11.006.

Acknowledgments

The authors wish to thank Raju Kucherlapati and Len Zon for material and technical support, Sarah Hutchinson for intellectual contributions, and Gavin Wright (and his student) for technical expertise. We wish to thank Chuck Kimmel for Alcian Blue-stained *furina*$^{-/-}$ mutant zebrafish, and Gage Crump for *dlx* plasmids. This work was supported in part by R01 HD047863-01 and by the Huntsman Cancer Foundation. Huntsman Cancer Institute core facilities, supported by grant P30 CA042014, also facilitated this work.

References

Benoit, Y.D., Lussier, C., Ducharme, P.A., Sivret, S., Schnapp, L.M., Basora, N., Beaulieu, J.F., 2009. Integrin alpha8beta1 regulates adhesion, migration and proliferation of human intestinal crypt cells via a predominant RhoA/ROCK-dependent mechanism. Biol. Cell 101, 695–708.

Bowen, M.A., Aruffo, A.A., Bajorath, J., 2000. Cell surface receptors and their ligands: in vitro analysis of CD6-CD166 interactions. Proteins 40, 420–428.

Brakebusch, C., Fassler, R., 2005. beta 1 integrin function in vivo: adhesion, migration and more. Cancer Metastasis Rev. 24, 403–411.

Bretaud, S., Allen, C., Ingham, P.W., Bandmann, O., 2007. p53-dependent neuronal cell death in a DJ-1-deficient zebrafish model of Parkinson's disease. J. Neurochem. 100, 1626–1635.

Burns, F.R., von Kannen, S., Guy, L., Raper, J.A., Kamholz, J., Chang, S., 1991. DM-GRASP, a novel immunoglobulin superfamily axonal surface protein that supports neurite extension. Neuron 7, 209–220.

Clouthier, D.E., Hosoda, K., Richardson, J.A., Williams, S.C., Yanagisawa, H., Kuwaki, T., Kumada, M., Hammer, R.E., Yanagisawa, M., 1998. Cranial and cardiac neural crest defects in endothelin-A receptor-deficient mice. Development 125, 813–824.

Clouthier, D.E., Williams, S.C., Yanagisawa, H., Wieduwilt, M., Richardson, J.A., Yanagisawa, M., 2000. Signaling pathways crucial for craniofacial development revealed by endothelin-A receptor-deficient mice. Dev. Biol. 217, 10–24.

Couly, G., Creuzet, S., Bennaceur, S., Vincent, C., Le Douarin, N.M., 2002. Interactions between Hox-negative cephalic neural crest cells and the foregut endoderm in patterning the facial skeleton in the vertebrate head. Development 129, 1061–1073.

Crump, J.G., Swartz, M.E., Kimmel, C.B., 2004. An integrin-dependent role of pouch endoderm in hyoid cartilage development. PLoS Biol. 2, E244.

David, N.B., Saint-Etienne, L., Tsang, M., Schilling, T.F., Rosa, F.M., 2002. Requirement for endoderm and FGF3 in ventral head skeleton formation. Development 129, 4457–4468.

DeBernardo, A.P., Chang, S., 1996. Heterophilic interactions of DM-GRASP: GRASP-NgCAM interactions involved in neurite extension. J. Cell Biol. 133, 657–666.

Degen, W.G., van Kempen, L.C., Gijzen, E.G., van Groningen, J.J., van Kooyk, Y., Bloemers, H.P., Swart, G.W., 1998. MEMD, a new cell adhesion molecule in metastasizing human melanoma cell lines, is identical to ALCAM (activated leukocyte cell adhesion molecule). Am. J. Pathol. 152, 805–813.

Depew, M.J., Lufkin, T., Rubenstein, J.L., 2002. Specification of jaw subdivisions by Dlx genes. Science 298, 381–385.

Dettlaff-Swiercz, D.A., Wettschureck, N., Moers, A., Huber, K., Offermanns, S., 2005. Characteristic defects in neural crest cell-specific Galphaq/Galpha11- and Galpha12/Galpha13-deficient mice. Dev. Biol. 282, 174–182.

Diekmann, H., Stuermer, C.A., 2009. Zebrafish neurolin-a and -b, orthologs of ALCAM, are involved in retinal ganglion cell differentiation and retinal axon pathfinding. J. Comp. Neurol. 513, 38–50.

Fashena, D., Westerfield, M., 1999. Secondary motoneuron axons localize DM-GRASP on their fasciculated segments. J. Comp. Neurol. 406, 415–424.

Graham, A., 2003. Development of the pharyngeal arches. Am. J. Med. Genet. A 119A, 251–256.

Heffron, D.S., Golden, J.A., 2000. DM-GRASP is necessary for nonradial cell migration during chick diencephalic development. J. Neurosci. 20, 2287–2294.

Holder, N., Klein, R., 1999. Eph receptors and ephrins: effectors of morphogenesis. Development 126, 2033–2044.

Ibanez, A., Sarrias, M.R., Farnos, M., Gimferrer, I., Serra-Pages, C., Vives, J., Lozano, F., 2006. Mitogen-activated protein kinase pathway activation by the CD6 lymphocyte surface receptor. J. Immunol. 177, 1152–1159.

Kimmel, C.B., Ballard, W.W., Kimmel, S.R., Ullmann, B., Schilling, T.F., 1995. Stages of embryonic development of the zebrafish. Dev. Dyn. 203, 253–310.

Kimmel, C.B., Miller, C.T., Kruze, G., Ullmann, B., BreMiller, R.A., Larison, K.D., Snyder, H.C., 1998. The shaping of pharyngeal cartilages during early development of the zebrafish. Dev. Biol. 203, 245–263.

Kimmel, C.B., Miller, C.T., Moens, C.B., 2001. Specification and morphogenesis of the zebrafish larval head skeleton. Dev. Biol. 233, 239–257.

Kopinke, D., Sasine, J., Swift, J., Stephens, W.Z., Piotrowski, T., 2006. Retinoic acid is required for endodermal pouch morphogenesis and not for pharyngeal endoderm specification. Dev. Dyn. 235, 2695–2709.

Kurihara, Y., Kurihara, H., Suzuki, H., Kodama, T., Maemura, K., Nagai, R., Oda, H., Kuwaki, T., Cao, W.H., Kamada, N., et al., 1994. Elevated blood pressure and craniofacial abnormalities in mice deficient in endothelin-1. Nature 368, 703–710.

Lawson, N.D., Weinstein, B.M., 2002. In vivo imaging of embryonic vascular development using transgenic zebrafish. Dev. Biol. 248, 307–318.

Miller, C.T., Schilling, T.F., Lee, K., Parker, J., Kimmel, C.B., 2000. sucker encodes a zebrafish endothelin-1 required for ventral pharyngeal arch development. Development 127, 3815–3828.

Miller, C.T., Yelon, D., Stainier, D.Y., Kimmel, C.B., 2003. Two endothelin 1 effectors, hand2 and bapx1, pattern ventral pharyngeal cartilage and the jaw joint. Development 130, 1353–1365.

Nair, S., Li, W., Cornell, R., Schilling, T.F., 2007. Requirements for endothelin type-A receptors and endothelin-1 signaling in the facial ectoderm for the patterning of skeletogenic neural crest cells in zebrafish. Development 134, 335–345.

Neff, M.M., Neff, J.D., Chory, J., Pepper, A.E., 1998. dCAPS, a simple technique for the genetic analysis of single nucleotide polymorphisms: experimental applications in Arabidopsis thaliana genetics. Plant J. 14, 387–392.

Noden, D.M., 1983. The role of the neural crest in patterning of avian cranial skeletal, connective, and muscle tissues. Dev. Biol. 96, 144–165.

Ofori-Acquah, S.F., King, J.A., 2008. Activated leukocyte cell adhesion molecule: a new paradox in cancer. Transl. Res. 151, 122–128.

Parant, J.M., George, S.A., Holden, J.A., Yost, H.J., 2010. Genetic modeling of Li-Fraumeni syndrome in zebrafish. Dis. Model Mech. 3, 45–56.

Piotrowski, T., Nusslein-Volhard, C., 2000. The endoderm plays an important role in patterning the segmented pharyngeal region in zebrafish (*Danio rerio*). Dev. Biol. 225, 339–356.

Piotrowski, T., Schilling, T.F., Brand, M., Jiang, Y.J., Heisenberg, C.P., Beuchle, D., Grandel, H., van Eeden, F.J., Furutani-Seiki, M., Granato, M., Haffter, P., Hammerschmidt, M., Kane, D.A., Kelsh, R.N., Mullins, M.C., Odenthal, J., Warga, R.M., Nusslein-Volhard, C., 1996. Jaw and branchial arch mutants in zebrafish II: anterior arches and cartilage differentiation. Development 123, 345–356.

Robinson, V., Smith, A., Flenniken, A.M., Wilkinson, D.G., 1997. Roles of Eph receptors and ephrins in neural crest pathfinding. Cell Tissue Res. 290, 265–274.

Robu, M.E., Larson, J.D., Nasevicius, A., Beiraghi, S., Brenner, C., Farber, S.A., Ekker, S.C., 2007. p53 activation by knockdown technologies. PLoS Genet. 3, e78.

Rosano, L., Spinella, F., Di Castro, V., Nicotra, M.R., Dedhar, S., de Herreros, A.G., Natali, P.G., Bagnato, A., 2005. Endothelin-1 promotes epithelial-to-mesenchymal transition in human ovarian cancer cells. Cancer Res. 65, 11649–11657.

Ruhin, B., Creuzet, S., Vincent, C., Benouaiche, L., Le Douarin, N.M., Couly, G., 2003. Patterning of the hyoid cartilage depends upon signals arising from the ventral foregut endoderm. Dev. Dyn. 228, 239–246.

Sato-Jin, K., Nishimura, E.K., Akasaka, E., Huber, W., Nakano, H., Miller, A., Du, J., Wu, M., Hanada, K., Sawamura, D., Fisher, D.E., Imokawa, G., 2008. Epistatic connections between microphthalmia-associated transcription factor and endothelin signaling in Waardenburg syndrome and other pigmentary disorders. FASEB J. 22, 1155–1168.

Thisse, B., Thisse, C., 2004. Fast release clones: a high throughput expression analysis. ZFIN Direct Data Submission. (http://zfin.org).

Thisse, C., Thisse, B., 2005. High throughput expression analysis of ZF-models consortium clones.

Walker, M.B., Miller, C.T., Coffin Talbot, J., Stock, D.W., Kimmel, C.B., 2006. Zebrafish furin mutants reveal intricacies in regulating endothelin 1 signaling in craniofacial patterning. Dev. Biol. 295, 194–205.

Walker, M.B., Miller, C.T., Swartz, M.E., Eberhart, J.K., Kimmel, C.B., 2007. phospholipase C, beta 3 is required for endothelin 1 regulation of pharyngeal arch patterning in zebrafish. Dev. Biol. 304, 194–207.

Weiner, J.A., Koo, S.J., Nicolas, S., Fraboulet, S., Pfaff, S.L., Pourquie, O., Sanes, J.R., 2004. Axon fasciculation defects and retinal dysplasias in mice lacking the immunoglobulin superfamily adhesion molecule BEN/ALCAM/SC1. Mol. Cell. Neurosci. 27, 59–69.

Welten, M.C., de Haan, S.B., van den Boogert, N., Noordermeer, J.N., Lamers, G.E., Spaink, H.P., Meijer, A.H., Verbeek, F.J., 2006. ZebraFISH: fluorescent in situ hybridization protocol and three-dimensional imaging of gene expression patterns. Zebrafish 3, 465–476.

Westerfield, M., 2000. The zebrafish book. A guide for the laboratory use of zebrafish (*Danio rerio*), 4th ed. University of Oregon Press, Eugene, Eugene, OR.

Wolman, M.A., Regnery, A.M., Becker, T., Becker, C.G., Halloran, M.C., 2007. Semaphorin3D regulates axon axon interactions by modulating levels of L1 cell adhesion molecule. J. Neurosci. 27, 9653–9663.

Zimmerman, A.W., Joosten, B., Torensma, R., Parnes, J.R., van Leeuwen, F.N., Figdor, C.G., 2006. Long-term engagement of CD6 and ALCAM is essential for T-cell proliferation induced by dendritic cells. Blood 107, 3212–3220.

CHAPTER 4

CONCLUSIONS

DGS, the most common microdeletion syndrome, is characterized by congenital heart disease, craniofacial and immune system abnormalities. The T-box transcription factor *Tbx1* has been identified as the gene responsible for causing DGS. However, the cardiac defects in the zebrafish *tbx1*$^{-/-}$ mutant have not been characterized so far. In this thesis I have shown that zebrafish *tbx1*$^{-/-}$ mutants have defects in heart morphology, looping, function and differentiation. My data suggests a model whereby heart looping and differentiation are regulated by *tbx1* in a linear pathway through *wnt11r* and *alcama*. Furthermore, I show that *alcama* plays a crucial, nonautonomous role in pharyngeal endoderm during zebrafish cartilage formation, a tissue highly affected in *tbx1*$^{-/-}$ mutants. I have demonstrated that Alcama functions downstream of Edn1, a downstream effector of Tbx1, to regulate NC differentiation and cartilage morphogenesis. Hence, my data suggests that Tbx1 regulates Alcama via Wnt11r in the heart and via Edn1 in the pharyngeal endoderm.

4.1 Tbx1 regulates heart morphology and differentiation

Tbx1-/- mice have a severe phenotype with single cardiac outflow tract (OFT) and aortic arch defects (Jerome and Papaioannou, 2001). The role of zebrafish *tbx1* in cardiac

development has not been extensively studied. By ISH analysis *tbx1* is expressed in the mesodermal progenitors of the cardiomyocytes from the commitment phase. Hearts in *tbx1*$^{-/-}$ mutants are incompletely looped, wider and shorter, and have weaker contractions and slower heart rates.

Previous data suggest that mouse *Tbx1* positively regulates SHF cell proliferation and SHF contribution to OFT, and negatively regulates differentiation in SHF (Chen et al., 2009; Liao et al., 2008; Xu et al., 2004). My findings in zebrafish show that while SHF cells are formed in *tbx1*$^{-/-}$ mutants, the BA is not normally formed and is undifferentiated. Combined with data from a recent report (Hami et al., 2011), I concluded that SHF cells fail to migrate and integrate into the BA in *tbx1*$^{-/-}$ mutants. Together these data suggest that the role of *Tbx1* in regulating heart morphogenesis, especially in the outflow tract, is conserved among species.

Study of zebrafish *tbx1*$^{-/-}$ mutants has given us further insight into the mechanism by which *tbx1* regulates heart morphology. Although the ventricle and atrium are specified correctly, *tbx1*$^{-/-}$ mutants lack differentiation markers for the specific regions of the heart such as AVC. Similar to the lack of looping, lack of differentiation/subspecification has not been observed in mouse *Tbx1-/-* mutants. Whether lack of differentiation causes the looping defect or is an effect thereof is unknown. Loss of function studies for these differentiation markers suggest that differentiation does not affect heart looping. For example, the zebrafish *bmp4* mutant and *notch1b* morphant do not have defective heart looping (Lorent et al., 2004; Stickney et al., 2007), suggesting that lack of expression of these differentiation markers accompanies but does not cause the looping defect. It is however possible that looping

affects differentiation as other zebrafish looping mutants and morphants have defects in subspecification of the heart (Brown et al., 2005; Garrity et al., 2002; Qu et al., 2008; Ribeiro et al., 2007; Tu et al., 2009).

The lack of looping and differentiation may be caused by a defect in cell proliferation and shape. Although initial heart development proceeds normally, *tbx1*$^{-/-}$ mutants develop a reduction in cell proliferation at the onset of looping that results in decreased numbers of cardiomyocytes by 48 hpf. While Tbx1 regulates cell proliferation in mouse SHF, this is the first demonstration of its role in maintenance of proliferation in PHF cells. The decreased cardiomyocyte number might result in increased extracellular spaces in the heart.

In addition, these cardiomyocytes fail to change their shape from rounded to elongated cells. While both proliferation and shape change have been shown to contribute to heart looping (Auman et al., 2007; Ribeiro et al., 2007), they have not been linked to heart differentiation. Hence, *tbx1* might be necessary for maintaining cell proliferation and inducing shape changes that might regulate heart looping and differentiation in parallel or sequentially.

4.2 *tbx1* regulates heart morphogenesis via *wnt11r*

While both *Tbx1* and *Wnt11r* signaling have been shown to be important in heart morphogenesis, no link has been established to date (Arnold et al., 2006; Belema Bedada et al., 2005; Eisenberg et al., 1997; Merscher et al., 2001; Pandur et al., 2002). I have demonstrated that *wnt11r* is downregulated in *tbx1*$^{-/-}$ mutants and that *wnt11r* $^{-/-}$ mutants have looping and differentiation defects similar to *tbx1*$^{-/-}$ mutants, suggesting that *wnt11r*

functions downstream of *tbx1* to regulate heart looping and differentiation. In support of this hypothesis, *tbx1*$^{+/-}$/*wnt11r*$^{+/-}$ double heterozygotes have defective heart looping and differentiation, while single heterozygotes are morphologically unaffected. Furthermore, I was able to rescue the heart looping and differentiation defect by injection of *wnt11r* RNA or *alcama* RNA, a gene downstream of *wnt11r*, indicating that *tbx1* regulates heart morphogenesis via *wnt11r* and *alcama*.

In contrast to heart looping and differentiation defects, *wnt11r*$^{-/-}$ mutants do not have the BA defects seen in *tbx1*$^{-/-}$ mutants. This suggests that Tbx1 regulates BA morphogenesis and differentiation by a mechanism independent of Wnt11r.

I observed an increase in extracellular spaces between the cardiomyocytes of *tbx1*$^{-/-}$ mutants. Increased extracellular spaces have also been observed in *Xenopus wnt11r* and *alcama* morphants (Garriock et al., 2005; Gessert et al., 2008). Alcama, a homophilic transmembrane adhesion molecule downstream of Tbx1, might be required for maintaining cell-cell contact. This would explain the increase in extracellular spaces obtained by knockdown of any of the three genes: *tbx1*, *wnt11r* and *alcama*. Close cellular contact might be required for the cardiomyocytes to communicate with each other leading to looping and differentiation. Hence looping and differentiation defects might be indirect effects of *tbx1* knockdown. Alternatively, Alcama might regulate heart looping and differentiation directly and close cellular contact might be required for Alcama to mediate signaling.

tbx1$^{-/-}$ cardiomyocytes in the outer curvature fail to change their shape from rounded to elongated cells. I did not analyze the *wnt11r*$^{-/-}$ mutant hearts for this defect. Wnt11 has been demonstrated to provide a directional cue to organize the elongation of

early muscle fibres via the planar cell polarity pathway (Gros et al., 2009). Hence it is possible that *wnt11r* regulates cell shape and secondarily heart looping via the planar cell polarity pathway.

edn1 has been shown function downstream of *tbx1* in zebrafish cartilage morphogenesis (Piotrowski et al., 2003). This is corroborated by the observation that mouse *Edn1-/-* mutants share craniofacial and heart defects similar to *Tbx1-/-* mutants (Kurihara et al., 1995; Kurihara et al., 1994). This leads to the possibility that Tbx1 regulates heart looping via Edn1. However, zebrafish *edn1* is not expressed in the developing heart and *edn1*$^{-/-}$ mutants are not reported to have cardiac defects. While it is still conceivable that *Edn1* functions downstream of *Tbx1* in regulating heart development in mammals, this possibility cannot be studied using zebrafish.

In conclusion, I have demonstrated that zebrafish *tbx1* is required for normal heart looping, function, and differentiation. A possible mechanism by which Tbx1 regulates heart looping is the maintenance of cell proliferation and induction of cellular shape changes. Finally, I propose a model by which *tbx1* regulates *wnt11r* that then regulates *alcama*, which in turn regulates heart looping and differentiation.

4.3 Alcama is required for normal cartilage morphogenesis

My data indicates that *tbx1* regulates heart morphogenesis via *wnt11r* and *alcama*. Analysis of *alcama* morphants revealed that the ventral anterior arch cartilages are changed in orientation, are shorter and are fused to their dorsal counterparts. Analysis of earlier stages revealed that NC, endoderm and mesoderm are patterned and specified correctly in *alcama* morphants. However, late NC markers such as *hand2* are strongly

reduced in the pharyngeal arches of *alcama* morphants, suggesting that *alcama* is required for NC differentiation. NC differentiation is a prerequisite to normal chondrogenesis and cartilage formation. Hence I concluded that similar to *tbx1*, *alcama* is required for NC differentiation and cartilage formation and thus *alcama* might function downstream of *tbx1* during cartilage morphogenesis in addition to heart morphogenesis.

4.4 Alcama functions downstream of Edn1 signaling

The cartilage and NC differentiation phenotypes observed in *alcama* morphants are characteristic of the *edn1*-class of cartilage mutants (Piotrowski et al., 1996; Walker et al., 2006; Walker et al., 2007). Edn1 is a small signaling molecule functioning downstream of Tbx1, that is required nonautonomously for NC differentiation into cartilage (Piotrowski et al., 2003). Edn1 signals the NC and induces ventralization of pharyngeal arch cartilage (Miller et al., 2000). My data suggesting that *alcama* functions downstream of *tbx1* in heart morphogenesis taken together with the similarity of cartilage defects between *alcama* morphants and *edn1*$^{-/-}$ mutants, lead me to hypothesize that *alcama* might function downstream of *edn1* during cartilage morphogenesis.

Indeed, Alcama protein levels are downregulated in *edn1*$^{-/-}$ mutants and can be rescued by injection of *edn1* RNA, indicating that endogenous Edn1 regulates the levels of Alcama protein. Surprisingly, *alcama* RNA levels do not correlate with the severe down-regulation of Alcama protein levels observed in *edn1*$^{-/-}$ mutants, indicating that *edn1* regulates Alcama posttranscriptionally, perhaps at the level of translation or protein stability. I used the proteasome inhibitor MG132 to reveal that Edn1 inhibits the proteasomal degradation of Alcama.

In contrast to *edn1*$^{-/-}$ mutants, *tbx1*$^{-/-}$ mutants have downregulated levels of *alcama* RNA as well as protein. However, Alcama protein levels are more severely downregulated than *alcama* RNA levels. This suggests that Tbx1 transcriptionally regulates *alcama* RNA levels and Alcama protein is downregulated in *tbx1*$^{-/-}$ mutants by a combination of decreased RNA expression or stability and increased protein degradation. Alternatively, *alcama* RNA and protein levels might be lower in *tbx1*$^{-/-}$ mutants due to a decrease in the number of endodermal cells. The higher severity of cartilage defects in *tbx1*$^{-/-}$ mutants as compared to *edn1*$^{-/-}$ mutants can be explained by this lack of endodermal cells or by downregulation of other Tbx1 target genes. In either case, the cartilage defects in *alcama* morphants, though less severe than either mutant, are more similar to *edn1*$^{-/-}$ than *tbx1*$^{-/-}$ mutants.

I further probed my hypothesis that *alcama* mediates Edn1 signaling by overexpressing *alcama* in *edn1*$^{-/-}$ mutants and assessing NC differentiation. Indeed, *alcama* overexpression can rescue the NC differentiation defect in *edn1*$^{-/-}$ mutants, suggesting that *alcama* functions downstream of *edn1* to regulate NC differentiation. Furthermore, knockdown of *alcama* can abrogate the rescue of *edn1*$^{-/-}$ mutants by *edn1* overexpression, suggesting that *alcama* expression is necessary for Edn1 function. Hence, I have demonstrated that Edn1 mediates its signaling in the pharyngeal endoderm via Alcama.

4.5 Alcama interacts with Nadl1.1 on NC to mediate Edn1 signaling

Alcama is a transmembrane protein expressed on the endoderm and not on NC, the tissue that differentiates to form cartilage. Nadl1.1, which has been shown to interact with Alcama in chick (DeBernardo and Chang, 1996), is expressed on NC. I have shown that knockdown of *nadl1.1* results in cartilage and NC differentiation defects similar to *alcama* knockdown. Furthermore I demonstrated that knockdown of *nadl1.1* abrogates the ability of *alcama* to rescue NC differentiation in *edn1*$^{-/-}$ mutants, suggesting that *nadl1.1* expression is necessary for Alcama to mediate Edn1 signaling. Due to lack of antibodies, I could not show direct interaction of Alcama on endoderm with Nadl1.1 on NC due to the absence of an antibody against Nadl1.1. However co-injection of suboptimal doses of *alcama* MO and *nadl1.1* MO resulted in NC differentiation and cartilage defects, indicating that Alcama and Nadl1.1 interact during cartilage morphogenesis. All these data lead me to conclude that Alcama interacts with Nadl1.1 to mediate Edn1 signaling and regulate NC differentiation and cartilage morphogenesis.

The difference in severity of cartilage defects between *alcama* morphants and *edn1*$^{-/-}$ mutants can be explained by the additive effect of two parallel pathways. *alcama* morphants have only one pathway blocked while *edn1*$^{-/-}$ mutants have both pathways blocked leading to a more severe defect. Similarly *ednra* morphants do not phenocopy the cartilage defects in *edn1*$^{-/-}$ exactly (Nair et al., 2007). According to my model knockdown of *ednra* and *ednrb* together will have a more severe defect as it will block both pathways. In addition, my model predicts that *ednrb* morphants should have downregulation of Alcama protein.

An alternative possibility is that Edn1 does not need to be secreted from the endodermal cells to regulate Alcama. Since both Edn1 and Ednrb are synthesized in the endodermal cells, they might bind in the endoplasmic reticulum and signal from there itself. This would explain the similarity between *furina*$^{-/-}$ mutants and *alcama* morphants (Choudhry et al., 2010; Walker et al., 2006). Endothelin remains in its uncleaved form in *furina*$^{-/-}$ mutants, hence Edn1 peptide is never secreted and never binds to its receptor on the neural crest, blocking one pathway. However, the uncleaved Edn1 may bind to Ednrb in the endoplasmic reticulum of endodermal cells and stabilize Alcama levels keeping the second pathway active.

Another possibility is that Edn1 regulates Nadl1.1 levels in the neural crest similar to how it regulates Alcama in the endoderm. While I have shown that *nadl1.1* RNA is unaffected in *edn1*$^{-/-}$ mutant, I have been unable to analyze Nadl1.1 protein levels due to the absence of a zebrafish Nadl1.1 antibody. In this case, both Alcama and Nadl1.1 levels will be under the control of Edn1, making Edn1 signaling highly potent and sensitive to levels of Edn1.

In conclusion, I have demonstrated that *tbx1* regulates heart looping and differentiation via *wnt11r* and *alcama* in the heart. In parallel, *tbx1* regulates *edn1* and *alcama* in the pharyngeal endoderm, which in turn regulate NC differentiation and cartilage morphogenesis.

4.6 References

Arnold, J.S., Werling, U., Braunstein, E.M., Liao, J., Nowotschin, S., Edelmann, W., Hebert, J.M., Morrow, B.E., 2006. Inactivation of Tbx1 in the pharyngeal endoderm results in 22q11DS malformations. Development (Cambridge, England) 133, 977-987.

Auman, H.J., Coleman, H., Riley, H.E., Olale, F., Tsai, H.J., Yelon, D., 2007. Functional modulation of cardiac form through regionally confined cell shape changes. PLoS Biol 5, e53.

Belema Bedada, F., Technau, A., Ebelt, H., Schulze, M., Braun, T., 2005. Activation of myogenic differentiation pathways in adult bone marrow-derived stem cells. Mol Cell Biol 25, 9509-9519.

Brown, D.D., Martz, S.N., Binder, O., Goetz, S.C., Price, B.M., Smith, J.C., Conlon, F.L., 2005. Tbx5 and Tbx20 act synergistically to control vertebrate heart morphogenesis. Development 132, 553-563.

Chen, L., Fulcoli, F.G., Tang, S., Baldini, A., 2009. Tbx1 regulates proliferation and differentiation of multipotent heart progenitors. Circ Res 105, 842-851.

Choudhry, P., Joshi, D., Funke, B., Trede, N., 2010. Alcama mediates Edn1 signaling during zebrafish cartilage morphogenesis. Dev Biol 349, 483-493.

DeBernardo, A.P., Chang, S., 1996. Heterophilic interactions of DM-GRASP: GRASP-NgCAM interactions involved in neurite extension. J Cell Biol 133, 657-666.

Eisenberg, C.A., Gourdie, R.G., Eisenberg, L.M., 1997. Wnt-11 is expressed in early avian mesoderm and required for the differentiation of the quail mesoderm cell line QCE-6. Development 124, 525-536.

Garriock, R.J., D'Agostino, S.L., Pilcher, K.C., Krieg, P.A., 2005. Wnt11-R, a protein closely related to mammalian Wnt11, is required for heart morphogenesis in Xenopus. Dev Biol 279, 179-192.

Garrity, D.M., Childs, S., Fishman, M.C., 2002. The heartstrings mutation in zebrafish causes heart/fin Tbx5 deficiency syndrome. Development 129, 4635-4645.

Gessert, S., Maurus, D., Brade, T., Walther, P., Pandur, P., Kuhl, M., 2008. DM-GRASP/ALCAM/CD166 is required for cardiac morphogenesis and maintenance of cardiac identity in first heart field derived cells. Dev Biol 321, 150-161.

Gros, J., Serralbo, O., Marcelle, C., 2009. WNT11 acts as a directional cue to organize the elongation of early muscle fibres. Nature 457, 589-593.

Hami, D., Grimes, A.C., Tsai, H.J., Kirby, M.L., 2011. Zebrafish cardiac development requires a conserved secondary heart field. Development 138, 2389-2398.

Jerome, L.A., Papaioannou, V.E., 2001. DiGeorge syndrome phenotype in mice mutant for the T-box gene, Tbx1. Nature Genetics 27, 286-291.

Kurihara, Y., Kurihara, H., Oda, H., Maemura, K., Nagai, R., Ishikawa, T., Yazaki, Y., 1995. Aortic arch malformations and ventricular septal defect in mice deficient in endothelin-1. J Clin Invest 96, 293-300.

Kurihara, Y., Kurihara, H., Suzuki, H., Kodama, T., Maemura, K., Nagai, R., Oda, H., Kuwaki, T., Cao, W.H., Kamada, N., et al., 1994. Elevated blood pressure and craniofacial abnormalities in mice deficient in endothelin-1. Nature 368, 703-710.

Liao, J., Aggarwal, V.S., Nowotschin, S., Bondarev, A., Lipner, S., Morrow, B.E., 2008. Identification of downstream genetic pathways of Tbx1 in the second heart field. Dev Biol 316, 524-537.

Lorent, K., Yeo, S.Y., Oda, T., Chandrasekharappa, S., Chitnis, A., Matthews, R.P., Pack, M., 2004. Inhibition of Jagged-mediated Notch signaling disrupts zebrafish biliary development and generates multi-organ defects compatible with an Alagille syndrome phenocopy. Development 131, 5753-5766.

Merscher, S., Funke, B., Epstein, J.A., Heyer, J., Puech, A., Lu, M.M., Xavier, R.J., Demay, M.B., Russell, R.G., Factor, S., Tokooya, K., Jore, B.S., Lopez, M., Pandita, R.K., Lia, M., Carrion, D., Xu, H., Schorle, H., Kobler, J.B., Scambler, P., Wynshaw-Boris, A., Skoultchi, A.I., Morrow, B.E., Kucherlapati, R., 2001. TBX1 is responsible for cardiovascular defects in velo-cardio-facial/DiGeorge syndrome. Cell 104, 619-629.

Miller, C.T., Schilling, T.F., Lee, K., Parker, J., Kimmel, C.B., 2000. sucker encodes a zebrafish Endothelin-1 required for ventral pharyngeal arch development. Development 127, 3815-3828.

Nair, S., Li, W., Cornell, R., Schilling, T.F., 2007. Requirements for Endothelin type-A receptors and Endothelin-1 signaling in the facial ectoderm for the patterning of skeletogenic neural crest cells in zebrafish. Development 134, 335-345.

Pandur, P., Lasche, M., Eisenberg, L.M., Kuhl, M., 2002. Wnt-11 activation of a nonccanonical Wnt signalling pathway is required for cardiogenesis. Nature 418, 636-641.

Piotrowski, T., Ahn, D.G., Schilling, T.F., Nair, S., Ruvinsky, I., Geisler, R., Rauch, G.J., Haffter, P., Zon, L.I., Zhou, Y., Foott, H., Dawid, I.B., Ho, R.K., 2003. The zebrafish van gogh mutation disrupts tbx1, which is involved in the DiGeorge deletion syndrome in humans. Development (Cambridge, England) 130, 5043-5052.

Piotrowski, T., Schilling, T.F., Brand, M., Jiang, Y.J., Heisenberg, C.P., Beuchle, D., Grandel, H., van Eeden, F.J., Furutani-Seiki, M., Granato, M., Haffter, P., Hammerschmidt, M., Kane, D.A., Kelsh, R.N., Mullins, M.C., Odenthal, J., Warga, R.M., Nusslein-Volhard, C., 1996. Jaw and branchial arch mutants in zebrafish II: anterior arches and cartilage differentiation. Development 123, 345-356.

Qu, X., Jia, H., Garrity, D.M., Tompkins, K., Batts, L., Appel, B., Zhong, T.P., Baldwin, H.S., 2008. Ndrg4 is required for normal myocyte proliferation during early cardiac development in zebrafish. Dev Biol 317, 486-496.

Ribeiro, I., Kawakami, Y., Buscher, D., Raya, A., Rodriguez-Leon, J., Morita, M., Rodriguez Esteban, C., Izpisua Belmonte, J.C., 2007. Tbx2 and Tbx3 regulate the dynamics of cell proliferation during heart remodeling. PLoS ONE 2, e398.

Stickney, H.L., Imai, Y., Draper, B., Moens, C., Talbot, W.S., 2007. Zebrafish bmp4 functions during late gastrulation to specify ventroposterior cell fates. Dev Biol 310, 71-84.

Tu, C.T., Yang, T.C., Tsai, H.J., 2009. Nkx2.7 and Nkx2.5 function redundantly and are required for cardiac morphogenesis of zebrafish embryos. PLoS One 4, e4249.

Walker, M.B., Miller, C.T., Coffin Talbot, J., Stock, D.W., Kimmel, C.B., 2006. Zebrafish furin mutants reveal intricacies in regulating Endothelin1 signaling in craniofacial patterning. Dev Biol 295, 194-205.

Walker, M.B., Miller, C.T., Swartz, M.E., Eberhart, J.K., Kimmel, C.B., 2007. phospholipase C, beta 3 is required for Endothelin1 regulation of pharyngeal arch patterning in zebrafish. Dev Biol 304, 194-207.

Xu, H., Morishima, M., Wylie, J.N., Schwartz, R.J., Bruneau, B.G., Lindsay, E.A., Baldini, A., 2004. Tbx1 has a dual role in the morphogenesis of the cardiac outflow tract. Development (Cambridge, England) 131, 3217-3227.